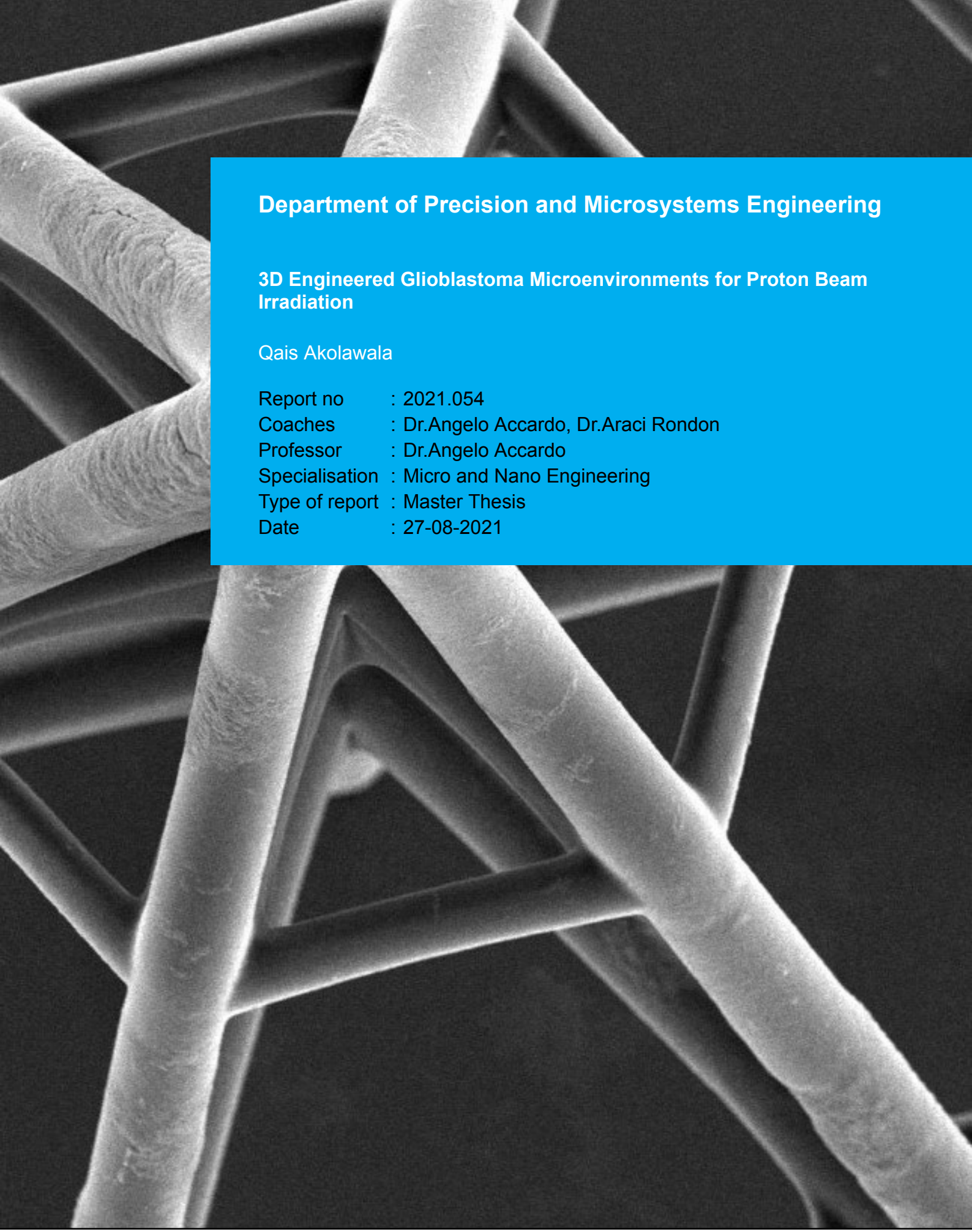

Department of Precision and Microsystems Engineering

3D Engineered Glioblastoma Microenvironments for Proton Beam Irradiation

Qais Akolawala

Report no	:	2021.054
Coaches	:	Dr.Angelo Accardo, Dr.Araci Rondon
Professor	:	Dr.Angelo Accardo
Specialisation	:	Micro and Nano Engineering
Type of report	:	Master Thesis
Date	:	27-08-2021

TU Delft Delft University of Technology

Challenge the future

3D Engineered Glioblastoma Microenvironments for Proton Beam Irradiation

by

Qais Akolawala

to obtain the degree of Master of Science in Mechanical Engineering
at the Delft University of Technology,
to be defended publicly on Friday August 27, 2021 at 10:00 AM.

Student number:	5044081
Project duration:	July 27, 2020 – August 27, 2021
Thesis committee:	Dr. A. Accardo, TU Delft, Supervisor
	Dr. A. Rondon, LUMC, Supervisor
	Dr. I. Buijnsters, TU Delft

This thesis is confidential and cannot be made public until December 31, 2022.

An electronic version of this thesis is available at http://repository.tudelft.nl/.

TU Delft

Preface

This project ”3D Engineered Glioblastoma Microenvironments for Proton Beam Therapy”, brings together principles of cancer cell biology, engineering design, and radiobiology. The project is very unique since it studies these parameters simultaneously: Directionally Engineered structures, cultured cancer cell lines, and their response to proton beam irradiation.

The project began in August 2020, and is a pilot project under the 'TU Delft Health initiative' award. This award supports the bringing of TU Delft expertise to research programmes that pioneer in health and life-sciences research. Under this vision, this project was aimed at creating reproducible, biomimetic microscaffolds for the growth of cells in 3D in *in-vitro* conditions. These samples were further tested with proton beam irradiation and study cellular response to it.

The project started with a 3-month long literature survey, which has been summarized in the introduction of this thesis. The literature survey was to familiarize myself with the topics, and to create a plan for the conducting the experimental research for this project. From November 2020 until July 2021, I developed the design for the structures, conducted cell cultures, proton beam experiments, and the analysis and evaluation of these experiments. The project is a result of a collaboration between three organisations: TU Delft, Leiden Univeristy Medical Centre (LUMC) and Holland Proton Therapy Centre (HPTC). I cannot thank the teams at these organisations enough for their continued support and guidance during this year-long project.

This thesis is a culmination of one year of my work on this project, two years of my masters at TU Delft, and many years of my ambition. I studied Mechanical Engineering during my bachelor's course, and always viewed biology and cellular studies with a wistful outlook. It always interested me, intrigued me, I would read and make amateur attempts at understanding it. This project provided the opportunity to bring my interest to fruition, and I am very glad I took it. It showed me that a steep learning curve can be overcome by the desire to strive forward. *'A little bit everyday'* has been my guiding refrain in this year. To keep trying to understand more, and keep attempting newer solutions.

I hope this thesis reflects my dedication toward this project, and that you can enjoy reading it, as much as I did writing it.

Qais Akolawala
Delft, August 2021

Acknowledgments

The collaborative nature of this project brought together teams from three different organisations and many different groups within them. This project has been made possible under the 'TU Delft Health Initiative Pilot Award' and I would first and foremost thank them for supporting this project.

I would like to then by thank my supervisors, Dr.Angelo Accardo and Dr.Araci Rondon. Dr.Accardo gave me with this opportunity, and his expertise provided me with the direction that I needed for this project. Without Dr.Rondon's constant support and expertise, it would not be possible for me to conduct the biology and cellular studies that are imperative in this project. The faith and confidence that my supervisors expressed in me and my work made me more confident in my work, and has helped me through this year. I would also like to thank Dr.Marta Rovituso at Holland Proton Therapy Centre, without whom the radiobiology experiments would not be possible. She was present every step of the way and helped me navigate the new territory of Proton Beam Irradiation.

I would also like to thank Prof.Dr.Henri Versteeg, under whose team and vision I worked at Leiden University Medical Centre. I must also thank Prof.Dr.Urs Staufer at TU Delft for his guidance invaluable perspective during the project.

Rob Luttjeboer and the Technical support staff at TU Delft have a big role to play in smoothly conducting any aspect of this project. I would like to thank them and the Einthoven lab team at LUMC where help was always enthusiastically available. I would also like to mention Wouter van Burik at HPTC, for his support during the experiments. The support of these teams has been invaluable in a project that is significantly experimental.

I would also like to thank the Nanoscribe users team at TU Delft, managed by Ahmed Sharaf. A lot of collaboration is required within the team to effectively work with the device, and help was always around the corner. I must thank Pieter, Damla, Halis, Nastaran, Jikke and Katerina for their very practical insights through the year and for making the environment at the lab so lively and energetic.

At LUMC, I must mention the Cancer Asssociated Thrombosis (CAT) team, for making me feel welcome at the lab and their constant support in an environment that was largely unfamiliar to me. I want to thank Rob van den Akker, Maaike Kapteijn and Monika Yvanovska particularly for their help and perspective at the lab.

I want to thank Thijs for helping me with the 'cell-box' design and printing it as a personal favour, and all my friends who made this year so much more memorable. Finally, I want to thank my parents, and my cousin– Enasha– for their support and encouragement in this year, even when things may have seemed hopeless.

Abstract

Glioblastoma (GBM) is a devastating cancer of the brain with an extremely poor prognosis. Novel *in-vitro* methods for the assessment of cancer response to drug and radiation are being developed. Compared to two-dimensional cell culture, three-dimensional cellular microenvironments provide a model closer to the *in-vivo* situation. In the context of cancer treatment, while X-Ray radiotherapy and chemotherapy remain the current standard, Proton beam therapy is an alternative with a compelling biological and medical rationale. It has shown to reduce the damage to healthy tissue with superior targeting abilities. In this report, a novel 3D engineered scaffold is designed and fabricated by two-photon polymerization (2PP). 2PP provides high-resolution and reproducible scaffolds are used to compare the response of cultured U251 cell line to Proton Beam irradiation. The cells are cultured on two- and three-dimensional scaffolds simultaneously for response comparison. Gamma-H2A.X is the marker used to identify the damage induced in the cells by the proton beams. The results show a higher DNA double-strand breakage in 2D cells as compared to those cultured in 3D. Differences in morphologies and proliferation are also observed. The discrepancy in proton radiation response could indicate a difference in the radioresistance of the cells, or a difference in the rate of repair kinetics between 2D and 3D cells. Thus, these biomimetic engineered 3D scaffolds can be used to routinely assess the effects of proton therapy on tridimensional GBM cell networks. These scaffolds have also been proved to be effective with evaluation methods such as immunofluorescence and scanning electron microscopy.

Contents

List of Figures

List of Tables

List of Acronyms

2D: Two-dimensional

2PP: Two-Photon Polymerization

3D: Three-Dimensional

CCK-8: Cell Counting Kit-8

CPT: Charged particle Therapy

DeMi Water: Demineralised Water

DMEM: Dulbecco's Eagle Modified Medium

DNA: Deoxyribonucleic Acid

DSB: Double strand breakage

ECM: Extracellular Matrix

FITC: Fluorescein isothiocyanate

GBM: Glioblastoma

HA: Hyaluronic Acid

HMDS: Hexamethylene Disilazane

HollandPTC/HPTC: Holland Proton Therapy Center

IF: Immunofluorescence

IPA: Iso-propyl Alcohol (2-Propanol)

ITO: Indium-Tin Oxide

LET: Linear Energy Transfer

LP: Laser Power

LUMC: Leiden University Medical Center

PBS: Phosphate Buffer Solution

PDC: Patient Derived Cells

PE: Phycoerythrin

PGMEA: Propylene glycol monomethyl ether acetate

qPCR: quantitative Polymerase Chain reaction

RBE: Radiobiological Effectiveness

SEM: Scanning Electron Microscopy

SOBP: Spread-out Bragg Peak

SS: Scanning Speed

TCGA: The Cancer Genome Atlas

WHO: World health Organisation

1 Introduction

1.1. Motivation

The brain is a complex organ, both in terms of its physiology and function. It is some way related to a variety of motor and physiological activities. It is the human seat of cognizance, understanding and our tool to understand the world around us. Any disease of the brain thus has insurmountable consequences to the lives that it affects. Cancer of the brain is one such disease, and Glioblastoma (GBM) its most aggressive known type.

The World Health Organisation (WHO) classifies glioblastoma as a grade IV glioma brain tumour[1]. The grade refers to it potential to grow and spread. Grade IV is the most serious and aggressive type. GBM continues to have one of the most dismal prognosis of any cancer in the body with the median survival rate at about 12-15 months, and less than 5% of cases surviving over 5 years after their initial diagnosis[2].

GBM causes tissue destruction, edema and epilepsy as its most notable symptoms. Depending on where it arises in the brain, the presented symptoms in patients can differ, including changes in personality, loss of language comprehension and formulation, loss of speech and motor functions. The deterioration is rapid, and the low chance of survival makes it imperative to understand the disease on a functional and fundamental level, to accurately target it and improve the lives of patients.

More is understood about the disease in recent times with the development of techniques to identify molecular genetic variations (mutations). The unrelenting nature of the GBM tumour is demonstrated by an experiment conducted by Dr. Dandy in 1928, where even after the resection of an entire hemisphere of the brain from a comatose patient, the tumour reappeared in the other half[3].

The current treatment regime includes removal of the bulk of the tumour by surgery followed by image guided radiotherapy and chemotherapy to control the regrowth of the tumour.The radiotherapy typically uses X-rays, and chemotherapy is done with drugs such as temozolomide[4, 5].

Photon beams, or X-rays are the current standard for radiation therapy for cancer patients worldwide. Advances in the technology have made it indispensable to patient care, but for some cancers in tough-to-access regions in the body–such as the brain–charged particle therapy (CPT) has more promising results. Proton beam therapy is a subset of CPT. CPT employs protons or other heavy ions instead of X-rays to induce damage to the tumours and cancerous cells. Compared to X-rays, proton beam therapy has improved targetting and can be controlled to have minimal dose deposition in surrounding healthy tissue.

The current standard of testing and studying GBM is with two-dimensional (2D) cell monolayer models. 2D monolayers are cultures of cells on plastic surfaces in flasks and petri dishes. The simplicity of its application and the development of reproducible protocols makes it an indispensable method of study. It also has certain disadvantages while studying GBM cells. These structures do not represent the milieu of the brain in which the cells grow, and causes phenotypical and organisational variations that lead to a change in cellular signalling and response to treatment.

To overcome this, three-dimensional(3D) models for cell culture are developed. 3D scaffolds or structures create an environment that has properties closer to that of the brain extracellular matrix (ECM).

They provide immense control over material, stiffness, architecture and geometry and therefore represent an important tool for *in-vitro* studies. Here it must be noted that these structures are not a fully accurate representation of the myriad complexities of the brain, but make it much easier to study parameters separately, and act as a bridge between the very simplistic 2D models and the complex 3D brain ECM[6].

The creation of these novel structures, and fucntionalising them for *in-vitro* cell culture applications is the first aspect of this project. The second is the application of Proton beam irradiation to these cultured cells, and the third is studying their *in-vitro* response to the treatment.

1.2. Background

In this section the background of the biology and experimental techniques associated with this project is listed. The section provides a short explanation to the rationale to the work conducted later, and is a description of technical information that is necessary to understand the project.

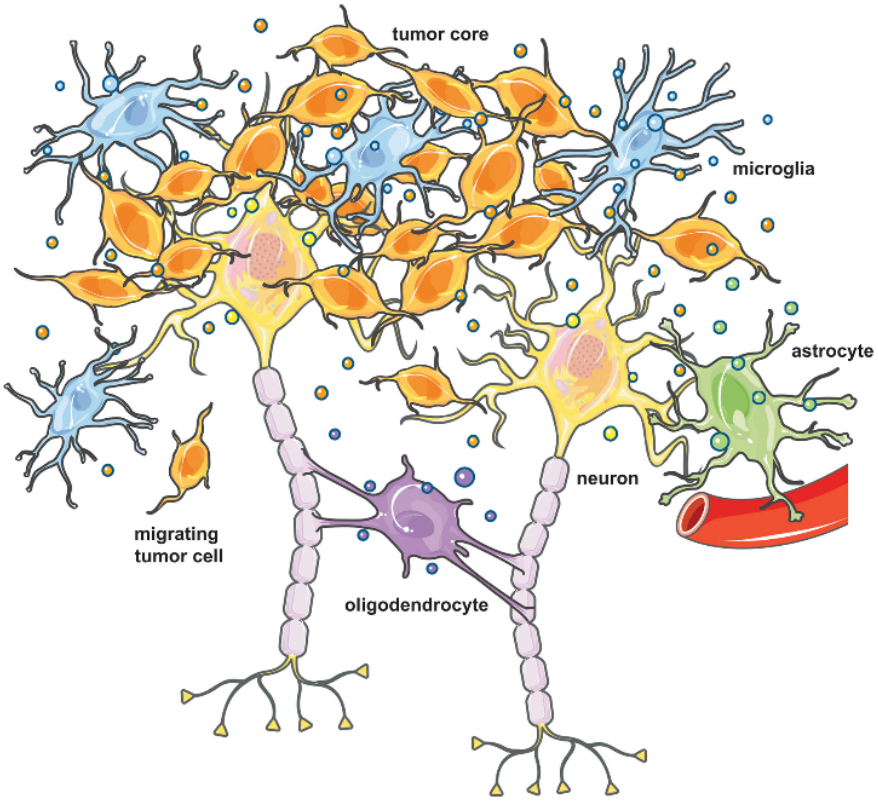

Figure 1.1: A schematic image of the GBM microenvironment, different cell types exist within the matrix[7].

1.2.1. Brain Tissue Composition

Firstly, we discuss the environment of the brain that is to be mimicked. The human brain has a complex composition. The brain not only consists of various types cells, but also other materials that assist in maintaining the structure and health of the tissue. Figure 1.1 shows a schematic image of this composition. The main components are:

1. **Neurons:** These are the cells that produce and transmit electric impulses in the nervous system. They make up approximately 8% of the composition of the brain[4].
2. **Glial cells:** Cells like oligodendrocytes, astrocytes and microglia. These cells do not produce electrical signals. They maintain homeostasis, form ECM protiens, and provide support and protection to the neurons. These cells form almost 72 % of the tissue volume[4].
3. **Extracellular Matrix:** This is the macromolecular scaffold that surrounds the cells.These materi-

als are synthesized by both the glial cells and the neurons. The ECM comprises of approximately 20% of the tissue volume [4, 8].

1.2.2. Glioblastoma

Classification:
Glioma collectively refers to cancers that arise from the glial cells (or their precursor cells). Gliomas are divided into low grade (I and II) and high-grade (III or IV), depending on their aggressiveness and growth potential[1, 9]. WHO classifies GBM as a grade IV central nervous system (CNS) tumour. It comes under the family of *'Diffuse astrocytomas and oligodendrogliomas'* which also contains other grade II and grade III tumours [1].

Earlier classifications of GBM were based on evidence found through microscopy. In their 2016 classification, WHO departs from this view, and integrates the genetic basis of the tumour into this classification [1]. Specifically, GBM is further divided based on the status of the isocitrate dehydrogenase (IDH) gene into IDH-wildtype and IDH-mutant type. The tumours that cannot be assessed are classified as GBM-NOS (not otherwise specified). **IDH-wildtype** is responsible for almost 90% of the GBM cases, and corresponds with the "primary" type, which originates directly from glial cells into a grade IV GBM. **IDH-mutant** type (~10% of cases), corresponds to secondary type which originates from lower grade gliomas. Each of these also show specific phenotypic expressions which are important for clinical evaluations.[1, 10]

Another system of classification of GBM on genetic variations was described by the study by The Cancer Genome Atlas (TCGA) network [11]. They classfiy GBM based on the recurring genetic abnormalities. Based on the variations studied from over 200 samples, the subtypes are Proneural, Neural, Mesenchymal and Classical. The nomenclature is based on the characteristic genetic expression, and terminology used to describe it in earlier research. The details of the genetic expressions have been published in the study by Verhaak et al. [12]

Both systems of classification have their merits. The WHO classification provides an integrated phenotypic and genotypic identification, while the TCGA study presents the complicated GBM genetic profile. These different methods of classification illustrate the complexity of GBM, and reiterate the necessity for more studies in the field.

Cellular biology:
GBM tumors show cellular heterogeneity not only between different tumours, but also within the same tumour. These differences are genetic and histological (microscopic anatomical variations in the tissues). This leads to variations in choice of treatments and its outcomes. GBM tumors express a characteristic termed as cellular plasticity [13]. It implies that GBM tumours are a dynamic target that can present in multiple phenotypes. Cellular plasticity is described as a dynamic equilibrium as opposed to a stable population of cells [13, 14].They are able to adapt to their surroundings, and even small changes in the composition or concentration of chemicals in the environment can cause significant changes in the behaviour of the cell. Factors such as acidity and hypoxia (low oxygen concentration), and the stresses caused by chemotherapy and radiation, can alter the gene expression and functional state of GBM cells [13, 15].

The tumors induce changes in the chemical composition and mechanical properties of the ECM. The tumors show an increased secretion of proteins which foster increased cell adhesion, proliferation and dispersion. The tumor regions show greater stiffness than the surrounding brain-tissue as indicated by neurosurgery ultrasound scans[16]. The tumors may remodel the ECM to provide spaces for infiltration and promote angiogenesis (formation of new blood vessels)[6, 9].GBM cells therefore have an extensive network of blood vessels within it. This high degree of vascularization can provide the structural and physiological framework on which the cancer cells grow.

In laboratory applications for studying the behaviour of GBM, usually two types of cellular models are used. They are listed below:

1. **Immortalised cell lines:** These are cell lines that have been isolated from the GBM tumour of a living organism. Regular cells normally do not proliferate indefinitely. These cells have undergone

mutations that evade the normal cell-cycle and allow them to grow indefinitely. The mutations can occur naturally or be intentionally induced for experiments. These cells can therefore be used for prolonged periods *in-vitro*. Some examples of GBM cell lines are U87, U251, T98G, A172 cell lines, which are all of human origin, and are available commercially. In this project, the U251 cell line is used.

2. **Patient derived cells (PDCs):** They are also referred to as primary cells. These cells have been extracted directly from tissues, and retain their morphological characteristics. These cells however, have a limited potential for cell renewal and differentiation. As these cells age, they undergo many changes. The initial behaviour of these cells also greatly depends on the characteristics of the patients they are extracted from.

Immortalised cell lines (or simply, cell lines), provide an inexpensive and stable platform to run tests in laboratory conditions. The PDCs have closer characteristics to *in-vivo* tumours, but need to be employed prudently. PDCs are expensive and more valuable. It must also be noted, that cell lines and PDCs express a lot of variation in their expression in culture. Their response to the substrate on which they grow, and other methods of signaling also have differences [17]. Trials and early experiments make use of cell lines, which can form a precursor for attempts with PDCs.

Blood Vessel Architecture

Farin et al. in their study show the behaviour of glioma cells in relation to the surrounding vasculature[18]. It is known that the cells grow in the region around the blood vessels, but the reason for that is usually hypothesized as a chemical attraction that maybe due to the blood gases or factors in the blood vessel. The study is conducted with blood vessels in slice culture (without any blood in it), and their conclusion is that the cells that form the blood vessels are secreting factors that attract the glioma cells. These factors have not been particularly identified in their studies, but the most promising ones include endothelial-derived growth factors such as PDGF(platelet derived growth factor), and chemokines such as SDF-1(Stromal-cell derived factor)[19]. Chemokines are signaling protiens created by cells that can induce directed chemotaxis in nearby responsive cells. Other possible factors can be ECM molecules such as tenascin[20, 21].

As shown in the schematic in figure 1.2, one of the principle observations of the study is that the cells multiply preferentially at the vascular branch points. Clearly the branch point provides some environmental cue for the cells to multiply. Based on the observations and information stated here, it seems credible that the blood vessels also provide a structural incentive for the preferential growth of the glioma cells. The branching nodes provide stable, nutrient rich sites for the cells to adhere, and colonize that region. This hypothesis has formed the basis of the designs selected for this project.

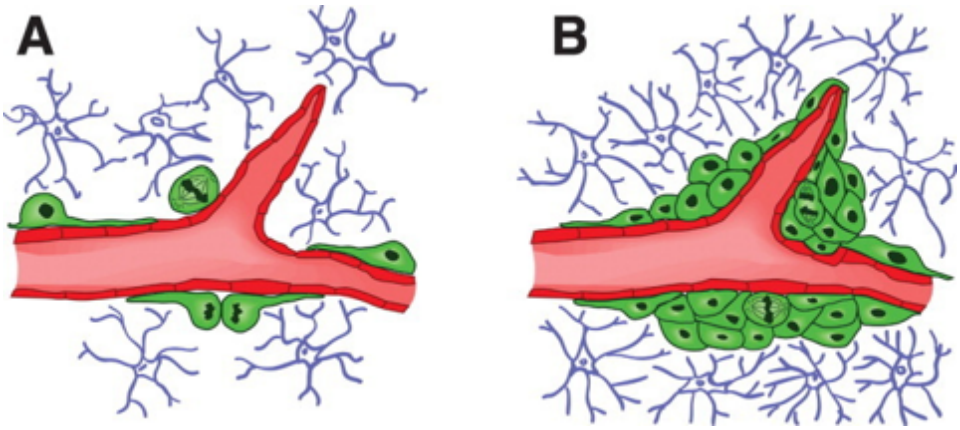

Figure 1.2: A: Glioma cells migrate along the blood vessels; **B:**Cells preferentially proliferate at the node[18]

1.2.3. Two-Photon Polymerization:

Two-photon polymerization (2PP) is a photolithographic method by means of which specific resins can be cross-linked by the simultaneous absorption of two photons. [22]When the beam of a femtosecond

pulse laser is tightly focused into the volume of a transparent, photosensitive material, the polymerization process can be initiated by non-linear absorption within the small focal volume pixel (voxel) as shown in the schematic in figure 1.3. These voxels can be maintained at sizes even below 100 nm. Consequently, the high-resolution of the structures manufactured with this method makes it possible to employ it to create various bio-mimetic designs such as bio-inspired blood vessels, microfluidic devices, and a range of scaffolds for improved cell culture. Among cell biology applications, it is extensively employed to better recapitulate disease models as well as for *in-vitro* drug and radiation testing. [22]

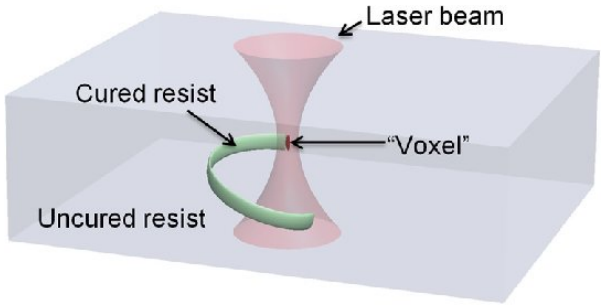

Figure 1.3: Schematic of the Photopolymerisation process. The material polymerises only locally at the voxel[23]

.

The workflow of the process is shown in figure 1.4. The slicing and hatching parameters of the manufacturing process control the resolution and surface features of the design. Slicing is the creation of multiple slices of the 3D structure with a varying cross section, while hatching controls the filling of each slice. The process of polymerisation happens according to these parameters in a layer-by-layer approach.

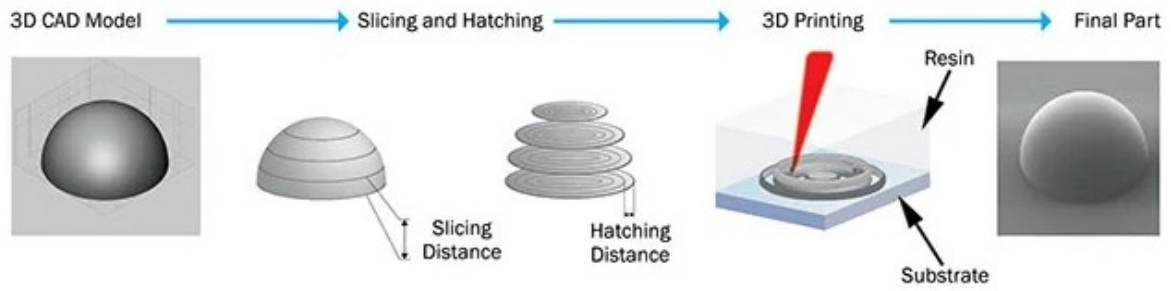

Figure 1.4: Work flow of the 2PP manufacturing process [24]

.

1.2.4. Proton Beam Therapy

Protons are usually sourced from ionized Hydrogen gas. These protons are then accelerated through Electric fields to achieve high energies and generate beams. Magnetic fields are used to steer the beam in the desired directions. X-rays on the other hand electromagnetic waves that are generated when an electron changes its energy states and releases photons.

Proton Beams vs. X rays

Protons and other charged particles show a variation of energy deposition with the depth of the beam, which is very different from that of X-rays. The dose refers to the amount of energy deposited per unit volume of the tissue. It is measured in a unit Gray (Gy). 1 Gy is equivalent to 1 Joule of energy being absorbed in 1 kg of the target material.

Charged Particle Beams have a characteristics energy deposition profile called the Bragg-curve. This curve is formed by the slowing of charged particles in air/water, where they lose energy by collisions with other particles. Figure 1.5 compares the depth-dose profiles of X-Rays and Proton Beams. The X-Ray beam (in black) exponentially decreases with depth as per the absorption law[25]. The proton

beams (in red and blue) are characterised by the sharp increase in energy in the curve, called the 'Bragg-peak'. The flat initial profile, also called the 'plateau', is a region of more-or-less constant dose. The sharp drop after the Bragg-peak is referred to as the distal fall-off. This sharp peak can also be modified by using multiple energy beams simultaneously to create a profile called the Spread out Bragg peak (SOBP), which provides uniform dose deposition in a certain range of depth of volume. Proton beams also show higher linear energy transfer (LET) than Photon beams. LET is defined as

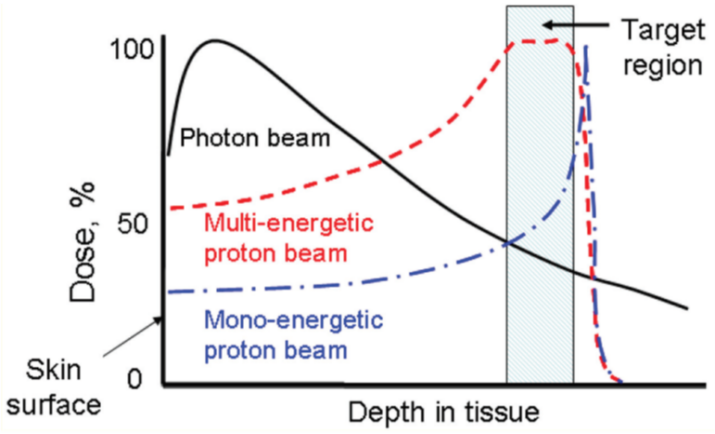

Figure 1.5: Depth-dose profile schematic comparing Proton beams and X rays. The Bragg peak forms a region of unifrm energy deposition at a greater depth than the X-rays. The characteristic distal end also shows much higher dose conformity[26]

the energy deposited per unit track in the tissue by charged particles. Its units are kilo-electron-volt per micron (keV/μm). LET depends on the ion charge and velocity. The increase in LET is more is more pronounced in heavier charged particles such as carbon. Nevertheless, a higher LET implies more effectiveness to kill a cell. Combined with the Bragg curve characteristics it makes charged particle therapy (CPT) an attractive method for cancer treatment.

High enough doses of radiation can kill any cell and sterilize tumours entirely, but all radiation will cause complications in healthy tissue and this hence demands a trade-off. Radiation (both X-ray and Proton beams) must achieve a high tumour control probability (TCP) with minimum damage to the surrounding volume. This requires fractionation of the total dose. 2 Gy per day, upto 60-80 Gy, depending on the cancers. Hence these factors greatly alter the treatment regime for the cancer.

The disadvantages with CPT is the paucity of available clinical data.This stems from the other issue of CPT being a very expensive treatment method. This is often cited as a reason to claim that there is not enough evidence for the superiority of CPT. [27] The biological, ethical and medical rationale remains compelling for further research in this field.In some specific cases such as Prostate cancer, the use of CPT has made it possible to double the dose to the target [27]. Hence the attempts to create and study pre-clinical and *in-vitro* models with CPT and Proton Beam irradiation is essential to build a body of evidence to support structured and broader clinical trials[27].

Depth-Dose Curve

A low dose is deposited at the region where the beam enters the tissue, maximum dose is deposited at region called the Bragg peak, and then a sharp distal fall-off. The regions and the profile is indicated on the graph in figure 1.6. Due to the low deposition of energy at the entrance,and the beam retains its energy, and reduces the damage to that tissue. At the Bragg peak the maximum dose is deposited to damage to the tumor. The distal fall of is the region after the deposition of the dose at the Bragg peak that shows a sharp decline in energy (especially for protons), which gives great dose conformity outside the tumour(keeping the dose deposited outside the tumor to a minimum). The occurrence of the Bragg-peak at a depth in the reduces the damage except where it is intended. The excellent ballistic characteristics and low exit energies of the particles make it possible for them to damage minimum healthy tissue around the target region[28].The energy of the beam can change the position of the bragg-peak. Several Proton beams can be targeted simultaneously to create a region of uniform

energy deposition which is called a Spread-out Bragg-Peak (SOBP). These have been shown in figure 1.6 Proton beams also have a sharp drop at the distal end. Heavy ions also have dose-tail behind

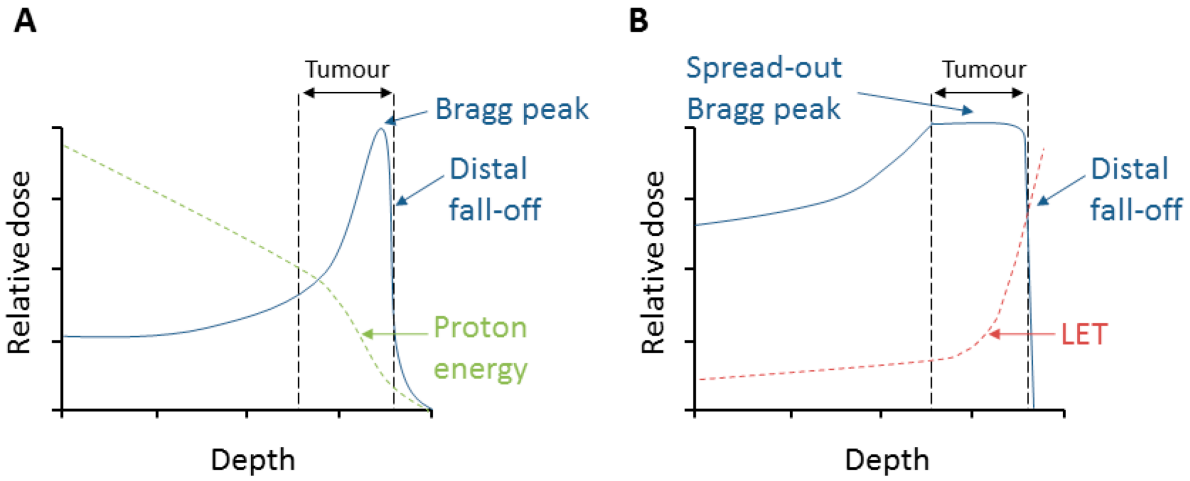

Figure 1.6: Depth–dose distribution of protons and relationship to energy and LET.**A:** An unmodulated (pristine) Bragg-peak produced by a proton beam. **B:** Several beams can be modulated such that they form a region of uniform dose deposition called the Spread-out Bragg peak (SOBP). It deposits a uniform dose in the region [29].

the Bragg-peak due to secondary collisions, creating a more complicated field. Comparatively, proton beams are able to present better dose conformity. The position of the peak can be precisely adjusted by changing the incident velocity of the beams[25].

1.2.5. Immunofluorescence

Immunofluorescence (IF) is a technique by which light emitting compounds–called fluorophores– are used to visualise specific cellular antigens. Antibodies bind to these specific antigen sites in the cells. The fluorophores bind to these antibodies. Fluorophores are compounds that absorb certain wavelengths of light, and emit other wavelengths. These compounds are what are detected in a biological sample by fluorescent and confocal microscopes.These sites can be used to visualise proteins and components within cells and tissues[30].

IF is of two types, direct and indirect. Direct IF is when the antibody is coupled with a fluorophore, and Indirect IF is when the fluorophore is a secondary antibody that binds to the primary one. The proteins or antigens can then be seen under a fluorescent or confocal microscope. The method can be used for qualitative and quantitative analysis of these antigens and regions of interest, depending on the outcome of the image. A schematic of fluorphores, and the principle is shown in figure 1.7. Both direct and Indirect methods of IF are used in this project.

Multiple antibodies can also be used in the same sample. Different fluorophores have different intensities of emission and excitation within a range of wavelengths. To successfully use multiple antibodies usually the ranges of excitation and emission spectra are selected such that they do not interfere with one another and cause and overlap in the images.

1.3. State of the Art

In this segment, I discuss the various methods that are currently employed for 3 dimensional cell culture, and methods to irradiate *in-vitro* cell samples.

1.3.1. 3D Cell Culture

Various methods can be implemented to create 3D cell culture samples. Synthetic and natural-derived materials are used with a variety of processes that create these scaffolds. The properties of these materials and the manufacturing process are important parameters in the feature sizes and resolutions that can be achieved.

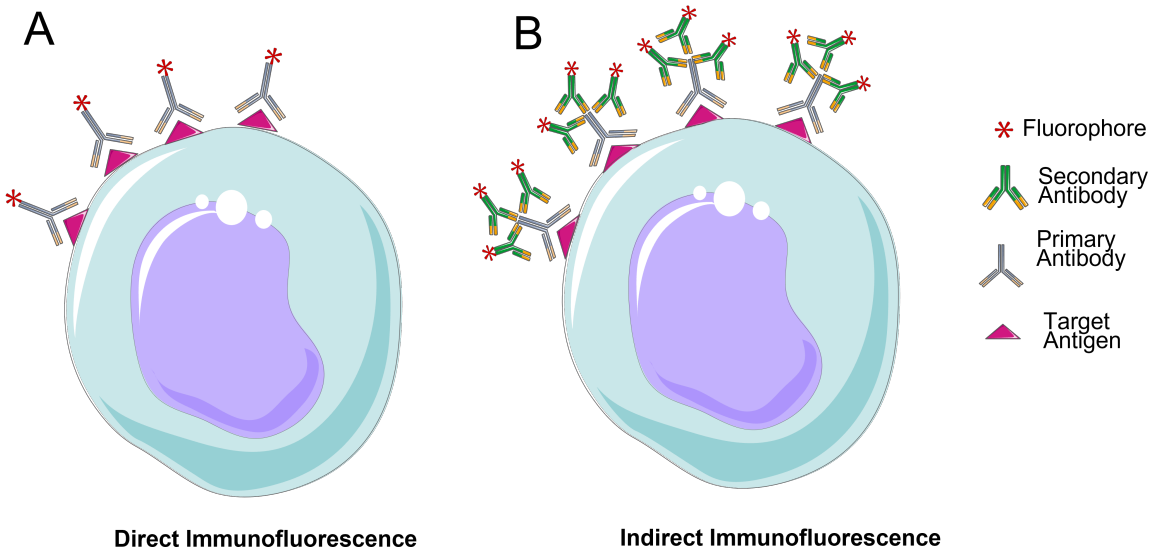

Figure 1.7: A: Direct Immunofluorescence with the primary antibody directly labelled with the fluorophore, and binding with the target antigen site. **B:** Indirect immunofluorescence with the primary antibody binding to the antigen, and the fluorophore-labelled secondary antibody binding to the primary[31]. *The image is created using elements from smart.servier.com*

Specifically, for methods such as two-photon polymerization (2PP), the material used is polymerised by the use of light, and needs to be functionalized for it, by the addition of chemicals called photoinitiators. It is an example where the material is altered to suit the manufacturing process.The cytotoxicity of the material components in particular, and their response to cells in general, plays an important role in the selection of the material or method.

2PP provides advantages in design and fabrication, and the current research using it is discussed in section 1.3.2.The other methods and materials used for 3D cell culture are discussed here. It is also summarized in table 1.1:

1. **Hydrogels:** Hydrogels are materials that have the unique property of retaining a large amount of water owing to their molecular structure and are hence good substrates for growing cells. Hydrogels can be created from natural polymers of the brain ECM in the hope to better mimic the ECM. These hydrogels include those derived from chitosan, hyaluronic acid (HA), chondritin sulfate polysaccharides, collagen/gelatin protiens and alginates[13].Hydrogels can also be manufactured synthetically such as Poly (ethylene glycol) diacrylate or PEGDA. These synthetic hydrogels, much like their natural counterparts, can also be manufactured through rapid chemical crosslinking, or by photocrosslinking[32].

   Hydrogels can be crosslinked covalently or non-covalently. The covalent linkages are stronger, but carry issue of cytotoxicity owing to the need of photoinitiators that are required to initiate a photopolymerization (solidification) process in presence of a light source. While hydrogels would form ideal materials for cell culture and to study cell-cell interactions, the manufacturing process with them can be quite complex, with reproducibility being difficult to achieve [33, 32]. Photocrosslinking these materials covalently can prove to be a time-consuming process that requires optimisation of not only the properties of the material but also the compatibility of the photoinitiator and subsequently only providing limited structural capabilities.

   Non-covalent composite hydrogels created with collagen and HA for 3D GBM cell cultures, exhibit biomimetic features such as control of collagen and HA composition, distinct microarchitectures, and physiologically relevant mechanical properties, which make them suitable 3D biomaterial scaffolds for neural cells [34, 35]. These materials have the disadvantage of not providing enough control on the design, which again, can affect engineered reproducibility.

2. **Natural and derived materials:** Scaffolds made of collagen, chitosan and HA undergo gelation at physiological temperatures. Scaffold fabrication can thus be done with simple methods like centrifugation or chemical crosslinking [33, 36, 37]. A number of different methods exploit different properties of the materials being used. Florcyzk et al. use lyophilizing (Freeze-drying) with chitosan and HA for creating a porous scaffold[38]. Another example is the use of a solid state foaming method to make porous polylactic acid scaffolds[5].

3. **Synthetic materials:** Polystyrene is the material that many 2D culture substrates are made out of.These materials are also used in commercial 3D scaffolds. Alvetex®3D scaffolds are an example of such a product.

   Hayman et al. create a solid and porous polystyerene scaffold to culture stem-cell derived neurons. While not a study on GBM, this study gives insight into the importance of the hole sizes of these scaffolds. Highly porous foams were prepared from poly(styrene/divinylbenzene) using a high internal phase emulsion. The creation of these foams makes small cavities of 5-20 µm in size, which is unsuitable for the growth of neurons, the neurite extensions of which sometimes extend to 500 µm. They process the foam with another chemical to increase the range of pore sizes to 50-100 µm[39]. This also shows how the sizes of the scaffold features can alter cellular behaviour, and even affect the success of the culture. The choice of these features is a parameter that is considered during scaffold design and manufacture.

Table 1.1: Summary of Minimum feature sizes for various 3D scaffolds

Cells	**Material**	**Pore/Minimum feature size**	**Reference**
G7, E2 (GBM PDCs)	Alvetex	42 μm	[40]
118-MG	Chitosan-Hyaluronic Acid	77.3 μm	[38]
U87	Polylactic acid	250-300 μm	[5]
U87	Collagen	50 μm	[41]
OSU2 Cells (GBM)	Collagen-HA in various proportions	Not reported, images with scale bar of 50 μm	[34]
Neuronal stem cells	Collagen-HA in various proportions	100-200 μm for various formulations	[33]
U87	IP-S	10μm	[42]
Neuroblastoma	IP-DiP	20 μm	[43]
Chondrosarcoma	Collagen	100 nm (Relevant for Proton beam irradiation)	[28]

1.3.2. 3D Cell Culture and 2PP

Many of the above techniques like gas induced foaming, fiber bonding, and phase separation have limitations for the production of scaffolds with reproducible architecture. These processes are carried out in the material in their bulk volume, without specific local alterations to form defined features. While the structures show some relevant features, they are not reproducible on the micrometer level. Considering how sensitive GBM cells are to their environment, local polymerization method such as such as two-photon polymerisation (2PP) provide the possibility to manipulate these structures reproducibly on a micrometer scale. A number of studies have used 2PP to create biomimetic scaffolds on which cells are cultured. A limited number of studies have been carried out with GBM cells in particular, but the rationale and results of studies with other cells also provide valuable insight into how the architecture of the scaffolds affects cell culture.

Spagnolo et al. demonstrate the use of micro-cages of differently sized pores to study the invasiveness of breast cancer cells. They use 2PP, and show that even the change of the spaces with a few micrometer-square can affect the invasive capacity of the cells. The size range of their pore sizes is taken proportionally to the size of the cell, to estimate the relationship between the gap sizes and the cellular sizes [44].Figure 1.8 shows the images of the 2PP scaffold.

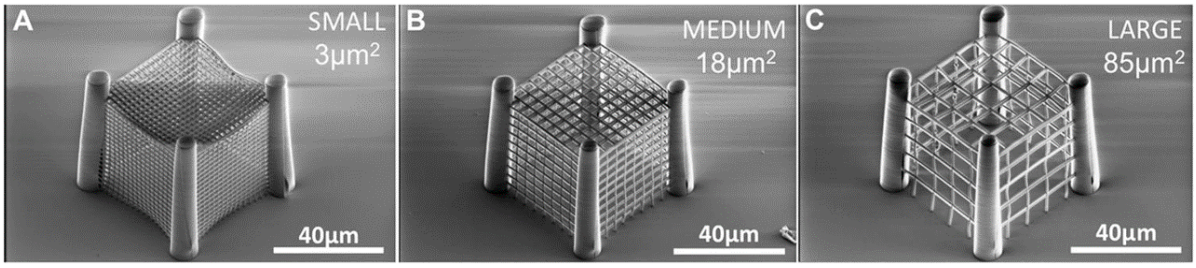

Figure 1.8: The images show the variation that it created with pore sizes. **A:** Smallest pore size**B:** Medium pore size and **C:** Largest pore size.An increase in the pore size showed an increase the invasion of the adenocarcinoma cells.[44]

Greiner et al. also demonstrate the use of a mesh-like structure to study the invasion of lung carcinoma cells, and compare their behaviour to other 2D structures. They used sizes of 10 μm, 8 μm and 7 μm, to create dimensional limitations to the chemotactic invasion study. A higher invasion was observed wehn compared to 2D cell cultures. Within the 3D culture a decrease in the mesh-size pores of the scaffold decreased the rate of migration of the cells across the structure [45]. Since the chemical attractant employed is the same, the change of pore sizes is a parameter that can tuned to make the scaffolds replicate *in-vivo* behaviour more accurately.

Another important study is by Tricinci et al, who use the 2PP approach for the manufacture of a microfluidic device mimicking the blood-brain barrier. This study uses GBM cells cultured on a micro-cage structure. The intent of the micro-cage was to form spheroids greater than 200 µm in diameter,and the design accomplishes that through pores and gaps which allow a flow of gases and nutrients to the cultured U-87 cells.This study also touches upon another important aspect of manufacturing with 2PP which is the use of the laser power values. Varying the laser power can change the stiffness values obtained in the structures which is an important characteristic of the created ECM for cell growth. The stiffness of individual beams of a structure can be low, but the design of the structure can improve the overall stiffness of the scaffold. Figure 1.9 shows the SEM image of the micro-cage. The design has large aspect ratios but still provides a stable framework for the formation of the tumour spheroids. From the image it can be observed that the diameter of the micro-cage is about 80µm, and the minimum features around 8-10 µm[46, 42].

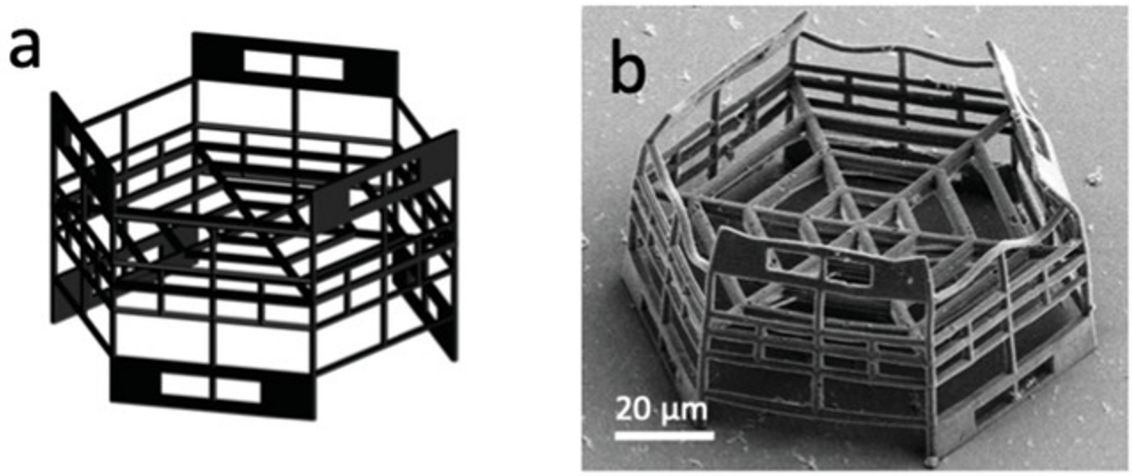

Figure 1.9: A:CAD Model of the structure, **B:**SEM image of the printed structure. This structure is able to create cell spheroids of approximately 200 μm diameter.[42]

In their manufacture of wood-pile structures, Accardo et al. also provide insight in the utility of 2PP as a tool for microstructure creation. They create the woodpile with a 60μm horizontal and 20μm vertical spacing for the easy penetration of the neuroblastoma cells used and to allow efficient imaging. The

regular nanogratings on the surface induced by fine-tuning the manufacturing parameters of slicing and hatching, provides smoother edges compared to square beams and aligning pathways to neuronal processes[43].

Lemma et al. in their study, present an overview of various designs and features used for human cell cultures, specifically in the case of cancer cell studies. As mentioned earlier cancer cells have higher migration rates and can invade through membranes and blood vessels. An overview of the various designs in literature is shown in figure 1.10[47].

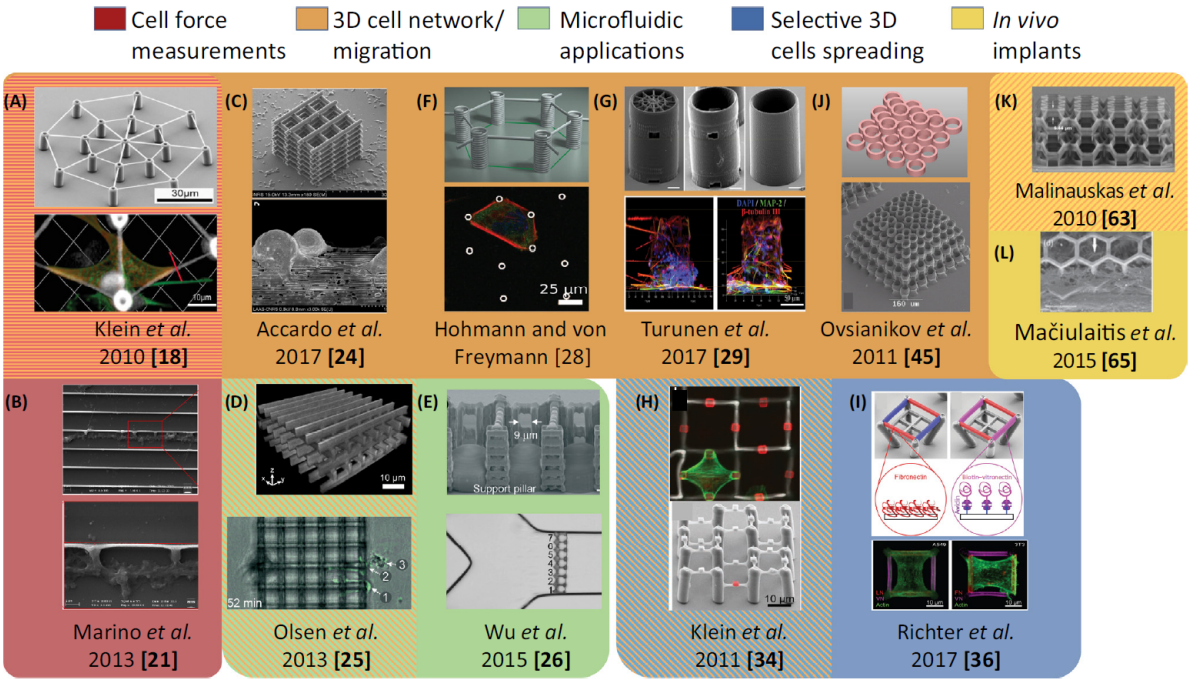

Figure 1.10: Overview of 2PP architectures created for applications with different cells. The specific geometries show the cell behaviour changes with changing ECM properties. (References of the images are as per the original paper.) [47]

1.3.3. Irradiation Studies:

Lopez-Perez et al. use the U-87 GBM cell line cultured in a monolayer configuration.[48] The study compares the effect of X-rays and Carbon-ion beams on these cultured cells. The effect is measured by quantifying the double strand breakage (DSB) of the DNA of the cells. They observe that that Carbon-ions radiation damages the cells more substantially when compared to cells irradiated with photon beams.They use Gamma-H2A.X to visualise the DNA strand breakage. Gamma-H2AX is created in the nucleus of the cells as repair-response to DNA damage, and is therefore an indicator for the DSB that occurs in the cell.Figure 1.11 shows a comparison of the Gamma H2A.X foci formation in the GBM cells. They also observed that cells irradiated with carbon ions also show a slower rate of DSB repair than those irradiated with photons.This was evaluated using colony forming survival assays. This study is important and relevant to this project as it is one of the very few studies that employ GBM cells with charged particle therapy (CPT), and their methods can be used to base-line protocols for newer research.

During the literature review, the search of 3D culture studies had to be expanded to other cancer cells since a direct search with GBM did not yield relevant results. The study by Hamdi et al, compares the effect of X-rays and Oxygen (O_{18}) ion beams. The set-up uses a collagen scaffold, and a culture of chondrosarcoma cells [28].

This study uses a collagen scaffold which does not have a designed structure. The orientations of the

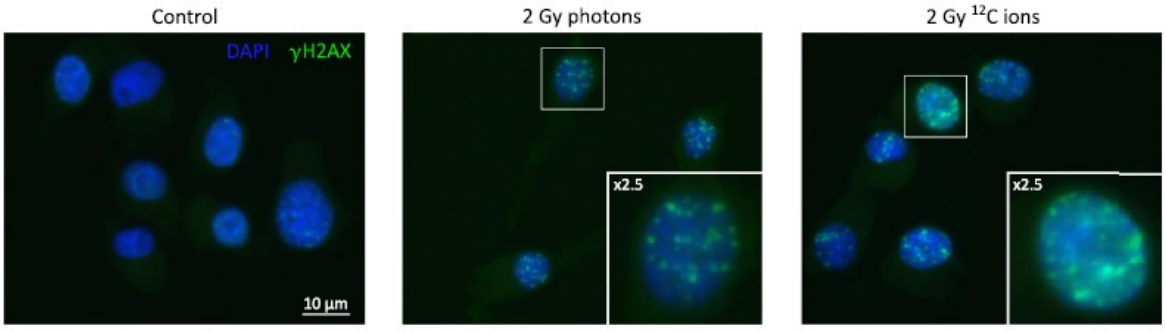

Figure 1.11: Higher levels of Gamma-H2A.X induction after irradiation with carbon ions compared to photon beams. The fluoroscent green spots in the blue stained nucleus show the formation of Gamma-H2AX, indicates higher extent of DNA damage[48].

collagen strands was not geometrically defined. The scaffold is shown in figure 1.12. This study uses a 96-well plate in which the wells are filled with the scaffold material. These scaffolds are irradiated vertically as shown in the figure 1.13. The O_{18} ion beam is optimised to deliver the planned dose of 2 Gy at the scaffold. The optimisation of the beam includes considering the plastic the holder, and the medium as these will also interact with the beam, and need to be accounted for.

A similar protocol to the one used by Lopez-Perez et al. is employed, with the use of Gamma-H2A.X and western blotting to evaluate the cells after and before irradiation.[48] An interesting outcome of the research is that the 3D cell culture with X-rays seemed to repair its broken DNA strands faster than the cells irradiated with the high-LET Oxygen ions, implying that high-LET charged particles induce more DNA damage.

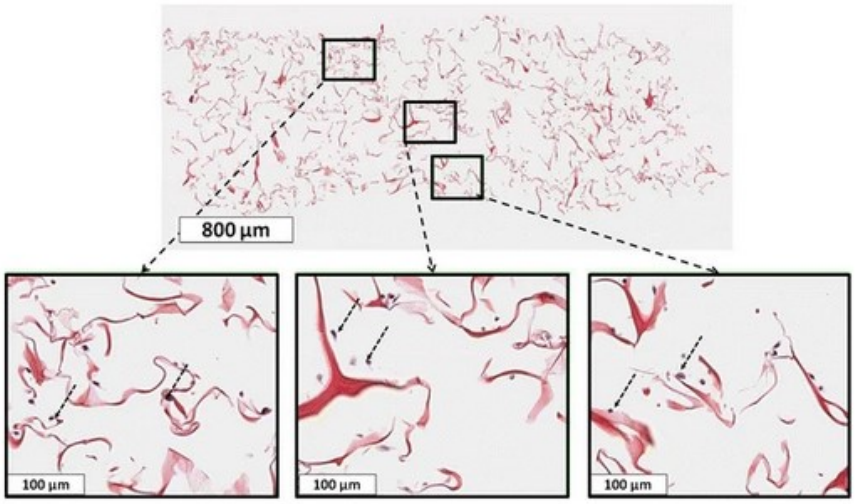

Figure 1.12: Collagen fibres shown in red, cultured cells marked with dashed arrows in the magnified sections (below). The cells attach to the fibers in the scaffold. The scaffold fibres itself are much larger than the cells cultured on them[28].

In the study by Roig et al. The study uses Fe_{56} ions, and lung carcinoma cells cultured on a 3D collagen matrix. The matrix, and irradiation set up is similar to the one seen in Hamdi et al. [28]. The conclusion of the research is that the DNA damage depends on the Bragg-curve energy distribution, and shows maximum cellular damage at the Bragg peak, and lower damage in the plateau region. They use the Gamma-H2A.X, DAPI and the Imaris software for a 3 dimensional reconstruction of the images, and make a map of the DNA damage observed [49]. The DNA damage response is mapped by using Gamma-H2AX and another DSB marker.

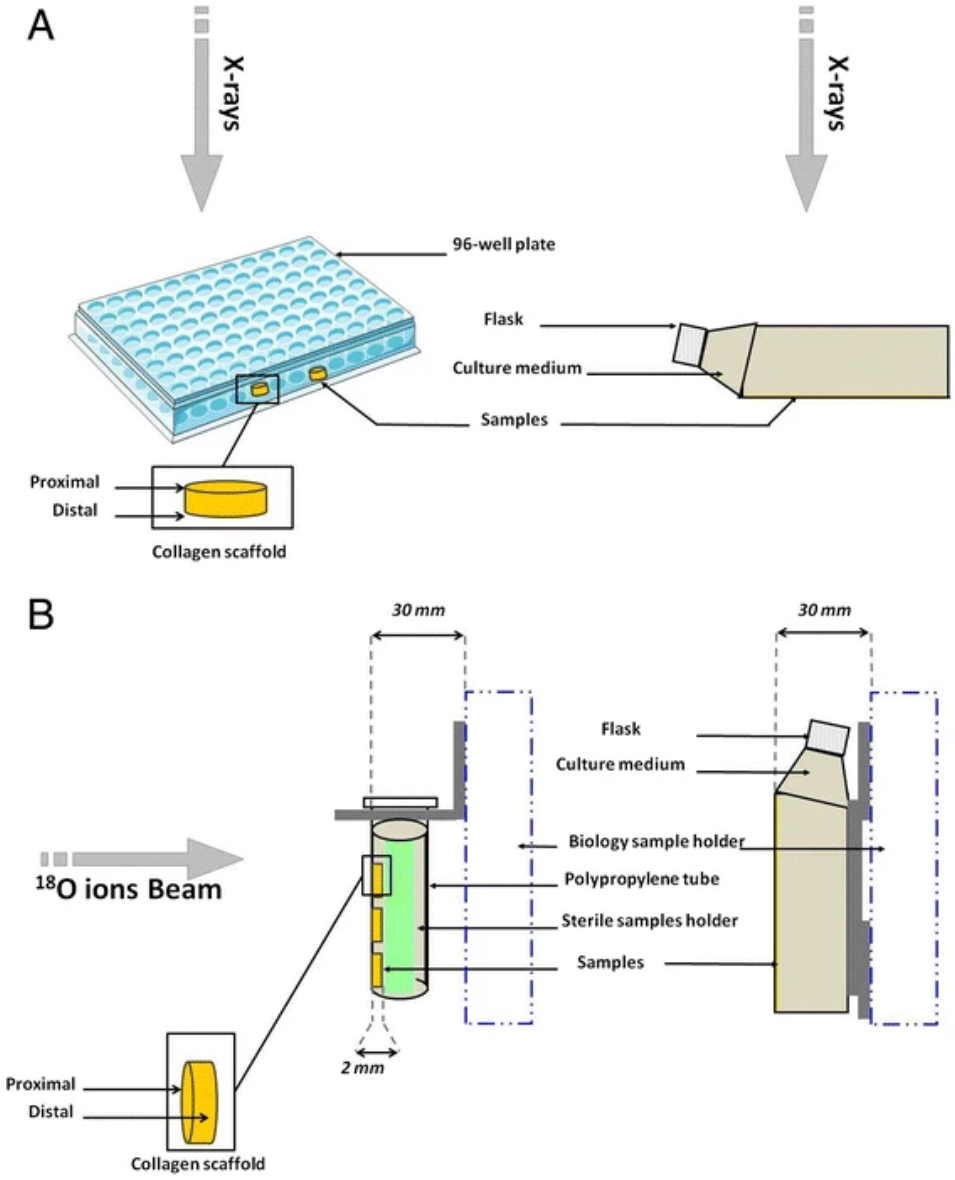

Figure 1.13: Schematic of set ups used for X-ray and CPT comparative studies. **A:** The flasks are oriented horizontally for X-ray irradiation. **B:**The flasks are oriented vertically for Oxygen-Ion irradiation. This is a typical difference between the setups for X-ray and CPT. The uniformity of particle beams is affected if there are too many intermediate surfaces[28].

Eke et al. in their study, culture four established GBM cell lines on 3D collagen scaffolds, and irradiate them with x-rays and carbon-ions, and compare the results. They specifically differentiate between the properties of migration, invasion and proliferation of the cells. Migration and invasion were studied temporally, and the proliferation studied with IF using Gamma-H2A.X and BrdU. BrdU is an antibody that is used to identify proliferating cells. While the use of Carbon-ion beams significantly decreases proliferation, Carbon-ions and X-rays both do not affect the invasiveness and migration of the cells. In conclusion of their research, they reiterate the clinical importance of CPT by stating its increased radio-biological effectiveness, and greater precision of the charged particle beam. It can therefore provide more targetted outcomes than X-rays[50].

The variation between conclusions of different studies is hence a point that must be considered during experiments and planning. It is possible that some effects maybe different when considering GBM cells with proton beams in particular,since the experiments use different ions and cell lines. Table 1.2 gives a summary of the 3D culture studies with CPT. The LET values, and nature of ions plays an important

role in the damage induced in cells. Hence it is imperative that the not only differences in methods, but also their rationale is accounted for while developing a project.

Table 1.2: Summary of Charged particle experiments conducted on 2D and 3D Cell cultures with different cell lines

Cells	Ion Beams	LET	Dose	Scaffold	Remarks	Ref
GBM cell lines	Carbon ions	120 keV/μm	2 Gy	Standard 2D cell culture	Compare DNA damage induced by X-ray and CPT	[48]
Chondro-sarcoma	Oxygen ions	103 KeV/μm	2 Gy	Collage Matrix	Comparison of DNA damage between X Rays and CPT	[28]
Lung Carcinoma	Iron Ions	307.7, 556.9, and 967.0 MeV/nucleon	0.3 Gy	Collagen matrix	Comparing effects of different energy levels	[49]
4 GBM Cell lines	Carbon Ion	Average 100 KeV/μm	2Gy	Collagen matrix	Compare migration invasion proliferation for High and Low LET	[50]

1.4. Research Gaps and Summary:

Through the courses of this literature survey, certain knowledge gaps have been identified. These gaps form the basis to the approach to the experiments. They have been summarized as follows:

1. Studies that use 3D cell cultures with charged particle therapy could be found, but none with two-photon polymerized scaffolds. The impact of the structure and its materials can provide important insights and challenges to the cellular behaviour and cellular response to CPT.
2. While there are some studies of GBM cells in 2D and 3D configurations with Charged particles (Specifically Carbon ions), no studies of GBM with Proton beams were found. Proton beams are expected to have a similar radiobiological effectiveness (RBE) to X-rays, but this information is not documented for GBM cells.
3. Although there is some evidence of GBM or other cancer cells on scaffolds made on proprietary materials of IP-Dip and IP-S by Nanoscribe GmbH there were no studies employing their new material IP-Visio. IP-Visio is specifically created for biological applications. The material exhibits almost no auto-fluoresence, and would not interfere with confocal imaging.No comprehensive information about its mechanical properties was available since it was new.

Studies have employed 2PP for GBM cell culture and drug-response testing. Other studies have used 3D structures manufactured with different methods and employed X-rays on them.There have been no studies which have employed 2PP structures that have been optimised for GBM cells and Proton-therapy simultaneously.

The aim of the project is to combine these aspects and create an efficient and reproducible bio-artefact that can be used for engineering GBM microenvironments and provide important reference for future pre-clinical proton beam treatment studies.

1.4.1. Research Questions

The gaps and the aim of the project can be condensed into the following research question:

How do 3D Engineered Glioblastoma microenvironments respond to Proton beam Irradiation?

Sub-questions:

1. Is replicating features of the vasculature effective for GBM?

2. What differences in proton beam radiation response of GBM can be seen between 2D monolayers and 3D scaffold cultures?

3. Do 3D scaffolds affect the efficacy of Proton beam irradiation on the GBM culture?

1.5. Approach to Experiment

From previous studies, the difference between cellular response in 2D and 3D environments is evident. This project will include: the design and fabrication of the structures, culturing the GBM cells, proton beam irradiation and validation of the samples by evaluating the response to this irradiation. These form the four main aspects of the project that have been detailed below.

1. **Scaffold Fabrication and Design:** The designs for the scaffold are inspired by the structure of the blood-vessels in the brain. The vascular branching sites provide notches in which the cells adhere. There is also differences in the angles, and multiple branches at the same point. The aim is to replicate these notches, and to include some variations in their angles. The design that was chosen for this is to utilise the slope of pyramidal structures to provide that variation in length, and to add lateral beams to increase the number of sites for cell adhesion. The apex conical or pyramidal structure could replicate the increasing distance between two vessels diverging from such a node.

   As per the information gathered from the literature–summarised in Table 1.1– the scaffolds should have features comparable to the sizes of the cells cultured. GBM cells vary in size from about 20-50 μm on flat pedestals or glass, and these dimensions are incorporated in the design. The 2D and 3D samples would be printed on the same substrate, to study cells on both environments simultaneously.

   Of the methods described 2PP can realise the design in terms of dimensions and fabrication throughput. IP-Visio is non-toxic and has low autofluorescence is therefore the final selected material. 2PP is able to provide the highest resolution and control on the design to create reproducible scaffolds. In 2PP scaffolds the extent of polymerization offers the possibility to control material stiffness, and to have that as a design parameter, which can be tougher with other methods.

2. **Cell culture**: The initial plan during the literature survey included studying multiple GBM cell lines in this project but realistically beginning with one cell line and validating the results was more practical option. The earlier considered cell lines included U87, U251, T98G and U118. The finally selected cell line is U251. U251 is a routinely used GBM cell line with a large body of research. It is a cell line that was also readily available at the laboratory at LUMC. The reasons for choosing U251 have been detailed in section 2.2.1

3. **Sample Irradiation**: Ideally, a range of doses in the proton beam experiment could validate trends of the antibodies that would be studied, but a larger range would imply a vastly greater number of samples and subsequent handling issues. Since the model itself was not yet validated, the justification for a study with a range of doses was not that high. Therefore a selection is made based on literature sources. The two doses selected for the experiments were 2 Gy and 8 Gy. These doses form the boundaries of minimum and maximum dose values that are used with the existing *in-vitro* experiments [48, 51]. The expectation was that the U251 cells would show a difference in response to these doses.

4. **Evaluation Methods**: The methods to evaluate the samples were narrowed down to immunofluorescence and Scanning Electron Microscopy. Immunofluorescence is a strong tool to use for these experiments. It has the advantage that the 3D and 2D environments could be studied separately, even when cultured together. Scanning Electron Microscopy allowed to study the morphology of the cells with respect to the scaffolds, and has a very high resolution of imaging. Methods such as Western Blotting and qPCR involve the removal of cells from the substrate for their analysis. In such a situation it would not be possible to individually assess the difference in characteristics of cells between 2D and 3D environments.

   Additionally, a viability assay was decided to be employed to validate the general effect of irradi-

ation on the samples, and confirm the expected outcomes of cell survival rates when irradiated with proton beams.

The research conducted included all four aspects, and many selections were made in the methods during the course of the project. The decisions and the rationale behind them have been detailed in section 2.

1.6. Planning and Risk Mitigation:

The project was carried out with a collaboration of 3 organisations. TU Delft, Leiden University Medical Center (LUMC), and Holland Proton Therapy Centre (HPTC). The project is financially supported by the TU Delft Health Initiative. The design, fabrication and mechanical characterization and SEM imaging of the scaffolds was carried out TU Delft. Cell Culture, IF staining, confocal microscopy and viability assays were done at LUMC, and the irradiation of the samples was done at HPTC.

The research plan for the project is shown in figure 1.14. This is the plan that was updated during the midterm review (April 2021), and varies from the initial one. The plan included alternate timelines to account for delays in the project. It was planned to conduct the beam-line experiments a total of 5 times, but due to COVID restrictions and delays is could be done successfully 4 times.

1.6.1. Challenges and Alternatives

1. **Scaffold structure:** There were concerns with the stability of 3D micro cage-like structures made with 2PP, raised by other colleagues working on it. A solution has been employed in terms of using a coating of a materials such as Ormoprime, for better adhesion of the material to the substrate.
2. **Cellular adhesion:** Since the IP-Visio is a new material, there might be issues with cell-adhesion, and the scaffolds may require coatings with bioactive materials such as Matrigel, laminin and fibronectin. But this can be easily tested with a simplified 2D structure made of IP-Visio and checked for cell adhesion. The preliminary tests at LUMC should suffice for this estimate.
3. **Design:** There is a rationale for the designs created, but it possible that the design could fail at the manufacturing or cell culture stage. Large aspect ratios in the design could lead to sagging of the beams. To overcome this the structure may need extra supports. These supports are not intended to be sacrificial, but integrated to foster cell colonization. It is also possible to increase the diameters of larger beams, such that they have a higher stiffness. These strategies can be applied to improve the structure iteratively.
4. **HPTC set-up:** Proton beam irradiation is carried out such that the beam is horizontal with respect to the ground. The position of the beam cannot be changed to vertically irradiate the samples. This therefore poses a challenge as the cell cultures and scaffolds are usually carried out on substrates that are flat and horizontal. The orientation of beam and the samples is discussed further in section 2. In usual cultures such as in the study by Hamdi et al, the scaffolds are sealed in multi-well plates or petri-dishes, and oriented vertically (see figure 2.9) to be irradiated by the proton beam. To overcome this, a specific holder will be created to suspend the cultures horizontally in the beam. Preliminary trials were conducted to test out the set up.
5. **Imaging:** It may not be possible to make a full 3D reconstruction of the scaffolds before and after irradiation. The presence of the material and cells could cause shadowing in the structure. Estimate may have to be made about the structure depending on the images that can be formed.
6. **COVID-19:** The pandemic is a rapidly evolving situation and its existence a general truth. The planning must consider this, and provide a certain degree of flexibility.

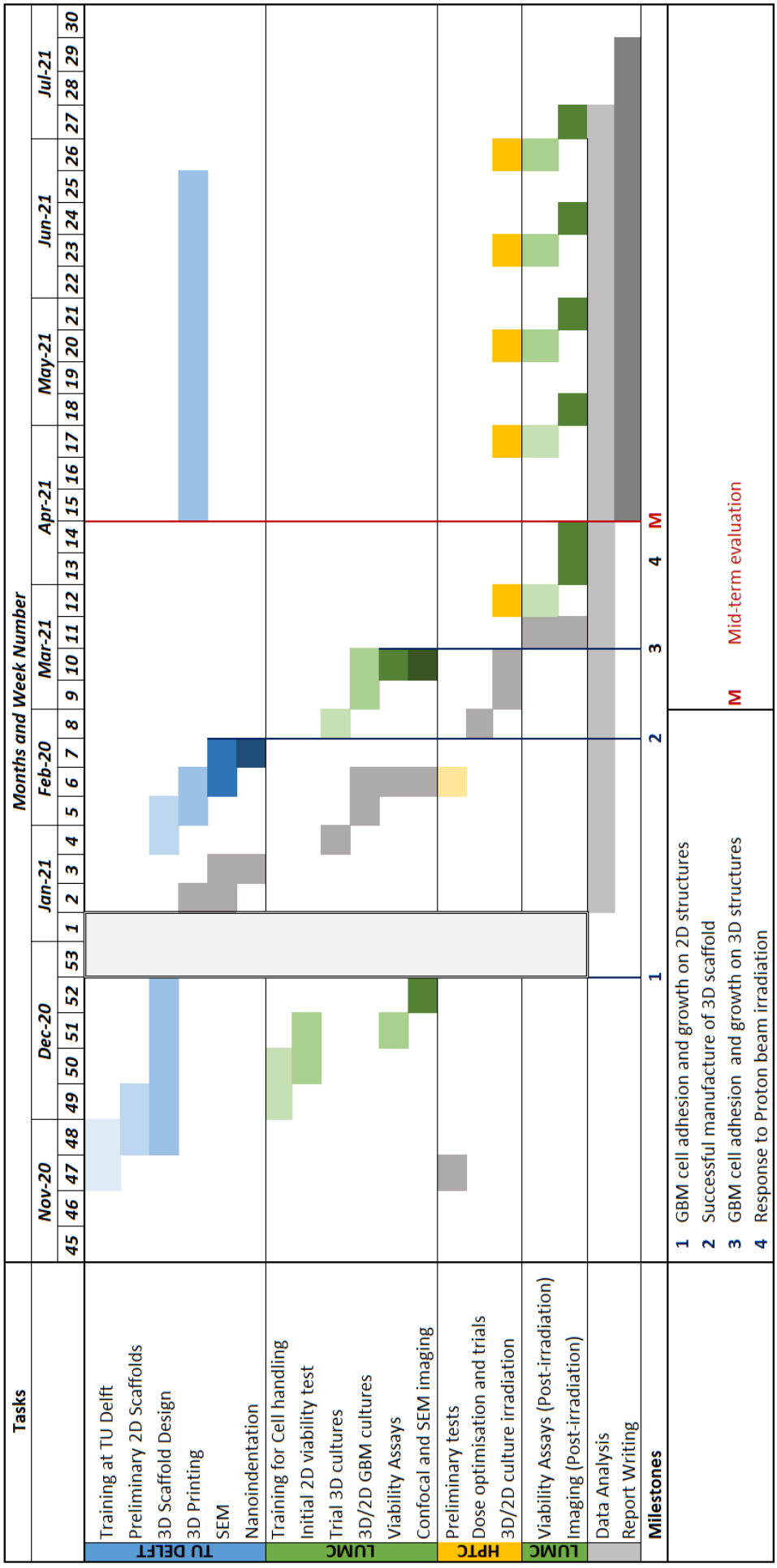

Figure 1.14: Gantt Chart for Research time plan

2

Experimental Methods

2.1. 3D Scaffold Fabrication with 2PP

Two Photon Polymerization was selected as the method for the fabrication of the cell culture scaffolds. 2PP provides a few advantages over the other methods discussed in the section 1.3. The advantages of using 2PP with IP-Visio can be summarised as follows

1. Higher resolution (Upto 0.6 μm when used with the 25x objective)
2. High reproducibility and reliability
3. Robust structures
4. Rapid fabrication Rates.
5. No cytoxicity in polymerized scaffolds
6. Low autofluorescence of IP-Visio

These factors, and the availability of the know-how for the *Photonic Professional GT2* printer by Nanoscribe GmbH at TU Delft, made it possible to pursue 2PP as a viable solution for the scaffold printing. The process of fabricating with 2PP undergoes a few steps after the training of the user to handle the device itself. The monomer resins are polymerized by the use of laser energy deposition. The resin is made of a methacrylate monomer and a photoinitiator that triggers the polymerization chain reaction in the presence of light. The general 2PP work-flow is shown in figure 2.1. A detailed protocol of the process that was used for this project is attached in appendix-D Two types of structures are printed

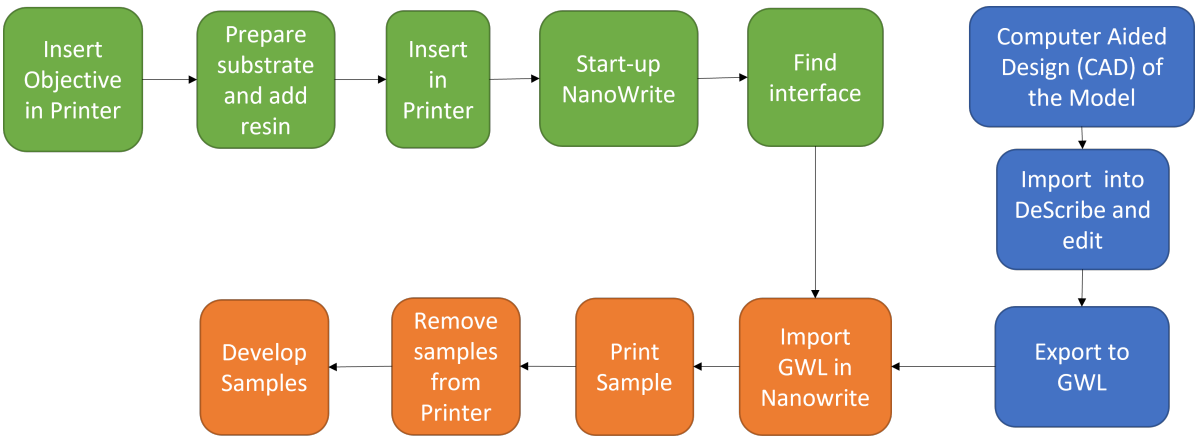

Figure 2.1: A chart of the general 2PP workflow. The CAD model is usually created on a separate software and brought to the DeScribe environment. DeScribe and Nanowrite are the software that are used to interact with the printer and give it commands.

on the samples. The 2D pedestals, and the 3D scaffolds. Both these structures were first modelled in a 3D CAD software (Autodesk Fusion 360) and then exported as .stl file. Fusion360 proved to be a

very easy and handy tool to model the 3D structures. These .stl files were then imported in DeScribe for printing. DeScribe is the modelling interface that is used with Nanoscribe to generate a code that directs the manufacturing process. The final code for the manufacture of the samples is attached in appendix-E. This code is then imported in another software called NanoWrite, which is used to give instructions to the device itself and carry out the print jobs.

2.1.1. Materials and Objective Lens:

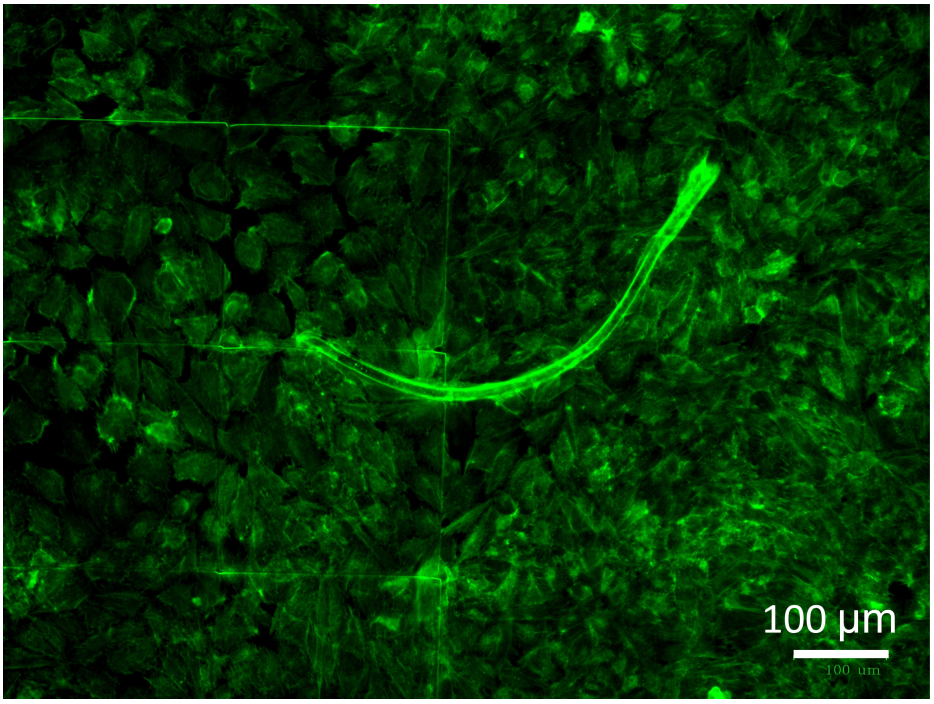

Figure 2.2: The image shows 2PP pedestals printed with IP-Visio. The structure does not interfere with the fluorescent image of the cells. The cells culture on the pedestal and show that it is not cytotoxic.

IP-Visio displays very low fluorescence and is non-cytotoxic. It is biocompatible and is suitable for cell studies in 3D and microscopy applications. Figure2.2 shows these properties. Structures with volumes of several cubic millimeters can be realized. IP-Visio is a proprietary material, and its recipe is protected. It is known that the material's functional group is *methacrylate*, which is responsible for its polymerization when exposed to light.

In this project, the objective lens of 25x (Numerical Aperture =0.8) was used to focus the laser into a voxel. The recipe available from Nanoscribe was optimised for this lens. The selection of the objective also depends on the resolution required by the design. 25x provides theoretical lateral resolutions down to 595nm, and axial resolution down to 3.3 μm when used with another material (IP-S), and a 780 nm laser. Figure2.3a shows an image of the lens used. The objective is also compatible with IP-Visio, and similar resolution range could be expected.This forms a medium feature-size set. The size that can provided by this objective is appropriate for these structures that have a minimum dimension of 7μm and a higher resolution objective of 63x would not be needed.

Slicing value refers to the axial distance between two layers of the structure, and hatching value is the lateral distance between two voxels. Typical slicing and hatching values are about 1 μm and 0.5 μm respectively for the 3D Medium features set. The combination of IP-Visio and 25X is used in the DiLL (Dip-in Laser Lithography) configuration. A schematic of the configuration and the image of the objective is shown in 2.3b.In it, the lens is dipped in the resin where it finds the interface with the glass, and prints the sample within the resin volume. The 25x objective provides a maximum print field of about 400 μm in diameter.The maximum working distance for 25x objective is 380μm. A sample of maximum this size can be printed by finding the interface at once. For designs that are larger than this size, the stitching conditions may have to be used with this objective.

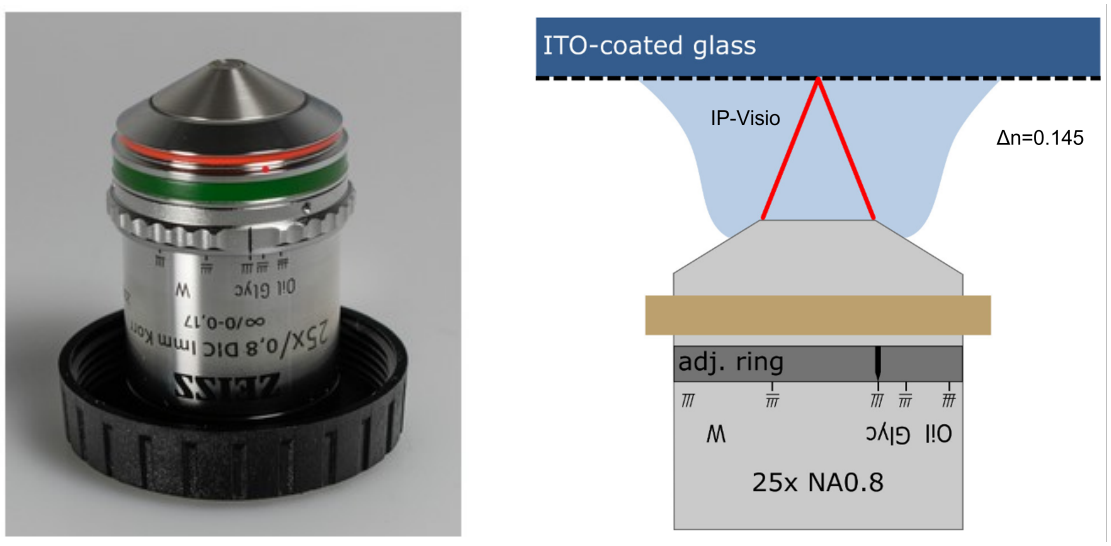

Figure 2.3: A: 25x Objective Lens; **B:** Schematic of the DiLL configuration with the 25X Objective, and a refractive index difference of 0.145.*The image is an edited version of the schematic from the Nanoguide*

The substrates are coated with 3-(trimethoxysilyl)propyl methacrylate (MAPTMS) before printing. This process is called silanization, and is also recommended by Nanoscribe to improve adhesion of samples on the substrate.

2.1.2. Dose Testing and Selection:

Dose is the amount of energy deposited by the laser in the 2PP voxel. This deposited energy determines the extent of polymerization that the material in the voxel region undergoes. The variation of the energy is controlled by two factors: Laser Power (LP) and Scanning Speed(SS). Dose testing is the process of finding the optimum of these two parameters for the given design, objective lens, resin and substrate combination. The dose is usually unique for a combination. If the design is very sensitive, a small change in the dose may also affect the print. A parameter sweep is done with varying these factors, and the dose is chosen for the clearest and sharpest print formed.

Laser Power: The degree of polymerization increases with the increase in laser power, since the dose increases with the Laser power

Scanning Speed: The degree of polymerization. decreases with an increasing scanning speed. The dose decreases with a faster scanning speed as lower energy is deposited per unit volume.

The variation of the dose and laser Power is depicted is the figure 2.4 .The optimum dose varies according to structures designs and the resolutions being used. The reasons for this variation is the geometry of the structure itself and how much the dose in the immediate region outside the voxel affects the material. For example, a thin structure would deposit a lesser dose in the monomer material surrounding it, while a thicker structure would probably require more passes to complete the print and deposit a higher dose.

The minimum dose required to begin polymerization is called the polymerization threshold. The dose must be at least greater than that to have a print. If the dose is lower than that, the monomer will remain as is. Very high values of the dose, it can cause the formation of bubbles due to overheating of the resin and can lead to damaged structures. Since the bubbles can also move in the resin, it is possible that may affect other structures in print too. The figure 2.4 indicates the trends between Laser Power, degree of polymerization and scanning speed.

For practical purposes, the laser power is indicated in a range of 0-100% of the total power of the machine. The power of the laser can decrease overtime, and using percentages keeps it easier for protocols. In using the medium features set, the structures are relatively large, and the variation of the

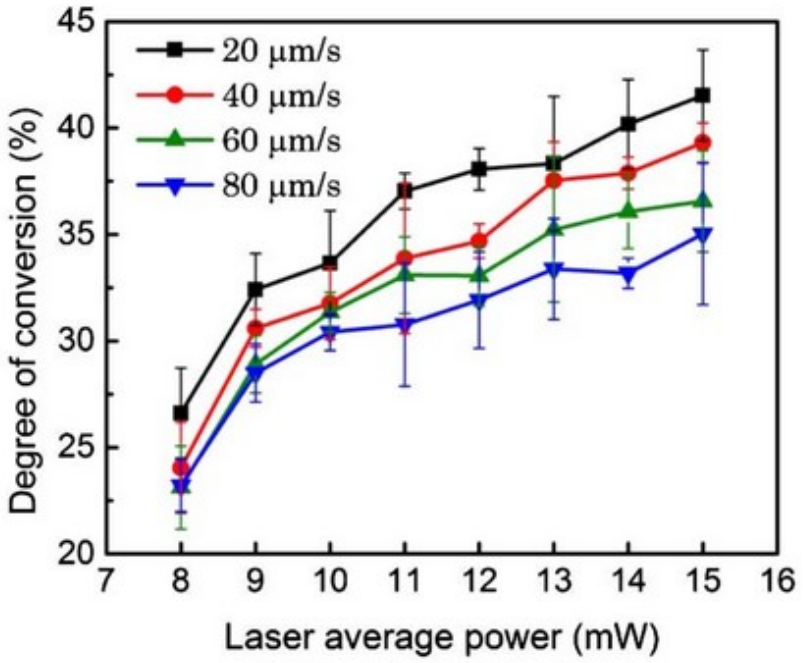

Figure 2.4: The percentage of conversion increases with the increase in laser power, but decreases with increase in scan speed. The optimum of these values must be found [52].

power was not enough to affect the print too much. It maybe a factor to consider in more sensitive structures, as this change can affect the actual energy being deposited in the voxel. This is also a practical reason to not use dose values very close to the polymerization threshold. The doses were selected based on the design and by carrying out a parameter sweep. The values that are determined for the 2D and 3D designs are detailed in section 3.1

2.1.3. Sample Development

After printing, the samples are removed from the printer, and developed in Propylene glycol monomethyl ether acetate (PGMEA). PGMEA, dissolves all the unpolymerized monomer around the sample, and only leave the polymerized material behind. The samples are then cleaned with iso-propyl alcohol (IPA) and allowed to air dry.

Using an air-gun to dry the samples can damage the delicate structures, and IPA evaporates quite easily at room temperature. This process may also require optimization and change in the protocol as this is a point where the samples can detatch from the substrate. In some cases another solution called Novec™7100, maybe additionally used. This solution evaporates faster than IPA, and therefore causes fewer deformations during evaporation. The standard protocol that was suggested by Nanoscribe only uses PGMEA and IPA, and that was sufficient for the designs in this project. The dried samples could be taken to cell culture. The protocol used is detailed in appendix-D

2.2. Cell Culture:

In-vitro methods involve the use of cells in controlled environments to study individual effects of factors. The experiments are organised to create reproducible methods, with minimum variation. The use of controls helps to establish causation in these experiments. GBM tumours have a complex heterogenity with a myriad of cellular mechanisms that are associated with these disease. Cell lines form an important tool to study these mechanisms, and to establish GBM behaviour on a molecular and genetic level. Cell lines may not entirely encapsulate the complexity of *in-vivo* tumours, but make an excellent starting point for further research.

2.2.1. U251 Cell Line

In this project, the GBM cell line U251 is used. The choice of using a cell line is justified since many aspects of the project are novel. The material, the design, the printing method utilised for GBM studies, and the combination of these with Proton beam irradiation. Establishing the validity of the model with cell lines is an important step in novel biological research before using the rarer and more expensive Primary cells. Primary cells also require more experience to handle.

U251 is a cell line that was established over 40 years ago in Sweden. It was extracted from a male patient who suffered from a malignant astrocytoma[53]. The cell line has been used extensively in research, and the large body of data makes it possible to characterize and study. This is also a cell line that is extracted from a *de novo* human brain tumor, and has an advantage over cell lines extracted from a clinical progression [54]. A *De Novo* tumor implies the first occurrence of that cancer in the body, while a clinical progression would imply secondary tumors arising from the mutated cells of an earlier tumour. This makes the characteristics of the U251 cell line closer to those of human brain tumor when compared to cell lines that are not of such origin. This, along with the team at LUMC using U251 as a part of a larger project make the choice of U251 for this study practical and mutually beneficial to both groups.

2.2.2. Selection of Culture Dishes:

Normal passage of cells can be carried out in various types of flasks, plates and dishes depending on their purpose. In this project a 60mm diameter petri dish is used. 5 ml of cell culture medium is sufficient in the dish to completely cover the slides, and provide enough cell medium for the cells to grow for the stipulated period of time. The cell medium used here is Dulbecco's Modified Eagle Medium (DMEM), with 10% Fetal Bovine Serum (FBS), 1%L-Glutamine (L-Glu) and 1%Pencillin-Streptomycin (Pen-strep). This composition of the medium is the standard that is used with this cell line. The dish adequately fits the glass slides on which the scaffolds were fabricated, without requiring any cutting or adjustment to fit it better. These dishes are also routinely used in cell culture and can be made of sterile plastic that does not allow contamination to settle in the material of the dish itself. Additionally, these dishes are 15mm in thickness, which would easily fit within the 25mm SOBP available at HollandPTC, and could be conveniently irradiated too.

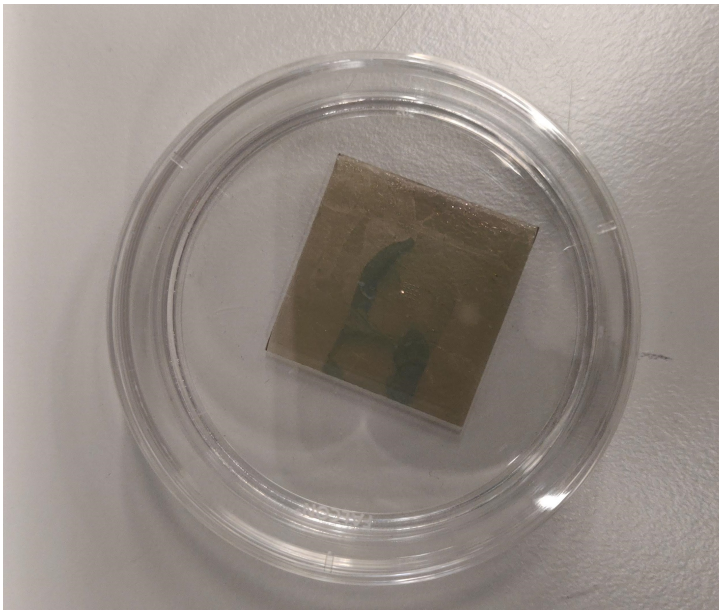

Figure 2.5: 60mm diameter petri dish with a representative sample

The other consideration was a 6-well plate, but that would require cutting the slides, an additional step that could lead to more damaged samples, and was not compatible with the microscopes used for the imaging of the samples. The 6-well plate would also cause mixing of media from different wells during irradiation or transport. The petri-dishes provided the cheapest, and most practical alternative for cell

culture.

2.2.3. Optimisation of Cell densities:

Carrying out the cell culture of the U251 Cells on the scaffolds involved preparation of the samples. Briefly, the fabricated structures were transferred to sterile petri dishes in a sterile environment. The glass slide with the scaffold were then immersed in 70% Ethanol rinsed with Phosphate Buffer Solution (PBS), and dried at room temperature. The cells were then cultured in these sterilised plates. A detailed protocol of cell culture is attached in appendix-A

Earlier in the process a very low density of cells of about 50,000 cells/ml was tested. This showed a very low density of cells on the samples, and did not colonise the scaffolds effectively. It was understood that a higher density of seeded cells at about 100,000 cells/ ml would be needed for effective colonisation of the structures.

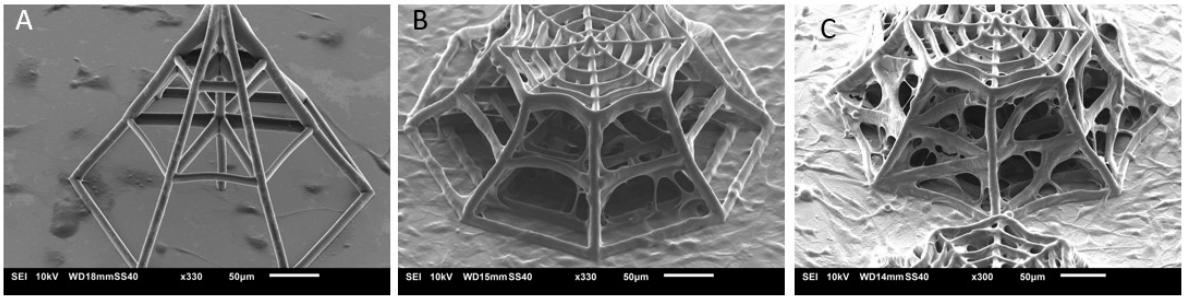

Figure 2.6: Optimization of cell densities. **A:** very few cells in the structure of the first hexagonal design with 50,000 cell/ml. **B:** Octagonal pyramid with with 100,000 cells/ml; **C:** Octagonal pyramid with side beams showing a greater colonisation of the structures with the same density of 100,000 cells/ml

Nonetheless during the design the densities went through some changes. Also when compared to the original tests, the duration of the cell culture period had to be increased from 3 days to 5 days, because of practical reasons of working in the lab. The final optimum was to use 50,000 cells per ml per scaffold. These densities would otherwise require a very large number of cells, as every experiment needed approximately, 12-18 separate petri dishes, with each dish further requiring 5ml of medium at these densities. The SEM images of the tests, with changing designs are shown in figure2.6

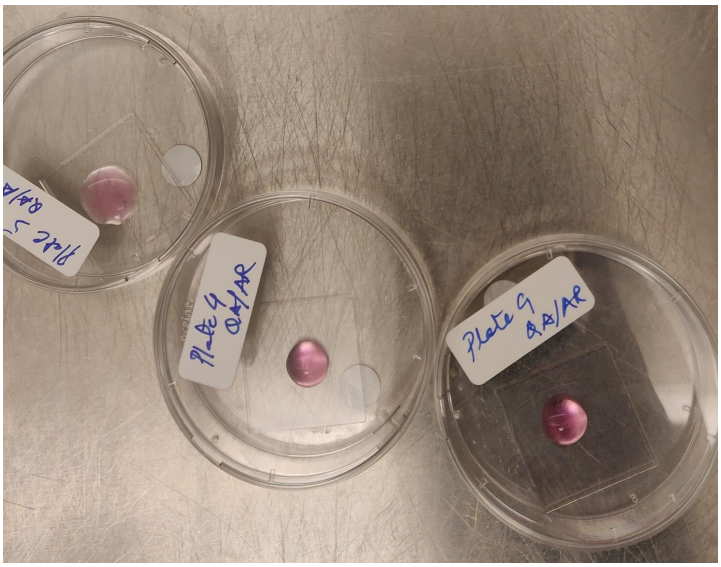

Figure 2.7: Final method of cell culture with a seeding density of 50,000 cells/ml in each droplet of 75 μL, in 60mm diameter petri dishes. These samples were left in the incubator for 1 hour, and then additional medium was added to the dishes.The droplets are the regions where the scaffodls are present.

The direct use of 5 ml of cell suspension per dish was leading to the cells not adhering to the 3D scaffolds and settling at the base of the glass slide. The solution to this problem, was the use of a small 75uL droplet of the cell suspension on the scaffold. Figure 2.7 shows the samples after seeding the cells, and before adding the extra medium. This reduced the number of cells required per experiment and improved the throughput of the experiment. On average the droplets of 8mm diameter were formed which was sufficient to cover the region of the slides where the scaffolds were present. There was also an attempt to use 2-well silicon inserts manufactured by Ibidi®, but those inserts could not be placed with ease on the glass surface and would damage the printed scaffolds.

Additionally, the high hydrophobicity of the glass slides ensured the intactness of the droplets, and did not allow it to spread too far in the dish. The cells were allowed to settle within this droplet region for an hour in an incubator at 37°C and 5% CO_2, after which 5 ml of fresh medium is added. This method significantly improved the adhesion of cells to the scaffolds, and lead to a better colonisation of the structures by the U251 cells. The cells are then cultured for 5 days before the irradiation experiment.

2.3. Proton-Beam Experiment:

The Proton beam experiments were carried out at Holland Proton Therapy Centre at Delft.HPTC has a cyclotron which is used to generate the Proton beams. There are 3 gantries through which the beam can be accessed. One of these gantries is dedicated for research purposes, and this is where the radiation experiments are carried out.

Table 2.1: Summary of the Proton experiment plan.

Experiment No.	Doses	No. of Samples
1	0, 2Gy	14
2	0,2 and 8 Gy	18
3	0,2 and 8 Gy	12
4	0,2 and 8 Gy	21

2.3.1. Dose Selections:

A dose is defined as the amount of energy transferred to the sample when irradiated with a Proton beam. Correlating with existing literature, the initial plan for this experiment was to irradiate the samples with a range of doses. 2,4,6,8 Gy being the most common one along with the control. The aim is to study the response of the cells with respect to different doses. With practical considerations, it was most efficient to study these samples with two doses and (2 and 8 Gy) and a control. A lower and a higher dose would sufficiently indicate the difference in response.Earlier studies conducted show a clear response between samples 2 Gy and 8 Gy [51]. These quantities of doses are also sufficient considering the small volume of the samples.

An earlier test was conducted in March 2021, with only 0 and 2 Gy, to test the validity of the experiments, and then the experiment with 0,2, and 8 Gy was performed 3 times during different available dates between May and June 2021. Table2.1 shows a short summary of the experimental plan.

2.3.2. Set-up

Proton beams are charged particle beams. The beam interacts with every material and surface in its path. The use of a petri dish in its conventional orientation would present many interfaces. The design of a petri dish would create additional plastic and air interfaces, at a varying cross section too, which would disrupt the beams uniformity and would require a larger Spread out Bragg peak. Figure 2.8 shows the 3D printed inserts that were used to keep the samples in the centre. The insert was made out of two halves which held the glass slide in between them, and then fixed with screws to make sure there was no movement. The inserts are about 60mm in diamater such that they fit well inside the plate, and the square gaps in the middle are 25mm by 25mm for minimum interference with the plate.All the parts were sterilised before introduction in the dish, as they would interact directly with the cell medium. The samples were held vertically with holders in the X-Y plane as shown in figure2.9. (Note: The planes are defined by the axes which are parallel to the plane. Hence the X-Y plane is the plane which is formed by the X axis and Y axis shown in figure2.9)

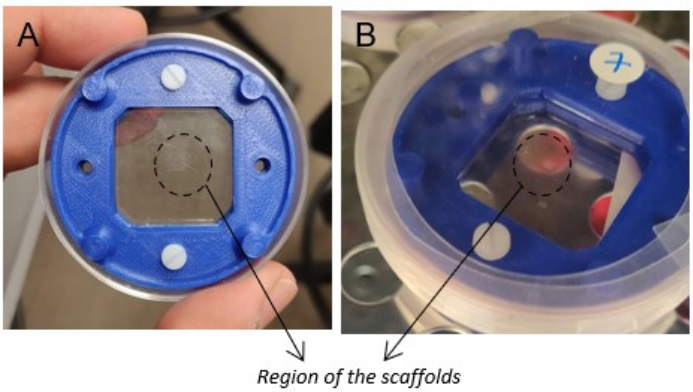

Figure 2.8: The insert used to keep the samples in place. A: Insert with two white screws, B:Insert inside the dish, with the dish sealed with parafilm to ensure no leakage of medium when it is positioned vertically

The set up used for the beam line experiments in shown in the figure2.9. With respect to the beam line, the direction of X, Y and Z axes are marked in the image on the left. The phantom is the object that is used to control the dept of the Spread out Bragg peak along Z-axis to ensure that the maximum dose is being deposited at the target of the sample. This phantom is calibrated such that it is equivalent to the same thickness of a water column ahead of the sample. Its referred to as a water-equivalent depth, and is routinely in radiobiological studies. The phantom in these experiments is made of a material called RW3 (Goettingen White Water) manufactured by PTW GmbH.The phantom absorbs a portion of the radiation to 'advance the SOBP to the posiiton required.

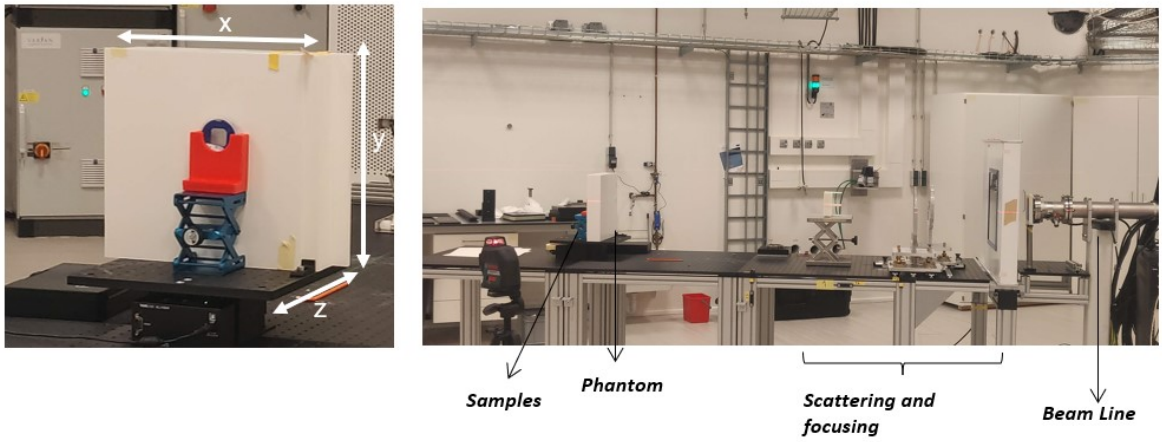

Figure 2.9: Right: Beam line set up, **Left:** Samples in petri dishes with the insert held in the X-Y Plane with a red 3D printed holder

The current set up has the capacity of a uniform dose deposition for a depth of 25mm i.e. the width of the Spread out Bragg Peak. The profile of the beam along the Z axis is shown in figure 2.10. The beam can be adjusted using the phantom to ensure that the Bragg peak occurs right at the petri dish. Using the dish in a vertical orientation was the solution that offered minimum interference. Within this 25mm, the Proton beam has a dose deposition uniformity of about 98%, which is very accurate. Figure 2.11 shows the cross section of the beam and shows the dose conformity in the Y-Z and X-Z planes respectively. Th energy of the beam used for these experiments is 796 nA with a dose rate of 1.61 Gy/minute. Irradiating 2 Gy would take about 1min and 12 seconds, and 8 Gy about 5 minutes of time.

The holders that hold the pertri dish vertically had two iterations of the design. The first used a 3D printed structure which was moved and adjusted manually, the second was an automated flipper design which could be moved with a lot more ease. The designs are shown in figure 2.12.

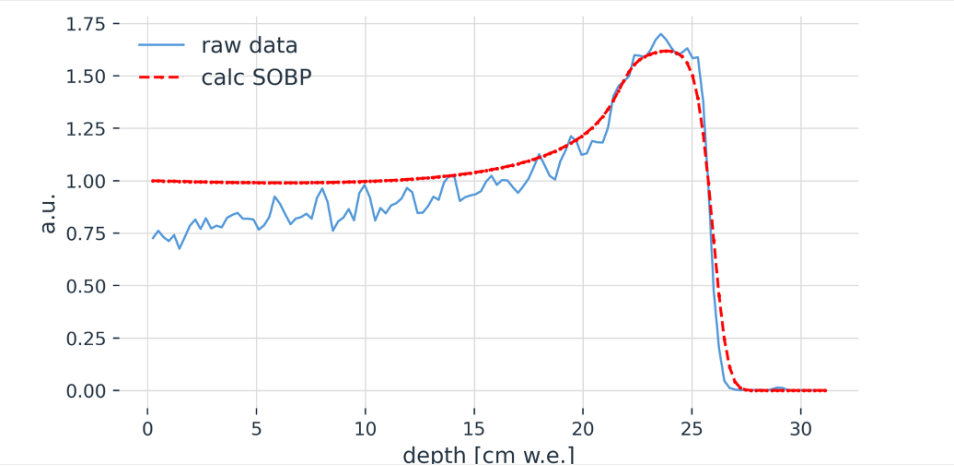

Figure 2.10: The Bragg curve from the data extracted from one of the beam line experiments, and the dose distribution profile along the Z-axis. *The image is the courtesy of M.Rovituso at HollandPTC*

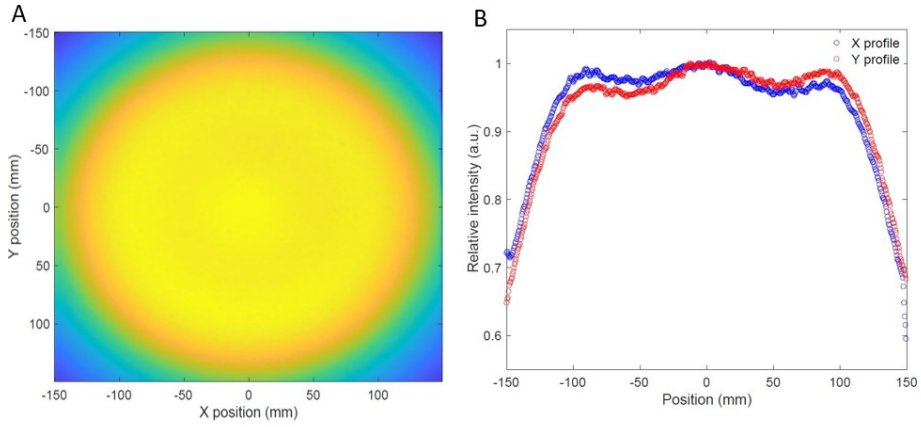

Figure 2.11: A: The yellow region shows the irradiated section of the sample when viewed in the X-Y plane. A square region of 100 mm by 100 mm in the centre of the circular region would be the region of interest with a unfiorm ose distribution. **B:** Shows the distribution of the profile in X-Z(Blue) and Y-Z (Red) planes. A uniformity of almost 98%, which is very accurate. *The image is the courtesy of M.Rovituso at HollandPTC*

All samples, including the control were sealed at the same time, to reduce variations in the stresses that would be introduced on the cells. After irradiation, the samples are allowed to decay to safe radiation levels before they could be handled, fixed and transported.

Transport: Live cells were sealed transported by car to and from HollandPTC. Cells would be outside the incubator for about an hour, brought a day in advance so that they could settle back down in the incubator, before they were irradiated on the following day. After decay, the cells were fixed at HollandPTC and transported back on the same evening to LUMC. Time-sensitive tests were conducted immediately, and the rest of the samples were stored until later days.

2.4. Immunofluorescence

Immunofluorescence (IF) is a method of cellular evaluation, in which antibodies are used to bind to specific sites or proteins in fixed or live cells. The principle of IF is described in section1.2.5. The antibodies can be visualised with a confocal or fluorescene microscope. A confocal microscope takes immunofluorescent images through a very thin cross section, and therefore can be used to visualise the cells layer by layer. In this project, the excitation, emission and capture of the images is done with the Zeiss LSM 710 confocal microscope. The images are captured on a computer using the Zen

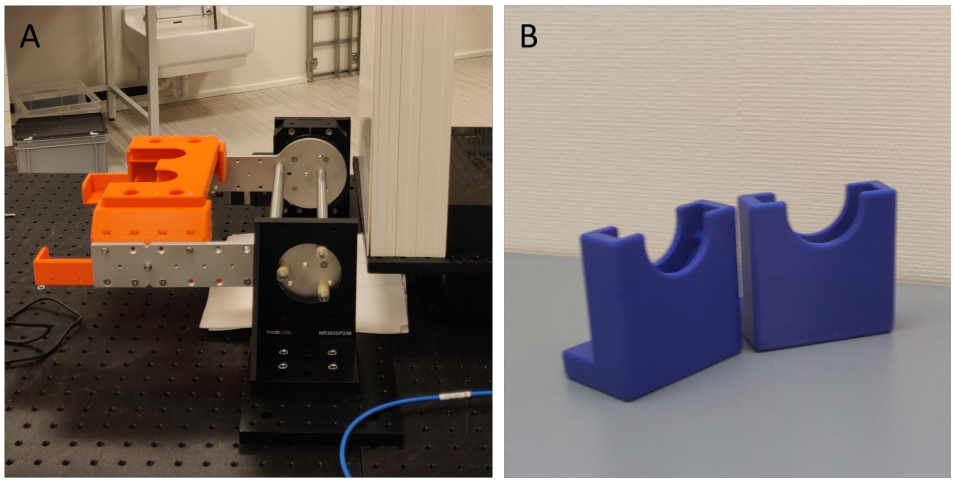

Figure 2.12: **A:**Automated flipper design that could be moved from outside the bunker where the irradiation is carried out. **B:**The earlier design of the holders Holders for manual adjustment of petri dishes

application (By Zeiss).

A variety of these microscopes are available, but the one used for this experiment is an upright microscope in which the lens in dipped in the solution in the petri dish, and then focused on the cross section of interest. IF is used for this experiment, as any of the other usually employed methods (Western blotting or qPCR) involve the removal of the cells from the substrate and after that it would not be possible to differentiate between 2D and 3D cells. Immunofluorescence is an image-based evaluation method, and the response of the antibodies can be seen, and compared between 2D and 3D environments. Different quantitative and qualitative techniques are used to evaluate the images that are formed. These techniques varied for the different antibodies used and have been discussed below:

2.4.1. DNA DSB antibody

Gamma H2A.X is the histone that is phosphorylated in the nucleus of the cell when the DNA undergoes double strand breakage(DSB). This damage is not exclusive to irradiation, but with the use of a control sample, the results of the proton beam damage can be evaluated. Gamma H2AX is a specific form of the H2A histone synthesized by the cells on the Ser-139, serine in the position 139 of DNA when the cell undergoes this double strand breakage[8]. There are various mechanisms by which the DNA can undergo damage. This particular one is studied and used because the antibody used for its detection, with the use of fluorescent markers, can form very distinct foci, which can be counted and used as a quantitative method of DNA damage analysis[55].

For the counting of these foci, imageJ was used.The Anti-Gamma-H2A.X antibody(ab81299, Abcam, UK) is used with the fluorophore FITC (Fluorescein isothiocyanate,A11008, Molecular Probes) as as a secondary antibody. It forms fluorescent green foci, and is counterstained with Hoechst33258 (Molecular Probes Inc, USA) that stains the nuclei blue. It allows to identify the region of the nuclei within which the foci form. The spectra of these fluorophores is shown in image2.14 Since both these stains do not interfere with each other, they can be easily used together. Using a macro, a binary image is generated of the Nuclei with certain thresholding settings. The same settings are used for every image sample. The macro then counts the bright spots formed in the image of the foci, by identifying bright pixels as maxima, only within the marked nuclear regions from the image of the other channel. This method ensures that no non-specific staining, or other artefacts or bright spots do not become included in the foci counting. The details of the macro and the counter are attached in appendix-B

2.4.2. Morphological Staining

Phalloidin (P5282, Merck Life Science, NL) stains the actin filaments in the cells, and counter stained with Hoechst. Phlloidin is a bicyclic peptide used to selectively stain F-Actin filaments in cells. Phalloidin used was already conjugated with the fluorophore FITC, and used direct IF for staining This staining

made it possible to visualise the morphology of the cells in 2D and 3D. The actin filaments are present throughout the cell, and form a part of the cell cytoskeletal structure and is therefore an indicator of the morphology and organisation of the intracellular environment.

The images that were formed with Hoechst-Phalloidin Staining were used for qualitative separation and identification of the cells and their structures. The confocal images from these samples were also used for the 3D reconstructions of the cells in 2D and 3D, and become a valuable tool for identifying nuclear organisation of the cells in these configurations.

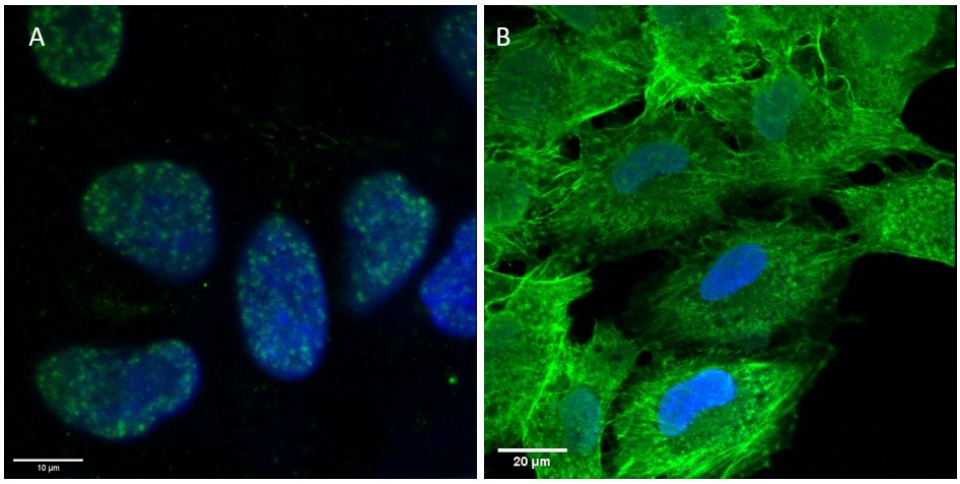

Figure 2.13: Images of U251 cells stained with FITC(Green) and Hoecsht(Blue) Fluorophores. **A:** An image of the DNA damage foci formed within the nucleus of the U251 cell, after 8Gy irradiation dose stained with the Gamma-H2A.X primary antibody.**B:** The Phalloidin antibody staining the actin filaments in the cytoplasm of the U251 cell

2.4.3. Live/Dead Immunofluorescence Assay

The Live dead IF assay was carried out using a combination of dyes. DRAQ7(ab109202,Abcam,UK), Calcein AM(C3099, ThermoFisher) and Hoechst. The three dyes have different excitation and emission bands and provide a good combination to work in for imaging.

1. DRAQ7 is a membrane impermeable dye that only stains double strand DNA of dead or permeabilised cells. Therefore the nuclei of such cells appears red in the confocal microscope when excited with a red laser. The maxima of the excitation and emission spectra are 647nm and 697 nm respectively
2. Hoechst stains all nuclei Blue (Live and Dead). The maxima of the excitation and emission spectra are 361nm and 497 nm respectively
3. Calcein AM only stains the live Cells in Green. Calcein AM is a cell permanent fluorescent probe that indicates cellular health. The maxima of the excitation and emission spectra are 495nm and 515nm respectively. Calcein AM has a similar excitation as FITC.

These spectra can be seen in image 2.14. These stains are used with direct IF as they are all fluorescent by nature. Unlike the other samples this test is carried out on an unfixed samples. The samples are stained with the dyes, incubated for 30 minutes and then imaged directly with the confocal microscope. The staining and imaging of this assay is carried out at about 2 hours after the irradiation.

2.4.4. Apoptosis Assays

AnnexinV: Apoptosis is a process of programmed cell death. The term encompasses a number of pathways and methods by which the cells enter into a cycle that eventually leads to their death. During apoptosis a number of different stages are seen. One of the initial steps is the inversion of the phospholipid membrane of the cell. These membranes change their organisation when the process of apoptosis begins. AnnexinV is the antibody which binds to these sites, and can be viewed by im-

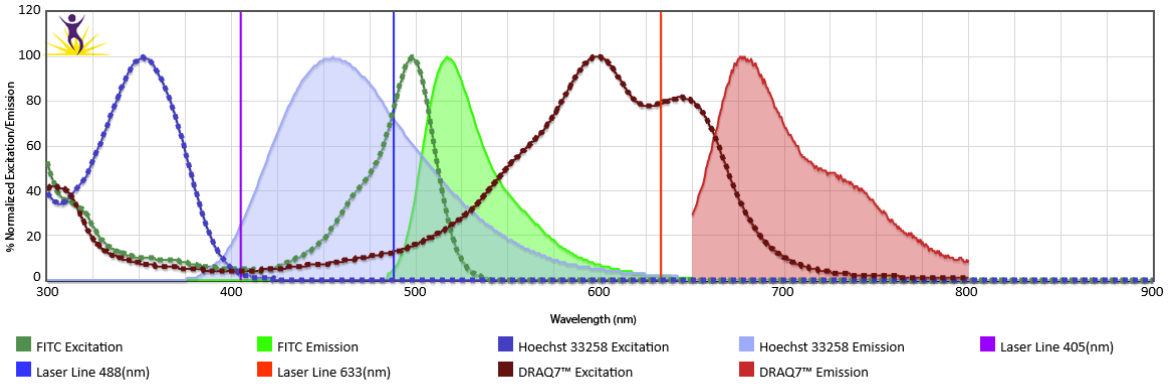

Figure 2.14: Blue: Hoechst, Green: FITC, and Red: for DRAQ7. The dotted lines are the excitation spectra and the solid blocks the emission spectra. The ranges of the spectra show a separation of the peaks, and can therefore be used well simultaneously. Image sourced from the Biolegend Spectral Viewer[56]

munofluorescence. For the proton beam experiment samples, AnnexinV conjugated with phycoerythrin (PE) is used. PE is a fluorophore with an excitation and emission spectra peak of 566 and 574 nm respectively. The staining therefore appears yellow in colour in the imaged samples. The cells were also stained with DRAQ7 (Red) and Hoechst (Blue) to distinguish dead cells from apoptopic cells. These samples are also stained live and immediately evaluated under a confocal microscope.

The recommended protocols for the AnnexinV include the preparation of special buffers and solutions, or would require ordering a specialised kit for its purpose. These kits being expensive, a justification would be necessary to attempt it. Due to the limited understanding of how apoptosis works in these cells, and a short time frame we opted not to use these protocols. Hence staining for AnnexinV was carried out using an existing simpler protocol.

2.5. Scanning Electron Microscopy

Scanning electron microscopy (SEM) is a method by which a high-energy electron beam is scanned onto a sample to produce images. In their interactions with the sample, the electron beam produces secondary and backscattered electrons, and characteristic X-rays. These signals are collected by one or more detectors to form images which are then displayed on the computer screen. SEM provides an advantage with the high resolution, and quality of images that can be formed. SEM also makes it possible to change the orientation of the sample in three dimensions, to visualise parts and features of the sample which could not be done from the top view or bottom view alone which is the standard for light microscopy.

For this project, SEM is a very valuable tool since it allows the user to be able to see the interaction of the cells with the scaffolds. The microscope used is a Jeol-JSM 6010LA. Since the structures were manufactured with a non-fluorescent material, or the most part, it was not possible to see the structure in confocal microscopy. While the lack of autofluorescence is very important to have minimum obstructions to the imaging of the cells, SEM became necessary to also see the structures, and the difference in cellular organisation in and around it.

The samples were fixed with Glutaraldehyde and dehydrated with a Protocol of alcohol and HMDS (Hexamethylene Disilazane), which has been detailed in appendix-C. For the earlier tests, where only and increasing alcohol concentration was employed, the results were not satisfactory. After an evaluation of the practical conditions in which the samples could be dehydrated, HMDS was chosen as the final solution. The details of the process are discussed in the next section.

The early protocol for dehydration was adapted from a study published by Accardo et al. [43]. This method utilises increasing concentrations of Ethanol in subsequent steps, to gradually dehydrate the samples without causing damage to the structures and the cells. While this process is a protocol that worked for the samples, and did not cause severe distortion in the structures, it could be observed that

cell images had a degree of loss of detail. Many of the finer processes of the cells that extend into the regions into the scaffold were not clearly observed.

This led to testing a different protocol for this method. Based on existing literature and the methods they employ for dehydration, two methods were short listed. The use of HMDS, and Critical Point drying.

HMDS: It is a chemical with a lower surface energy than Ethanol and makes the transition from a hydrated state to a dehydrated state of the sample in a gentler manner. The method involved gradually increasing the concentration of HMDS and decreasing ethanol in tandem. The final step allows the HMDS to evaporate from the samples overnight, and gives a dramatic difference in the details that can be seen in the cells.

Critical Point drying: Is a method in which the Ethanol is pumped with CO2 at higher temperatures and pressures, and the ethanol being replaced with liquid carbon dioxide. The Carbon dioxide then flash evaporates, inducing very little stress on the samples, and creating very well preserved samples.

In comparison, the detail that could be seen in the imaged samples after, showed the HMDS samples to have a marginally better preservation. Additionally, the critical point drying method requires specialised equipment, and is a much longer process, while HMDS method can be easily carried out in a lab. At least with respect to U251 cells, HMDS proved to be a more practical method with a better output that critical Point drying. The comparative images of the samples is shown in figure 2.15

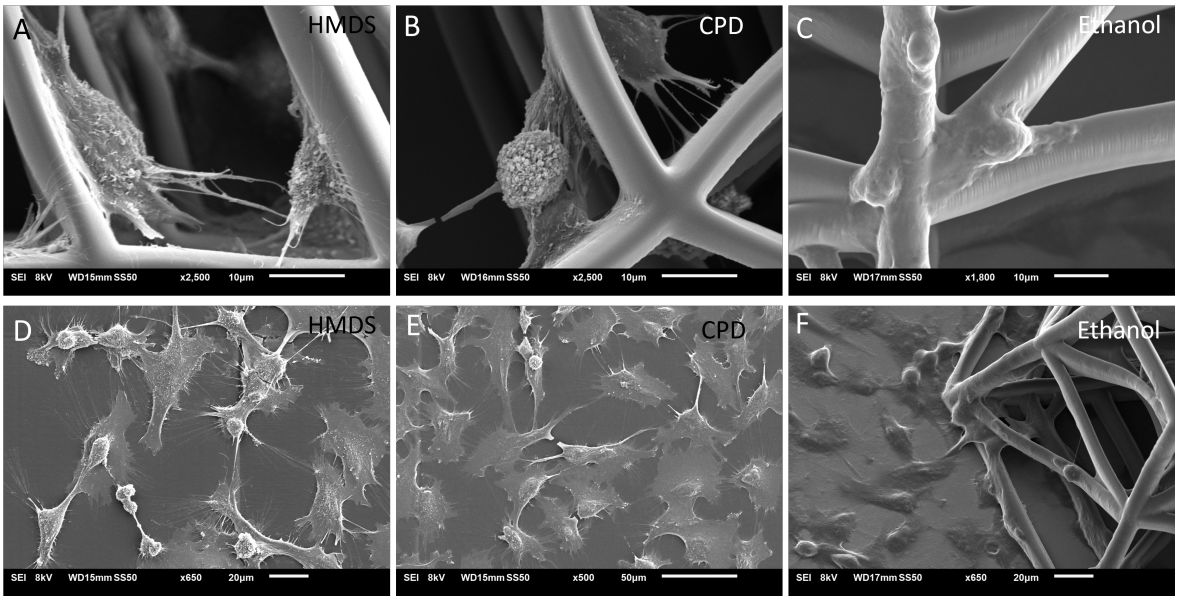

Figure 2.15: The protocols used for the method is marked in the image. HMDS and CPD are similar, and both better that the ethanol protocol.**A,B,C:**Cells on the 3D scaffolds. **D E,F**shows cells in the 2D configuration. The conditions of HMDS, CPD and Ethanol are marked in the top right corner of the images.

After dehydration, the samples were sputtered with gold in the JEOL JFC-1300 Auto Fine coater to make it conductive for the electron beam in SEM. The sample is coated at an inclination of 45°, rotated, and sputtered one more time. The coating is done at 20mA for 20s each. The sample is at an approximate distance of 25mm from the top, and a uniform coating of 13nm would form on the sample. The samples were then extensively imaged.

2.6. Viability Assay

Viability refers to the number of living cells present in a sample. To evaluate the proportion of living cells in the samples after irradiation, a viability assay is performed. The assay is conducted using Cell Counting Kit-8. (CCK-8, 96992, Merck Life Sciences, NL). The kit contains of a solution of WST-8 (2-(2-methoxy-4-nitrophenyl)-3-(4-nitrophenyl)-5-(2,4-disulfophenyl)-2H-tetrazolium, monosodium salt), which is bioreduced by cellular hydrogenases to produce an orange formazan dye, that is soluble in cell cul-

ture medium. The image 2.16 shows the colour that is formed in different samples. The amount of the dye produced is proportional to the number of living cells. The Kit solution requires no other steps, and is simply added to the solution and analysed using a plate reader. Fresh medium with the CCK-8 in a 1:10 dilution is added to the cells, and the cells are allowed to incubate at 37°C for 1.5 hours before extraction and analysis in the reader. The protocol for the method is added in appendix-F

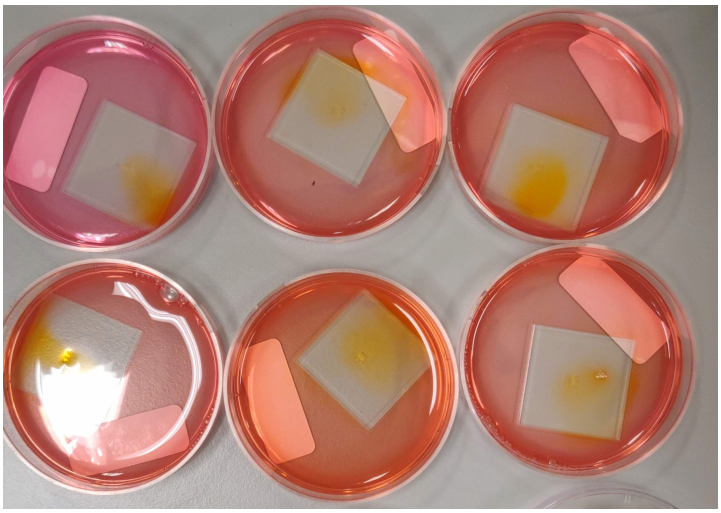

Figure 2.16: The dye can be seen being formed at the centre of the slides. That is where the cells have been seeded. The sample on the top left has fewer living cells and therefore appears closer to the pink of the cell culture medium.

96-well plates are used in the reader, with the wells containing the solution extracted from the plates. The plate reader was set to use light of wavelength 450nm, and gives the output as a proportion of the amount of light absorbed by the medium. A higher value in the plate reader output (absorbance), implies a greater number of living cells in the extracted medium.

The detailed reader layouts for the experiments are attached in the appendix-F. But in general, the plate the extracted medium added in triplicate, and a dilution of 1:10 for a better resolution of the differences if they are very low or seemingly imperceptible. The plate values are also standardised by using wells with only medium to baseline the colour of the formazan formed, as the colour of the medium can also sometimes vary slightly. The output of the reader is shown as a bar graph of each of the values and can be used as a quick tool to evaluate cell viability in samples.

3

Results and Discussions

The results of the designs, fabrication of these scaffolds with 2PP, mechanical characterization by nanoindentation, fluorescence imaging, and SEM imaging are discussed in this section. The results section also discusses the process and outcomes of the methods used for sample preparation for 2PP and SEM, for which structured investigations and evaluations were carried out. The reported findings are comprehensive and discuss some of the results that may be unexpected and inaccurate, and the reasons for them.

3.1. Two-Photon Polymerization

3.1.1. Substrate

For the fabrication of the IP-Visio scaffolds the recommended recipe from Nanoscribe uses glass substrates with an Indium Tin-Oxide (ITO) coating to satisfy the refractive index requirement for interface finding. This substrate is the standard one used in conjunction with a 25x objective, for structures with medium sized features. The reason for using these substrates is the difference in the refractive index. For successful interface finding, with a 25x objective, a difference in the refractive indices of the materials must be at least 0.1. IP-Visio has a refractive index of 1.479 in the liquid form, and 1.505 in the polymerized form with a 780nm wavelength laser. At the same wavelength only ITO coated Glass and silicon substrates have a high enough refractive index, which can maintain the 0.1 difference required. Despite a high difference of index, silicon substrates cannot be used because they are opaque. Transparency of the substrates is necessary for confocal imaging of the samples. The only transparent substrate with a difference greater than 0.1 is ITO-coated glass. A short overview of the available substrates and the refractive index difference is shown in table 3.1.

Table 3.1: Differences of refractive index with IP-Visio (=1.479) of available substrates. All values are taken from the *Nanoguide* website.

Substrate Material	**Refractive Index @780nm**	**Difference with liquid IP-Visio @780 nm and 20°C**
Fused Silica Glass	1.454	0.025
Soda-Lime Glass	1.518	0.039
Borosilicate Glass	1.517	0.038
Silicon Substrates	3.710	2.231
ITO-Coated Glass	1.624	0.145

3.1.2. Parameter Sweeps and Dose Selection

Parameter sweeps are a methodical way to find the optimum dose for a particular design, resin and objective combination. Usually, the Laser Power(LP) and Scan speed(SS) are varied in a grid to create LP,SS combinations. The actual (or a similar representative) structure is printed with these combinations and the optimum is selected.

In practise, the laser power is selected from a scale from 0 to 100% of the total laser power, and the

scanning speed varies from 0 to 100 mm/s. For IP-Visio, the suggested optimum dose provided by the company on their online manual for the printer, *Nanoguide*, is 100% laser power at 100 mm/s printing speed. This represented a good initial point to begin optimizing.

In the first iteration of manufacturing parameter sweeps (also referred to as Dose tests) were carried out for 2D pedestals and then subsequently for 3D structures. Some selections of the extent of the parameter sweeps also have to be chosen depending on the time available on the printer. The pedestals for the dose tests were 220μm by 220μm in area, and 10μm in thickness. The first 2D parameter sweep had an LP and SS range of 20-80% and 40-90mm/s respectively. For LP values of 40% and below, little to no polymerization is observed. The polymerization threshold can be assumed to be fairly lower than the 60% LP value. Figures 3.1, shows SEM images of the first dose test. In the second parameter sweep the LP and SS are in the range of 60-100% and 50-90mm/s respectively. Almost all the pedestals printed with a 100% LP showed the formation of bubbles and defects. Figure 3.2 shows an optical microscope image of the second dose test. It established 90% as the approximate upper LP limit for the pedestals. The optimum is therefore between 60 to 90% LP. Table 3.2 gives an summary of the dose tests that have been carried out in this project.

Table 3.2: Parameter sweep description

No.	Type	LP Range (%)	Step	SS Range (mm/s)	Step	Remarks
1	2D Pedestals	20-80	20	40-90	10	Threshold at about 60% tests needed for higher values
2	2D Pedestals	60-100	10	50-100	10	80%, 50mm/s and 90%, 60mm/s show good prints
3	3D Square Pyramid	80-100	5	50-90	10	Most samples have deformations, lower SS tests needed
4	3D Hexagonal Pyramid	90-100	5	15-30	5	100%,15mm/s show the best pedestals with no bending

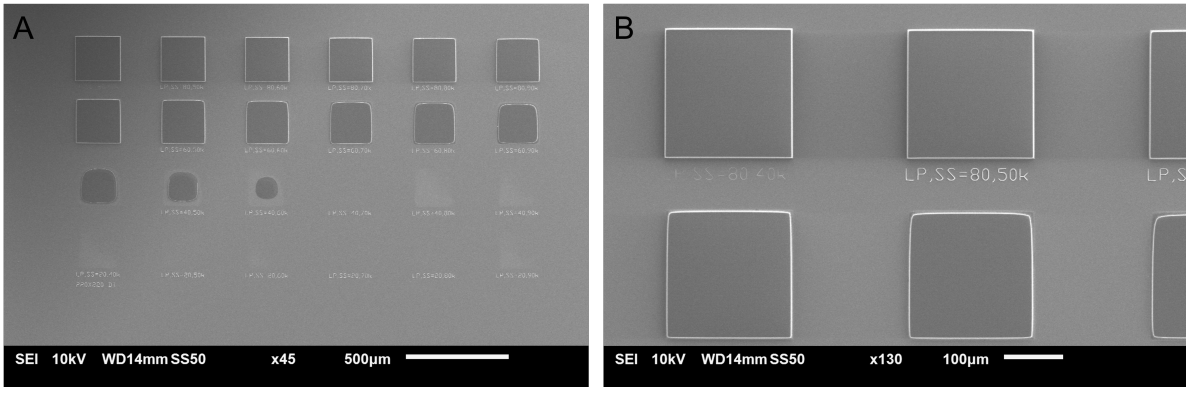

Figure 3.1: A: First Dose test.The SS increases from left to right (each column is a different value), and the LP increases from bottom to top (Each row is a different value). LP values below 40% have no pedestals present. **B:** Zoomed-in image on the left-top corner of image A. The pedestal marked with ”LP,SS=80,50k” is the optimum that was finally chosen. The sharp edges of the indicate a well-polymerized print.

The optimum selected was 80%,50 mm/s. It was the ideal dose at which the resin did not bubble and formed sharp edges in the pedestals. Another dose, 90%, 60mm/s also showed a good print in the dose test, but had bubble formations during the printing of final pedestals. Although the print would be marginally slower, the 80%,50mm/s combination did not have this issue was hence made the standard for pedestal prints. The samples were developed in PGMEA and IPA. This is the suggested protocol from Nanoscribe. The test-prints showed no deformations after development and the method was standardised for this print. Most samples have been developed with this protocol and the data is not

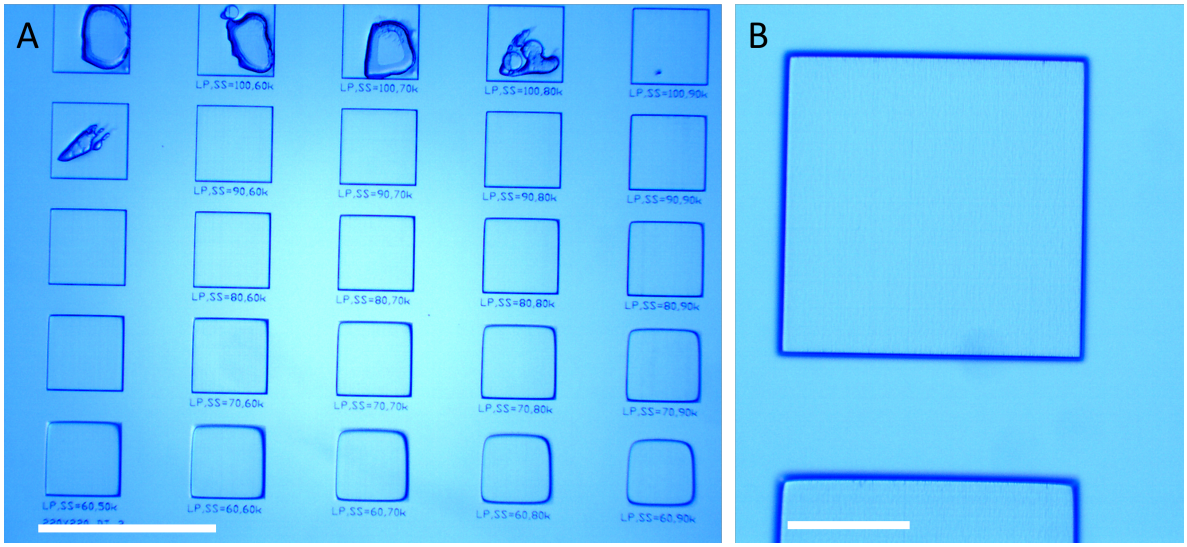

Figure 3.2: A: Second dose test. The SS increases from left to right (each column is a different value), and the LP increases from bottom to top (Each row is a different value). The top-most row is 100% LP which shows the formations of bubbles and defects. Scale bar= 500μm. **B:** Zoomed-in image on the pedestal with 80%,50mm/s. The darker edge is because of the microscope used, but is the clearest pedestal formed. The sharp edges of the indicate a well-polymerized print.Scale bar= 100μm

separately shown.The protocol is attached in appendix-D. Similarly, for 3D scaffolds, two parameter

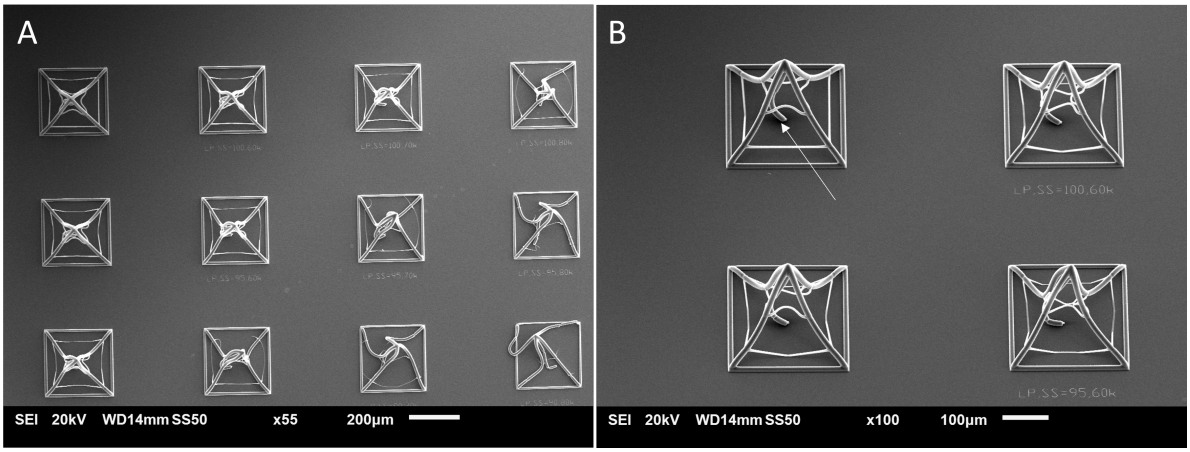

Figure 3.3: A: First 3D Dose test.The SS increases from left to right (each column is a different value), and the LP increases from bottom to top (Each row is a different value). The structures which have not been polymerized with a high enough dose have a lower stiffness and cannot hold shape. **B:** The white arrow marks the bending pillar on the sample with 100%,60mm/s, which was looked for in the later test.

sweeps were carried out. The first one was done using a preliminary square pyramid design that was not used for any samples. The pyramids were 220μm by 220μm at the base, and 300μm in height. A similar method to the 2D pedestal dose test was used. These pyramids can be seen in image 3.3. The LP and SS ranges were 80-100% and 50-90mm/s respectively. The optimization was started from the value used for the pedestal.The figure 3.4 shows the bending in the beams, and damage of the structures at higher scan speeds. Even for 100% laser power the dose is not enough. To increase the dose the SS would have to therefore be reduced. That was the objective of the second dose test. In which the LP is from 90-100% and lower SS in the range of 15-30mm/s. The design used for this was a pyramid with a hexagonal base. The diameter of the base is 300μm and 300μm height. Figure 3.4 shows the samples in the second test. In top view, all of the samples seem to have a good structure, but when observed at a 30° angle shows bending in the middle beam of the pyramid. This beam is

a structural element, and would be important for the scaffold to be robust. 100%,15mm/s is the only sample that shows an erect pillar, and was therefore selected as the final dose for 3D structures. Even with changes and iterations in the design, the dose remained the same and was able to give reliable reproducible structures for all prints carried out.

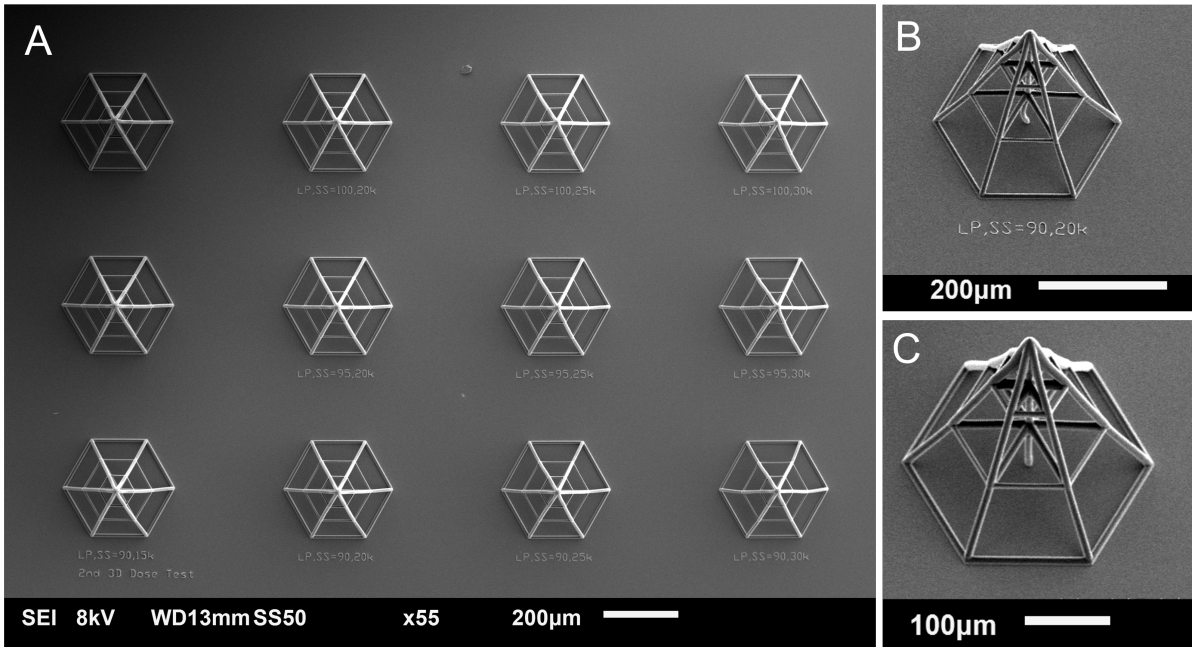

Figure 3.4: A: Second 3D Dose test.The SS increases from left to right (each column is a different value), and the LP increases from bottom to top (Each row is a different value). Structures seem to be stable in the top view **B:** Structure with LP,SS=90%„20mm/s also showing the central pillar bending. **C:** Structure with the final dose of 100%,15mm/s with the erect central pillar.

3.1.3. Scaffold Design:

2D Pedestals

The 2D pedestals are of 10μm thickness, and made of blocks of 250μm by 250μm in area. Since the print field for a 25x objective is a maximum of 400μm diameter, a square of 285μm x 285μm is the maximum possible square that can be printed at a time. The size is chosen it to be an easy way to scale printing, depending on the availability of the printer. The dose worked also for overlapping edges with overlap by about 3μm, which was ideal to fill up any gaps in the structure and the edges to make continuous pedestals. Figure 3.5 shows the difference between using an 3μm overlap and printing pedestals with no overlap.

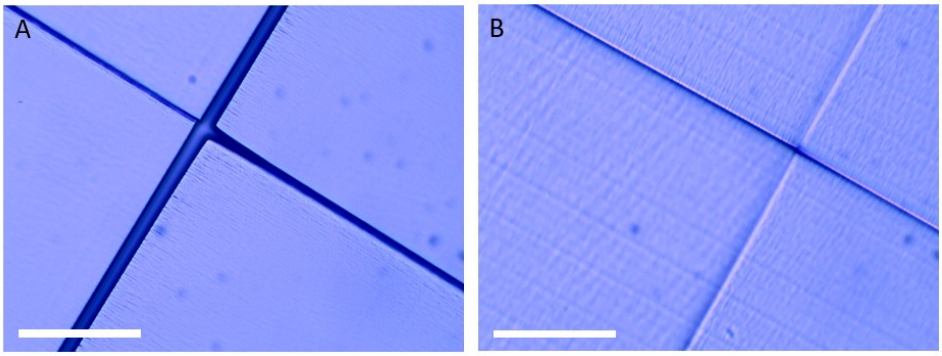

Figure 3.5: A:Pedestal Blocks printed without the 3μm overlap B: Pedestal blocks printed with the overlap. Scale bars= 50 μm

The aim was to have a standard, measurable area of the pedestals on which the cells were being cultured. In the final design, the total size of the pedestals is 1000μm by 1000μm. The printing of multiple pedestals next to each other could also be carried out by using the 'stitching' option in DeScribe, but the methods did not show much difference in the output. Using the stitching option would involve more intermediate steps in DeScribe, and increase the chance of error. Using the overlap method for printing the pedestals was an easier and more practicable way to print the pedestals. Each complete pedestal (1000μm by 1000μm) would take approximately 10 minutes to complete printing. Multiple such pedestals were printed in each sample to account for printing errors or small inclusions.The default value of slicing and hatching values generated by DeScribe for this design were at 0.8μm and 0.5μm respectively. These values provided good results in the design, and were not changed.

3D Scaffolds:
The 3D scaffolds went through a few design iterations and underwent modifications based on the response in cell culture. The process was iterative and attempted to maintain the scientific justification for the design. The scaffolds were modelled to replicate the vascular branching points of the blood vessels. The aim of using a pyramidal structure was to create a variation in the size and length of the lateral beams within each scaffold. IP-Visio, as suggested by Nanoscribe, is optimised for the printing of independent structures, each fitting within a single print field. Hence, these independent structures were printed in an array to offset the possibility of damage and to visualise a quantitatively relevant number of cells.

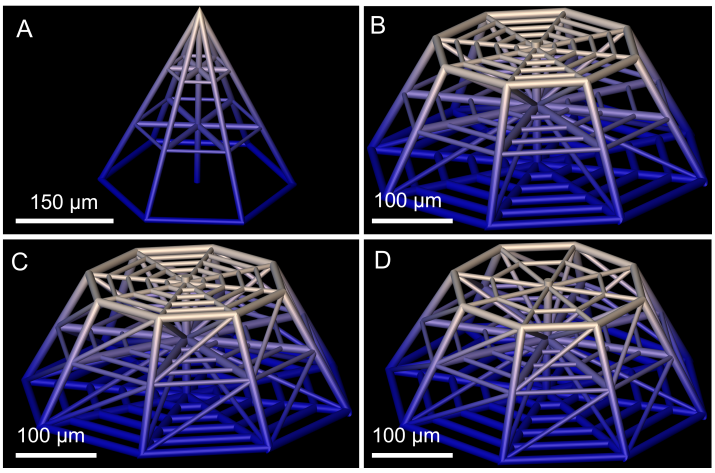

Figure 3.6: A: Hexagonal Pyramid of height 300 μm. (HexV1) **B:** Octagonal Pyramid with base sides of 150 μm and a height of 140μm (OctV1)**C:** Octagonal Pyramid with side beams(OctV2). **D:** Octagonal Pyramid with reduced lateral beams on the top (OctV3).

The initial Design was a hexagonal pyramid, with hexagonal base of diameter 300μm and a height of 300μm. It had 2 intermediate horizontal beams and a sparse structure. When cultured with cells, the cells did not colonize this structure. IP-Visio itself is biologically inert and did not provide any chemical incentive for the cells to migrate onto it. Additionally, the structure itself has wide gaps through which the cells could fall through before they adhere to the structure. The spaces had to be adjusted to be more comparable to the size of the cells, so that they could attach on the structure and proliferate on it. The very large height of 300μm also would make it more difficult for cells to migrate to that high.

The other consideration was for imaging. Since confocal microscopy is only performed at one plane at a time, it would be necessary to have a broader top to be able to visualise a quantitatively relevant number of cells. With a "pointed" Pyramid structure, the number cells would be fewer at the top, where the imaging would be clearest. This lead to the truncation of the top of the structure, and the addition of more lateral beams to trap the cells. The diameter of the circumscribed circle for the base of the octagon was increased to 380μm. The maximum print field (400μm diameter) of the 25x objective lens cannot be varied, and the design was changed from a hexagonal pyramid to an octagonal one to further increase the surface area of the samples. This would make it possible for a greater number of cells to

be trapped. The height was also decreased from 300μm to 140μm for the structures. The central pillar and the mainframe of the structure is made of beams of 10μm diameter, and all additional beams are of 6μm diameter. Table 3.3 gives a summary of the designs and the changes made. Although Blood vessel architecture in the brain can vary significantly in size, these dimensions are chosen such that the structures have comparative size to the U251 cells. This has been discussed in section 1.5.

Table 3.3: 3D Design Iterations

No.	Design Abbreviation	Description	Base Diameter (μm)	Height (μm)	Improvements
1	HexV1	Hexagonal Pyramid	300	300	Wide structure, does not effectively trap cells.
2	OctV1	Truncated Octagonal Pyramid	380	140	Greater surface area, lower height. Cells get trapped and can proliferate more.
3	OctV2	Truncated Octagonal Pyramid with side beams	380	140	Greater number of cells on the outer surface of the scaffold:better for SEM imaging
4	OctV2	Truncated Octagonal Pyramid with fewer lateral beams	380	140	Structure and Cell density not affected, less interference for deeper confocal imaging.

The iterations were carried out in tandem with the cell density optimisation. As is seen in figure 3.7, the gaps on the sides were quite wide, and did not have cells across them. The addition of diagonal beams made it possible for the cells to migrate through it, and formed the final design that is seen. The number of the lateral beams were optimised to have a relevant number of cells, as well as have enough space to not interfere with the confocal imaging of the cells. It was intended to take deeper images of the cells inside the structure, and too many lateral beams might have caused more interference. The figure 3.8 shows the colonization of the structures with different number of lateral beams. The densities used for both these samples is the same, and the number of cells not impacted. The scaffolds are also not affected structurally. The figure 3.6, shows the iterations of design used.

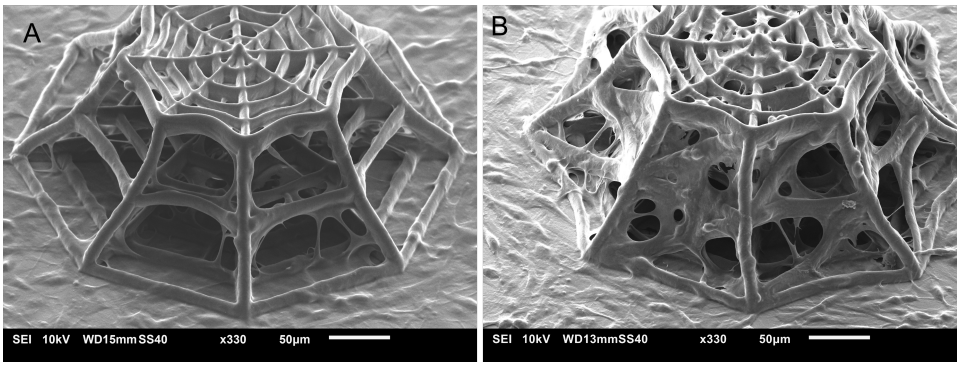

Figure 3.7: A: Octagonal Pyramid without side beams. The cells are present deeper inside the structure, but are not easy to visualise. **B:** Octagonal Pyramid with diagonal beams, which show a higher number of cells on the external surface. The presence of cells on these beams implies that they are being used as migration routes for the cells.

There was an attempt to create overlapping structures and increasing the complexity in the design used, but it did not add justifiable value to the design in terms of the improvement or variation, and would make the imaging tasks more inefficient.

The 2D and 3D structures were printed together on the same substrate to ensure that there is minimum difference between the cellular densities between 2D and 3D scaffolds. The cells on both structures would be subject to the exact same conditions and would make the experiments more precise. Typically,

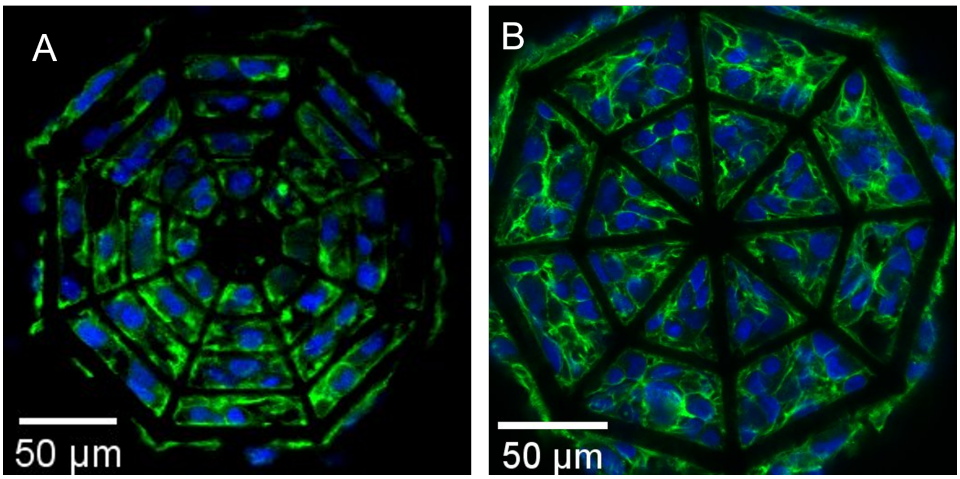

Figure 3.8: A: Sample with higher number of lateral beams **B:** Sample with similar densities with fewer lateral beams on the top surface.

in each sample, there are three 1000μmx 1000μm pedestals and fifteen 3D scaffolds arranged in an array of 3 columns and 5 rows. Each pedestal takes about 10 minutes to print, and each scaffold takes about 4 minutes to print. Collectively, each sample would take 1.5 hours to print. It was important to keep the total fabrication time low as large number of samples had to be printed for each experiment. A maximum of 9 samples could be printed in a 14 hour overnight job at the Nanoscribe. The final samples are shown in figure 3.9. The DeScribe code used to print these samples is attached in the appendix-E

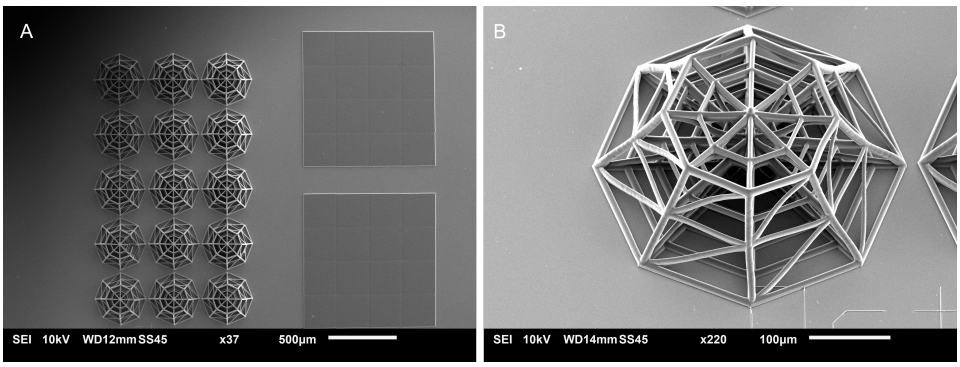

Figure 3.9: A: Samples used for Proton beam therapy **B:** Final 3D scaffold structure

3.1.4. Pedestal Delamination

Before cell culture, the samples have to be sterilised. Sterilisation was carried out with 70% Ethanol to remove any contamination. The samples are then washed Phosphate buffer solution (PBS), and then allowed to air dry, before the introduction of the cell culture medium with U251 cells. Hence, the solution around the structures changes twice after they are developed. Since IP-Visio was largely untested at the time, the response of the material was not known to these pH and stress (of washing the solution) changes. A test was preemptively carried out for these samples. The samples were left overnight in demineralised (DeMi) water, and the response of the samples to being submerged in water was checked. The samples were left in water for upto a week, which would be the approximate duration of the cell culture. The samples showed some seepage of water under the surface after a few days, but these effects were negligible. A trial cell culture was also carried out for these samples. Figure 3.10 shows that sample.

Although the trial was successful, subsequent pedestals delaminated from the glass substrate in most samples cultured after that. It was also surprising since the delamination was very rapid in these samples. The pedestals delaminated in a typical ‘rolling’ fashion, with the corners getting lifted first and

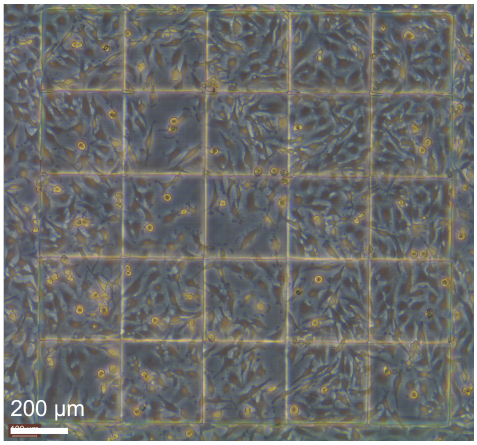

Figure 3.10: The sample was imaged after being cultured for two days in the incubator.

folding over itself. This led to a methodical investigation into the reason for this delamination.

The rolling of the pedestals implies that the structures were swelling causing stresses in the materials, delaminating it. Without these residual stresses, a roll would not be observed. It is also possible that the adhesion of the materials with the ITO surface was not strong enough and would disintegrate during cell culture. The possible postulated reasons for these stresses, and the reduced adhesion were heat, pH changes, and slicing and hatching parameters not having enough adhesive strength. Another reason could be the surface area of the pedestals, since 3D scaffolds printed on the same plate were not undergoing this delamination, and were printed with a higher dose.

Heat and pH changes could be accelerating a process that would otherwise take a much longer time to occur. But these are not parameters that could be altered, since the scaffolds have to sterilised, and have to be incubated at 37°C for the cells to culture. The applicable solutions were therefore:

1. Increase the adhesion with coatings such as MAPTMS and Ormoprime®08
2. Reduce the surface area of the pedestals
3. Change the slicing and hatching parameters
4. Changing the stitching parameters of the pedestals
5. Increasing depth of the interface during printing
6. Higher dose for the base layer of the pedestals
7. Curing in UV and heat post-fabrication to increase polymerization in the samples.

All the tests were carried out with control samples with samples printed with the original configuration of 80% and 50 mm/s. For slicing and hatching changes and area condition changes, the different configurations were printed on the same glass slide in an array. The samples were tested with PBS, and with medium, and in the incubator. Figures 3.11 and 3.12 shows the delamination that occurred while using different testing methods.

The coating with Ormoprime®08 (Adhesion promoter solution from Micro resist technology GmbH) showed only marginal improvement in adhesion. The changes in slicing and hatching parameters showed no improvement, and increasing the base laser dose to 70% and 60mm/s also did not show improvement. These parameters were also attempted in combinations with each other, with one varying across the X axis and the other on the Y axis, when printed in an array. No reliable conclusions could be drawn from any of these changes.

The silanization with MAPTMS gave the most reliable outcomes, as can be seen in figure 3.13. MAPTMS made the surface of the structure of the ITO glass slide more hydrophobic, and made the adhesion of the structures stronger. While this method worked for most samples, some batches of prints (which were carried out at various times through the year) would still show some delamination, but it would be

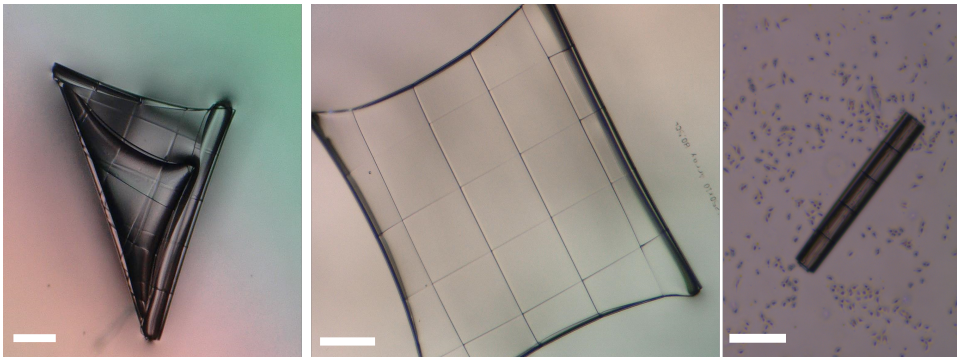

Figure 3.11: All the samples were tested by leaving in the incubator in solution mimicking conditions of cell culture. **A:**Delamination occurring after UV curing the samples, **B:**Delamination after Heat treatment, **C:**Delaminated samples after treating the surface with Ormoprime .

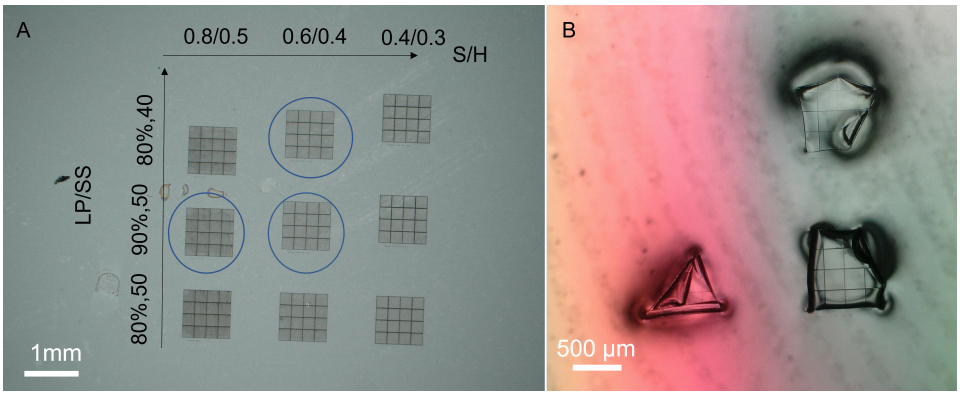

Figure 3.12: A: Parameter sweep with changing Dose (LP/SS) and Slicing and Hatching (S/H) Parameters. The scan speed is in mm/s and the S/H parameters are in microns. **B:** Results of samples from A when tested in the incubator, only the samples marked with blue circles from A are visible in the image, since the rest float away in the medium

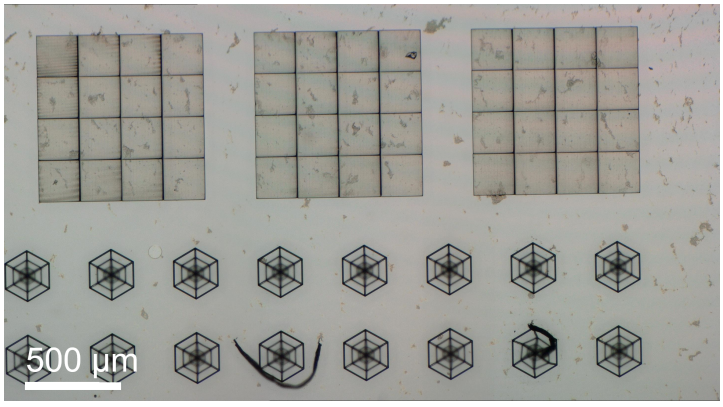

Figure 3.13: The sample with a coating of MAPTMS on the ITO-coated glass. The sample showed no delamination after sterilization, and 1 hour in the incubator at 37°C.

partial, and would not affect all the pedestals, since each sample had 3 printed pedestals. Increasing the concentration of MAPTMS (to 2% v/v in Ethanol) used for the silanization process improved the adhesion, but variation between batches of prints of the sample was observed. An additional attempt was made to change the development protocol of the samples. After 25 minutes in PGMEA and 5 minutes in IPA, the samples were put in Novec™7100 for five minutes. Novec is more volatile than IPA, and would exert lesser stresses on the samples as they dry. There was a shortage of Novec in

the laboratory (due to COVID-19), and since the protocol didn't show any particular difference than the existing one, it was not used further.

While MAPTMS provides a functional solution to the problem and could be utilised for cell culture, the fundamentals of why this variation occurs, and the reasons for the inconsistency could also lie in other factors such as decreasing laser power of the printer, changes in humidity and temperature, and differences between bottles of IP-Visio. These changes are unavoidable, and the protocol must be robust enough to compensate for it. There was a major overhaul pending for the machine, and a varying laser power and alignment could lead to reduced adhesion. An investigation into the polymerization of the materials and a deeper study could identify the fundamental issue that leads to delamination.

3.2. Compression Testing

A compression test was carried out for a configuration of the 2D pedestals, using the Femtotools Nanoindenter. The tip has a cross section of 50μm by 50μm, and was placed in the centre of the pedestals. The pedestals for this test had a height of 50μm to avoid effects of the substrate in the compression test. The test was carried out for a number of samples and yielded that IP-Visio has an average Young's Modulus of 1.46E+09 Pa . A schematic of the test set up and the data output can be seen in figure 3.15 The brain ECM has a very low young's modulus (0.1-100kPa)[57]. Achieving that

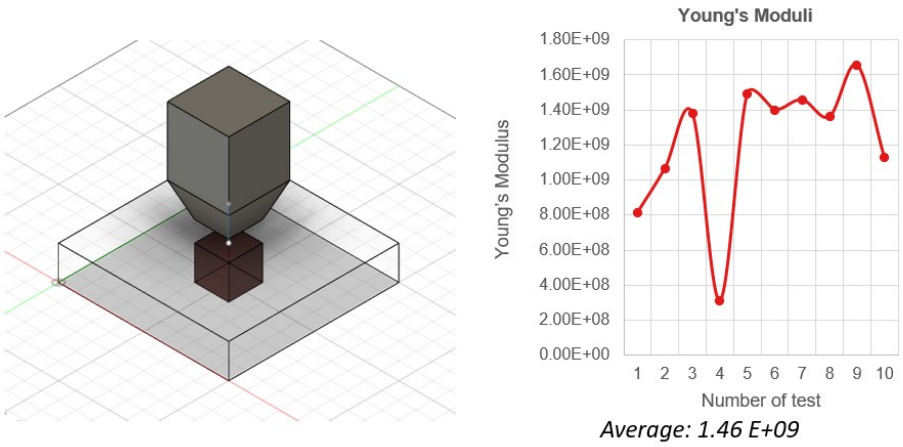

Figure 3.14: Left: Schematic of the test set up, with the Nanoindenter tip shown, Right: Graphical representation of the output. Outliers in the data can be explained by possible slippage of the tip from the edge of the sample during the test.

is difficult as the lower stiffness makes it difficult to model the designs intricately or extensively. The scaffolds would have lower stability and might collapse under the cells and stresses. While the IP-Visio structures do not have values of stiffness that low, the value of young's modulus is almost half of that glass (3.3 GPa) and makes this design and structure a good starting point for the further development of low stiffness scaffold structures for *in-vitro* brain tissue engineering.

3.3. Immunofluorescence Imaging

3.3.1. Gamma H2A.X:

Gamma H2A.X foci formation is directly proportional to the extent of double strand DNA damage in a cell. The event of double strand breakage (DSB) may not occur exclusively by ionizing radiation, but it increases the rate of DSBs in cells. The Anti-Gamma H2AX antibody is an established marker to study the formation of such foci for radiation-induced DSBs[58, 59, 60]. This marker has also been specifically studied for U251[51, 61].

In these experiments, Gamma-H2A.X foci formation clearly depends on the irradiation dose. Cells exposed to a greater dose show higher foci formation. The samples were studied with 2Gy and 8Gy proton beam radiation doses. Figure 3.16 shows the distinct difference seen between cells with these doses. In the image, the samples are fixed with 4% paraformaldehyde solution (in PBS) 30 minutes

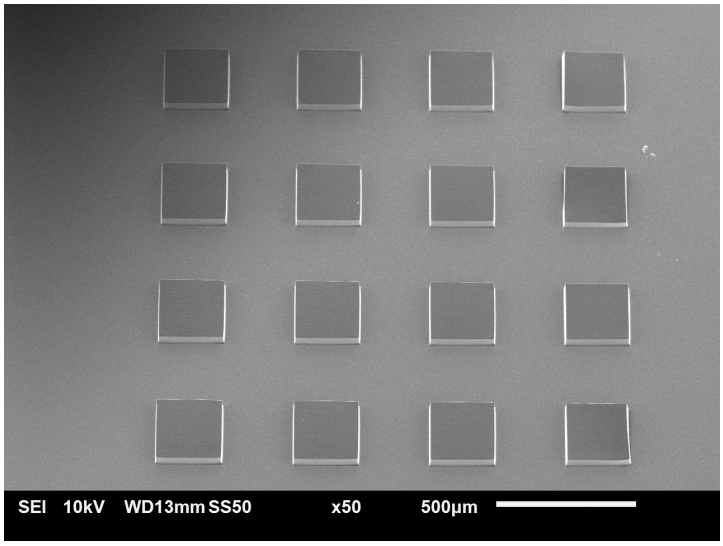

Figure 3.15: SEM images of the 50μm IP-Visio pedestals used for compression testing.

after irradiation. This time point was done for only one set of samples. The usual fixation time is at 1 hour. Gamma-H2A.X foci visibility peaks at the 1 hour time-point and decreases after that[48]. 1 hour is also a more practical time-point since the samples need to decay to safe radiation levels before they can be handled and fixed.

The samples also show some unintended staining of the cell cytoplasm, and is called non-specific staining. This may occur when the antibody binds to non-specific sites in the cells, or a combination of other ionic and hydrophobic interactions.[62]. The amount of non-specific staining seems to decrease in regions of the samples where the cells are more sparse. A blocking step is carried out decrease such non-specific staining, but it is still possible for it to be visible. That being mentioned, the foci that are formed are much brighter than the background staining as can be seen in figure 3.16. Additionally, for the quantitative analysis, the ImageJ macro only counts the bright spots(as local maxima) within the nuclear regions in the images, and the effect of non-specific staining in the analysis is thus avoided.

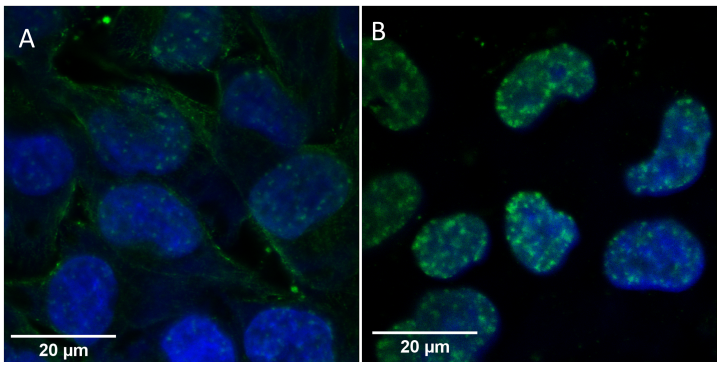

Figure 3.16: A: Cells in the 2D configuration fixed 30 minutes after 2Gy irradiation. **B:** Cells in the 2D configuration after 8Gy Proton beam irradiation. The green foci are distinctly formed in the nuclei of the cells. A higher number and intensity in visible in the cells exposed to higher doses.The images are taken with a 63x magnifixation lens.

The samples also show difference in the number of foci formed in the 2D substrates and the 3D scaffolds. This difference can be seen in figure 3.17. The figure shows a comparison of the foci formation between Control, 2Gy and 8Gy samples, in both the 2D and 3D configuration. The control sample is important for every experiment since the Gamma-H2A.X foci formation is not exclusive to radiation-induced DSBs. The control sample represents all the other stresses that the cells undergo, and makes the conditions of each experiment more comparable. For all the experiments conducted, the cells in 3D

show lesser foci, than in the 2D substrates. The number of the formed foci are distinct integer values and can therefore be counted. Additionally, The results also show that the percentage of cells that are positive for Gamma-H2A.X foci are also higher in 2D as compared to 3D. These experiments were repeated thrice at different dates, and similar results have been obtained. This can be seen quantitatively in the figure 3.18.

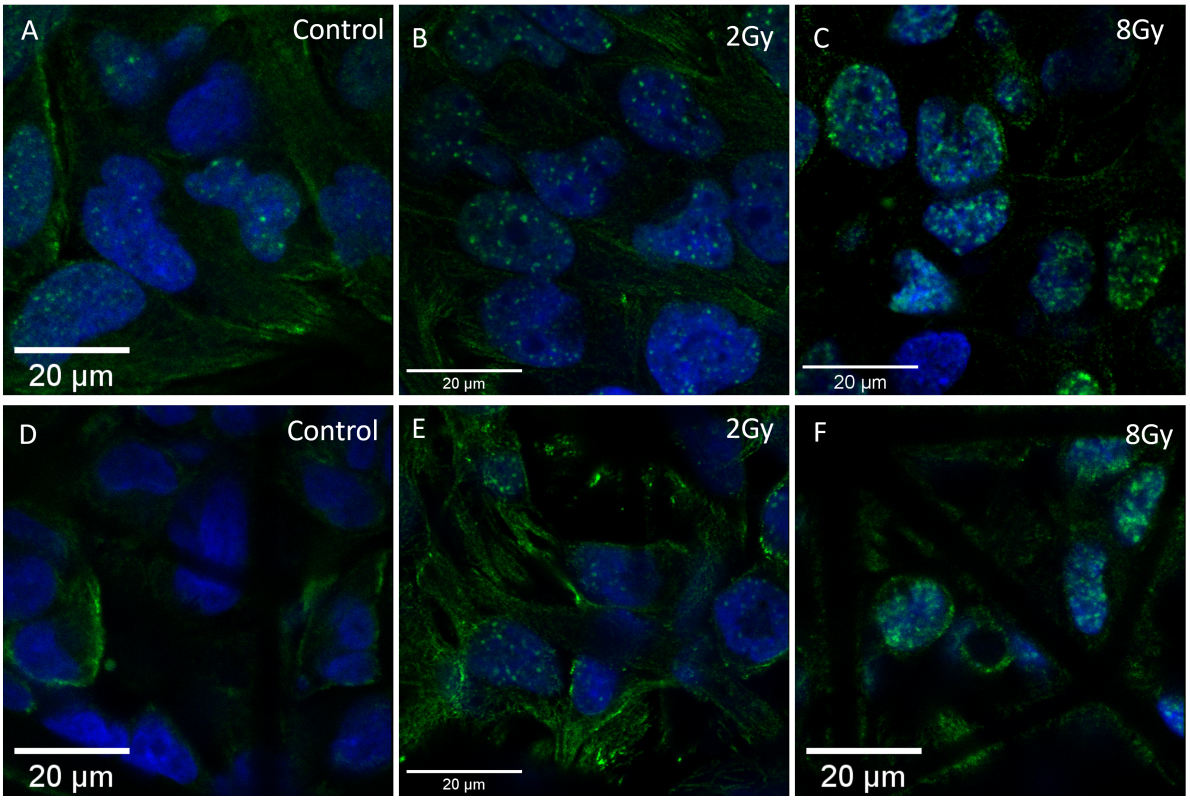

Figure 3.17: Regions of the samples with U251 cells on 2D pedestals and 3D scaffolds, with different doses of radiation. **A,B,C:** Cells on 2D pedestals. **D,E,F:** Cells in the 3D scaffold top layer. **A,D:** Control samples, **B,E:** 2Gy Samples. **C,F:** 8 Gy Samples. The number and density of the foci distinctly increases with the increase in dose. Cells in the 2D configuration have more foci than their 3D counterparts. The control sample in A also shows the some foci,since DSB damage is not exclusively caused by radiation. The images are taken with a 63x magnification lens.

It has been established that the ECM plays an important role in the regulation of proteins and other markers for GBM cells that make changes to its morphology, cell-cell interaction and cell-matrix interaction[63, 64].This difference in the formation of the number of foci, implies that these differences of the cells between 2D and 3D scaffolds are a result of the organisation of the cells. Using a 2D pedestal eliminates the possibility that these differences are caused because of a chemical interaction (with the material) alone. It can be said with a certain amount of confidence that the addition of the 3rd dimension to these cells affects the response of the cells to irradiation.

The process of sensing and responding to mechanical stimuli is known as mechanotransduction. Cell migration, differentiation, proliferation, apoptosis, gene expression, and signal transduction are all influenced by mechanical stimuli [65, 66].Hence, a difference in ionizing radiation response variation between 2D and 3D is an expected outcome [67]. The results and the data of this experiment consistently show a difference in the response of the cells in 2D and 3D environments.

The tumor microenvironment plays a very important role in the resistance of cells to treatment [68]. Studies of GBM cells also show more radioresistance in *in-vivo* orthotopic xenograft models than in corresponding *in-vitro* cultures[68]. Cells in spheroid cultures too have shown to have higher surviving fractions when treated with radiation [69]. Orthotopic xenografts are models in which cell lines or PDCs are transplanted into a host of a different species. This provides a more relevant environment for

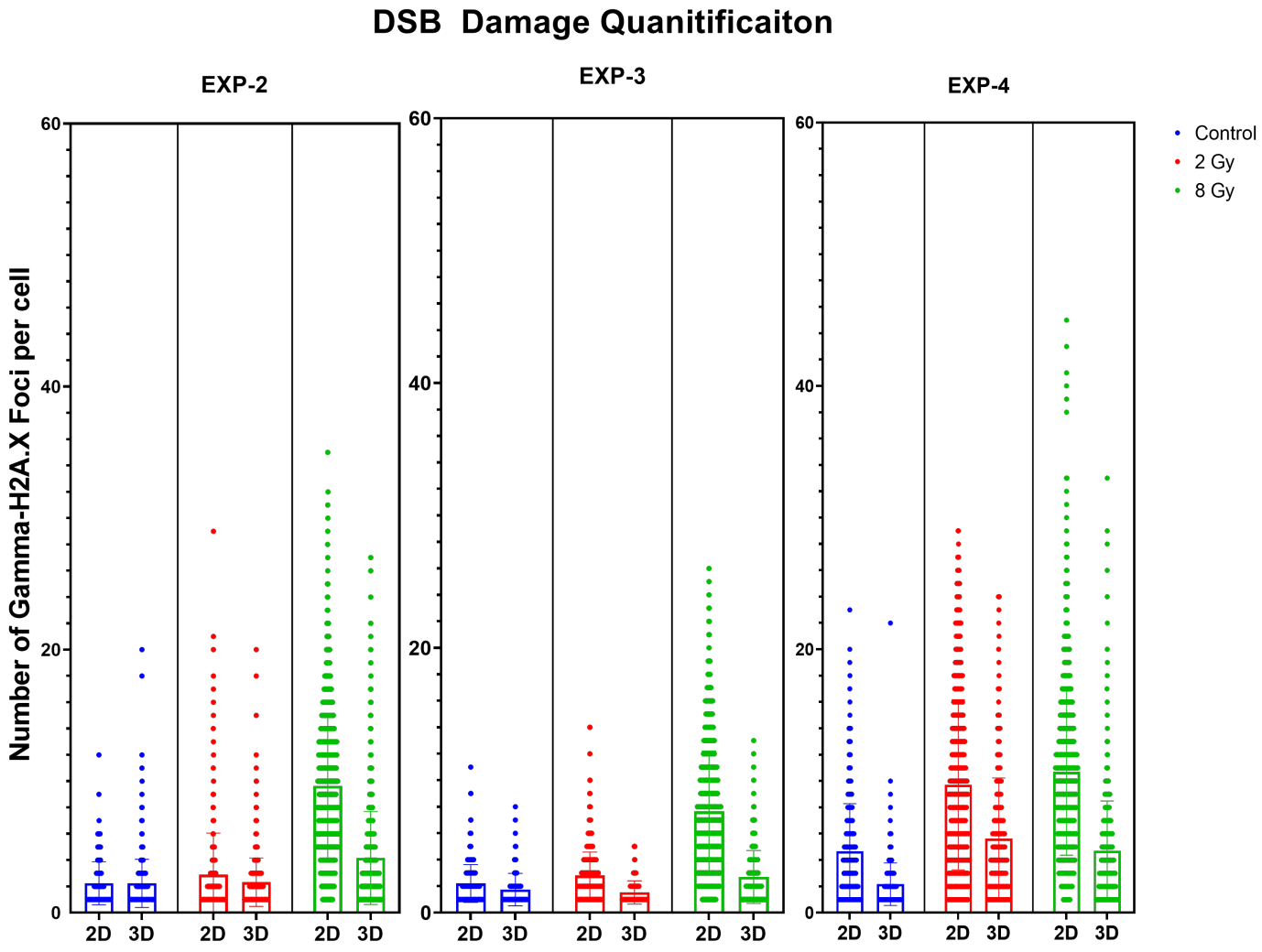

Figure 3.18: Each graph shows the scatter distribution of the foci formed. The longer width of the horizontal bars represents a greater number of cells with that number of discrete foci. The data correlates for all three experiments, and follows a similar trend. The bar-graph shows the mean, with error bars.

studying the tumour. 3D models of other cancers also show higher radioresistance in 3D [70].

In their study, Jamal et al. compare the radiation response of a GBM xenograft model to a 2D *in-vitro* cell culture model. They find that the *in-vivo* xenograft shows fewer Gamma-H2A.X foci formation than the 2D culture of the cells. An *in-vivo* environment can greatly differ from the limited 2D culture environment [71]. It can be reasonably assumed that the cells in an *in-vivo* environment are also growing in a 3D environment among other conditions. Considering this, the results of the current study correlate with the findings of Jamal et al. Fewer foci formed in the 3D scaffolds can suggest that even without the other factors (proteins, nutrients and ECM components), only adding a 3rd dimension to GBM cell culture can make the cells more resistant to radiation. Hence

This makes the 3D model also a more effective tool better estimate the response that ionizing radiation would have *in-vivo* while using a fully *in-vitro* model.

Another possibility to this outcome is that, in 3D cell cultures the repair dynamics of the cells are different. Many factors can affect the efficiency and extent of DSB repair in Glioblastoma cells[72]. Studies show that repair kinetics are different in 3D cell models, as compared to 2D[73, 74]. There is therefore precedence to speculate that GBM cells in a 3D environment may also exhibit different DSB repair

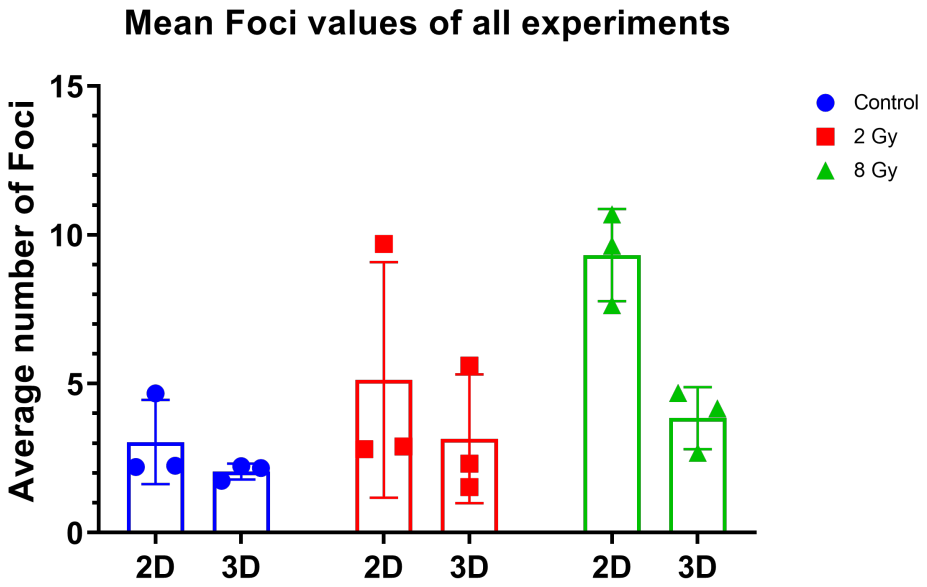

Figure 3.19: This graph shows the mean values of each experiment shown in figure 3.18. The mean values of the foci increases with an increasing dose even when averaged across multiple experiments.The mean foci formed are always lower in 3D scaffolds cells than 2D monolayers

kinetics than 2D. The result of this would affect the number of foci formed. Since for all the samples 2D and 3D are compared at the same time points, and fixation of the cells for this assay did not make it possible to visualise the same cells over a period of time to see the changing DNA damage response. This can form an interesting direction to further study the mechanisms of DSB repairs in GBM cells.

This result is the most significant of the project, as it validates the functioning of the scaffold design and proves that it effectively models an environment closer to *in-vivo* conditions. It also validates the methods and protocols–many of which are novel–used to carry out the experiments.

3.3.2. Cell Morphology

The Hoechst-Phalloidin staining was used to visualise the morphology of the cells in 2D and 3D. With 2D substrates the morphologies of the cells were more spread out and occupied a much larger area with the cytoplasm spread very thin. In 3D, the cells organised around the scaffold structure and formed long processes that extended across the scaffold.

The Hoechst-Phalloidin staining was used in tandem with the SEM imaging that allowed to visualise the structures also and give a qualitative image of the interaction of the cells with the matrix. In regions of very high confluency it would not be possible to separate one cell from the other. The reduction of cell densities created areas in the cells where the confluency was lower and the cells could be effectively visualised.

Not only in their confocal images, the Hoechst-Phalloidin stained samples also made it possible to have 3D reconstructions of the samples. These reconstructions gave an indication of the nuclear arrangement within the cell, and its organisation shape and size. 3D reconstructions of the samples with the Imaris (Oxford Instruments, UK) software give a vivid visualisation of the morphologies of the cells in these structures. Figure 3.21 gives an overall view of the cell proliferation in the scaffolds. By combining layers of each confocal image taken, the software can render 3D visuals of the images. A sectional view of the 2D cells also shows the arrangement of the nucleus and the cytoplasm in the cell. The cytoplasm is spreads in all directions under the nuclei, and can sometimes be indistinguishable from neighbouring cells.

While the intention with these 3D reconstructions was also to get an image of the cells deep inside the

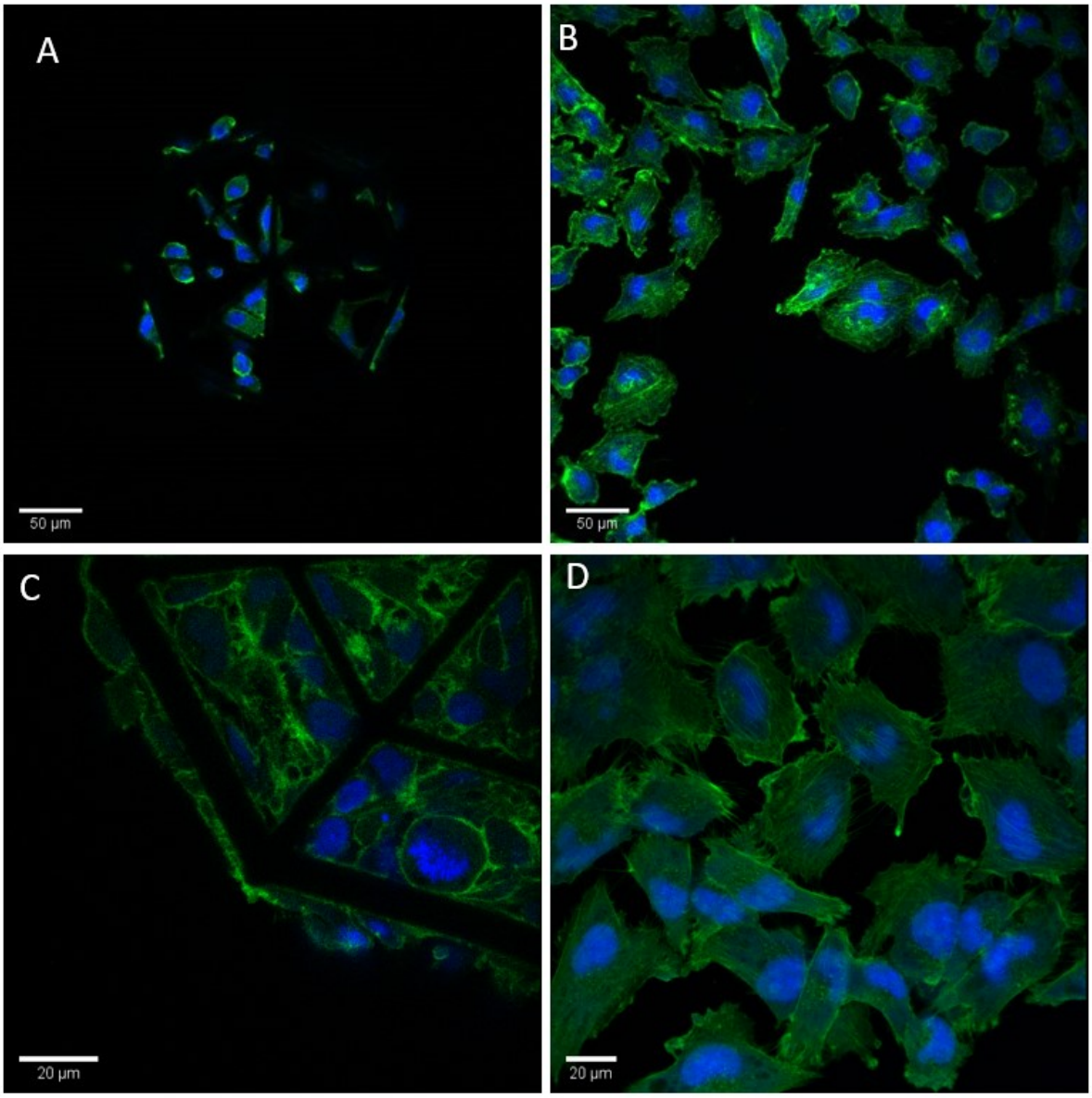

Figure 3.20: Morphological visualisation of cells in 2D and 3D. The cells in 2D show a typical spread out morphology, while the cells in 3D are more spherical and organised around the scaffold.**A:** 3D cells at a lower magnification(20x lens) **B:**2D cells at lower magnification Scale bars= 50μm;**C:** 3D cells around the scaffold at a high magnification,**D:** Cells on the 2D pedestal at a high magnification (63x lens) Scale bars= 20μm

structure, a high laser power would be needed to form those images due to a shadowing effect of the other layers of cells and the scaffolds around it. A high laser power would increase noise and image unclear, and have more leakage of signal from the edges, as well as cause bleaching of the sample which would led to a loss of information. The scaffolds were modified to make such deeper imaging possible but the images formed were not very clear. This is seen in figure 3.22

The Hoechst-Phalloidin and SEM samples were subjected to the same radiation doses as the other samples, and similar time points of fixations. The cells may have presented a change in the size of the nuclei, but not consistently across samples and experiments. Another setback with quantifying the information of the samples with respect to the scaffolds has been the difficulty to visualise the 3D structures in confocal imaging. Corresponding brightfield images could be used to super-impose the structures with the confocal images but this was not possible with the Zeiss LSM710 microscope. Another interesting observation has been the position of the nuclei with respect to the surrounding cell

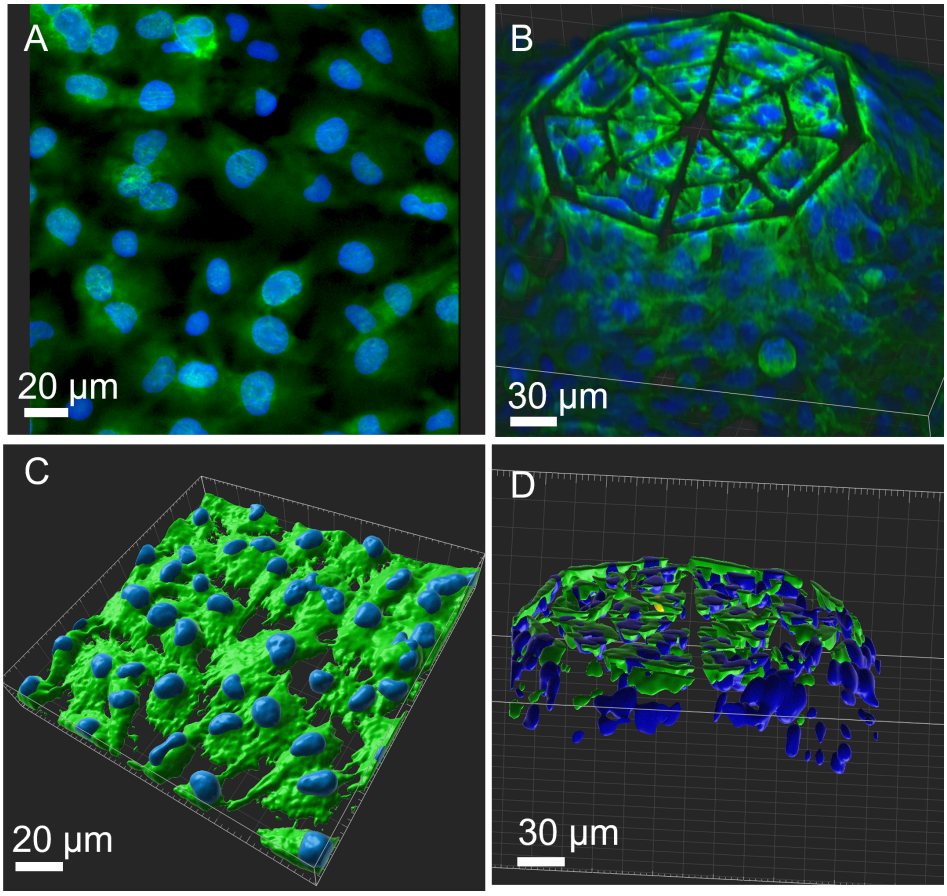

Figure 3.21: A: 3D fluorescent Image of 2D cells. The nuclei are in focus while the cytoplasm is in a different layer under the cells **B:** 3D fluorescent image of the 3D scaffold, C:Reconstruction of the 2D samples in Imaris, D Reconstruction of the top ring of the 3D structures in Imaris

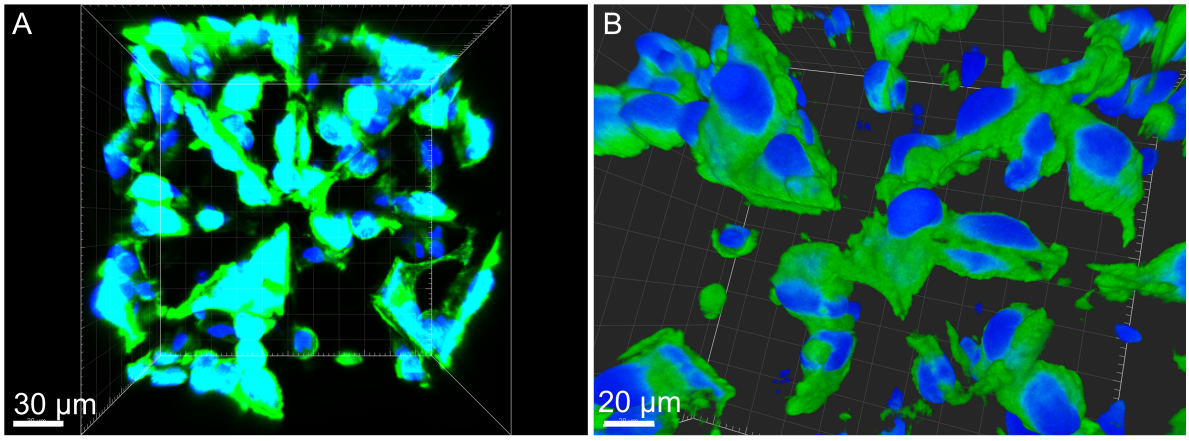

Figure 3.22: A:3D image of a deeper layer of the sample. **B:**3D Reconstruction using Imaris; The images show a lot of noise, and regions of very high fluorescence due to the high laser power. It leads to some distortions.

cytoplasm. In the figure 3.23, the sections of the 3D confocal images are seen. In the 2D configuration, the nuclei of the cells are always above the cell cytoplasm, and in the 3D organisation the cytoplasm surrounds the nucleus. This becomes an indicator of the cellular organisation in the scaffolds, and shows that there is a greater interaction of the cells with their surrounding scaffold. The cells alter their morphology to suit the environment. The table in figure 3.24 summarizes the differences between the

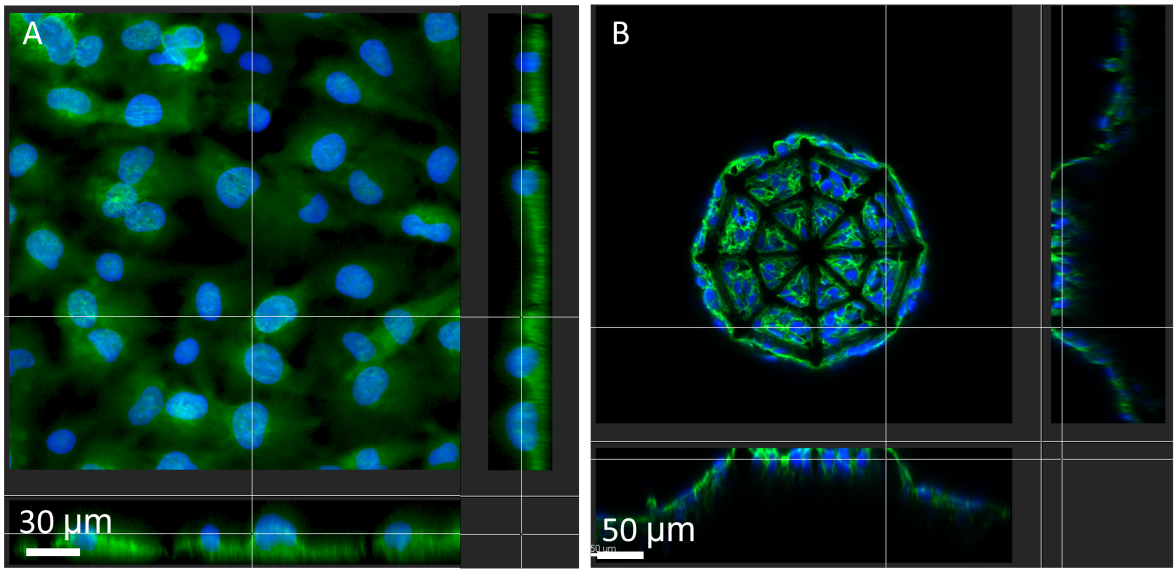

Figure 3.23: A: the sectional view of the 2D cell culture **B:** Sectional view of the 3D cell culture

2D	3D
Spread-out cellular morphologies	Relatively Spherical morphologies
Attach and proliferate on the substrate	Spindle like projections adhere on scaffolds
Cell multiplication in all directions	Migration along scaffold beams
Higher cell densities	Lower cell densities
Nucleus above most of the cell body	Nucleus embedded within the cell body

Figure 3.24: Summary of Morphological differences in cells in 2D and 3D

morphology of the cell in 2D and 3D.

The images of the cellular morphology correlate to those seen in earlier publications, with the morphology of the 3D cells being more spindle like, with numerous extensions anchoring the cells to the scaffold, while for a cell on 2D, the cells grown in an uncontrolled manner, and spread into larger sized areas on the pedestals[75]. The spherical nature of the cells in 3D better mimics the cell-morphology *in-vivo*. The morphology being a key factor in radiation response of the cells makes these scaffolds more effective than 2D glass plates[75].

3.3.3. Live/Dead Immunofluorescence

The Live-Dead IF assay shows the live healthy cells in green (stained with Calcein AM) and the Nuclei of the dead cells in red (Stained with DRAQ7™). In the observations of this assay, the number of dead nuclei observed were very few on the 3D structures, and virtually none on the 2D pedestals. The low number of dead cells in the samples could be explained by two phenomena:

1. The first one being that there is very low cell death occurring in the samples as is also understood

by the viability assays, and that the time frame at which the assay is conducted is not enough to visualise dead and compromised cells.

2. The other being that dead cells are not present on the structures because they float away in the medium. The cells are present on a small, concentrated region in the sample and not throughout the plate. Since dead cells detach and float in medium, the cells do not remain confined, but can float through the petri dish in the medium. A change of the solution from cell medium to PBS (which is required by the protocol), would aspirate any dead nuclei present. This could also be exacerbated by the transportation of the samples from HollandPTC to LUMC, during which the samples are inadvertently agitated, and could lead to the expulsion of the dead cells into the medium, which is subsequently aspirated.

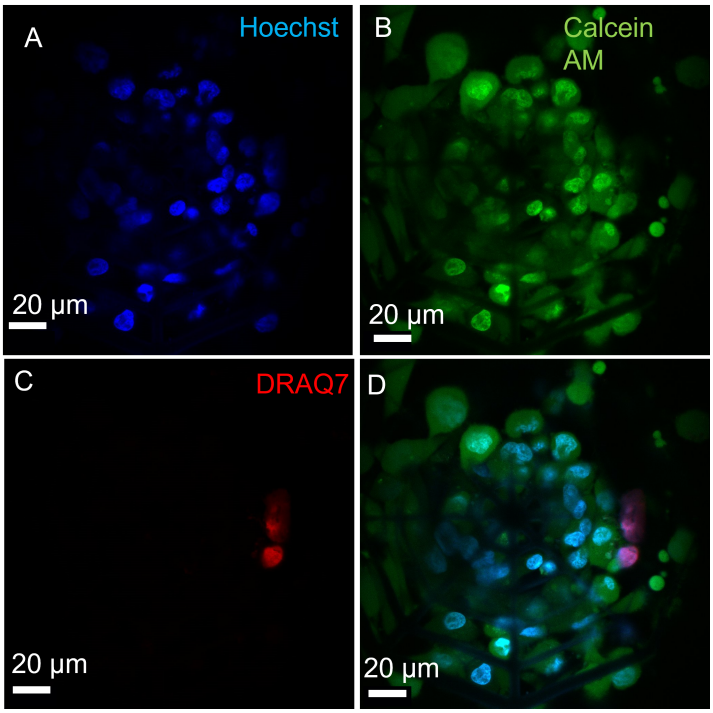

Figure 3.25: Live-Dead Assay imaging on the 3D scaffolds. Cells cultured on the scaffolds are simultaneously stained with multiple dyes.**A:**Nuclear staining with Hoechst 33258**B:**Live cells stained in green with Calcein AM **C:**Dead Nuclei stained with DRAQ7™**D:** Composite image of A,B,C

The advantage of utilising an IF method for quantification of the Live/Dead evaluation of the cells can be differentially conducted for the 2D and 3D samples. This justified the use of this assay. It would allow a qualitative and quantitative analysis of the irradiation effects on the samples. The tests and the experiment conducted with this method gave excellent images and it is a simple, high throughput protocol. This protocol is attached in appendix-A The disadvantage being that presence of dead cells on the samples would be unreliable due to medium changes and transportation, and both of these are not avoidable for conducting the proton beam experiments on the samples.

3.3.4. AnnexinV-DRAQ7

Apoptosis in cells is a complex process that can occur through several pathways. Cells enter a process of programmed death which can occur over varying periods of time and the response varies across cell types and cancers especially in cancer cells which have a very high rate of regeneration. AnnexinV is a marker that is used to indicate the early stages of apoptosis when the cell membranes becomes compromised.

The assay is conducted with live, non-fixed cells. In the images of this assay, the AnnexinV antibody is visible along the membranes of the cells. In some cells, it could also be seen that the AnnexinV completely lights up the cell body too. This could be possible with particular cells that have membranes that

have been compromised due to other stresses and have too much of the antibody penetrate through it. The brightest spots of the AnnexinV staining correspond to the cells indicated with DRAQ7, and support this explanation as dead cells have fully compromised membranes that do not serve as a barrier to external materials anymore

It is also observed in the live staining of the cells with Hoechst33258, that the 3D scaffold structures are also more fluorescent. This has not been observed to this degree in the fixed staining with Hoechst. This can be seen in figure 3.26 The dye seems to somehow also affect the structures or bind to them, but not in samples that are fixed. This phenomenon is not fully understood, but the observation is noted.

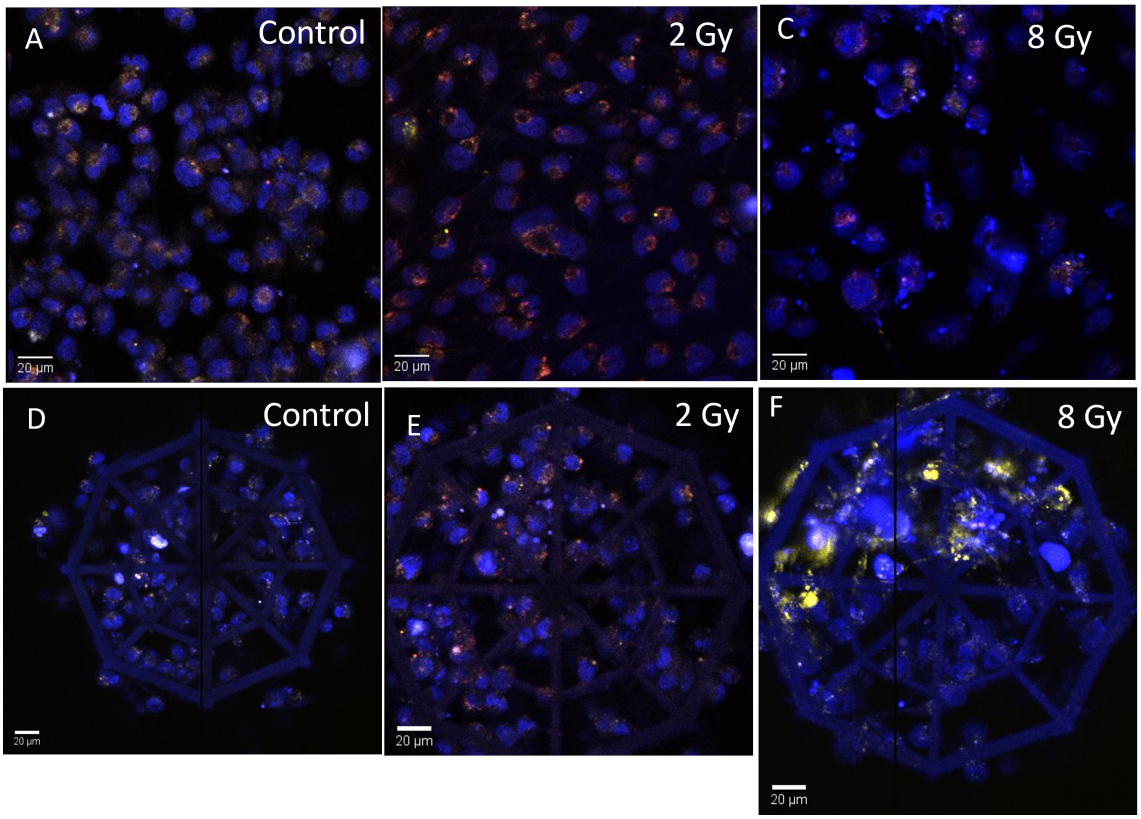

Figure 3.26: The samples are stained with AnnexinV (Yellow), DRAQ7 (Red) and Hoechst (Blue). **A,B,C:**Cells on 2D substrates **D,E,F:** Cells on the 3D substrate. The doses of radiation are marked on the upper right hand corner. The yellow spots are the fluorescence of the AnnexinV-PE conjugate. All Scale bars =20μm

Staining with DRAQ7™further makes it possible to differentiate between cells that have died. Qualitatively, the images of samples undergone radiation and the control do not show a large difference in AnnexinV positive cells. There seem to be the formation of brighter AnnexinV-PE spots in some images but it is not clear if these spots are on the membrane or are a result of non-specific staining. The spots in figure 3.26F could also be a result of accumulation in the membrane. It does not form the expected clear cell boundaries. The optimisation of the antibody dilutions used could yield better results for the imaging. The protocol is attached in appendix-A

3.4. Viability Assay

The CCK-8 assay was implemented for various samples throughout the experiment. It is important to note that the viability assay only measures the proportion of living cells in each sample that it is tested with. The output that is provided is also an average of the 3D and 2D samples and all the cells present on the plate, and does not distinguish between them since the scaffolds are printed on the same glass slide. The test was carried out for sets of samples with the control, 2Gy and 8 Gy, after it had been optimised for the solution that would be required per petri dish. The expected outcome

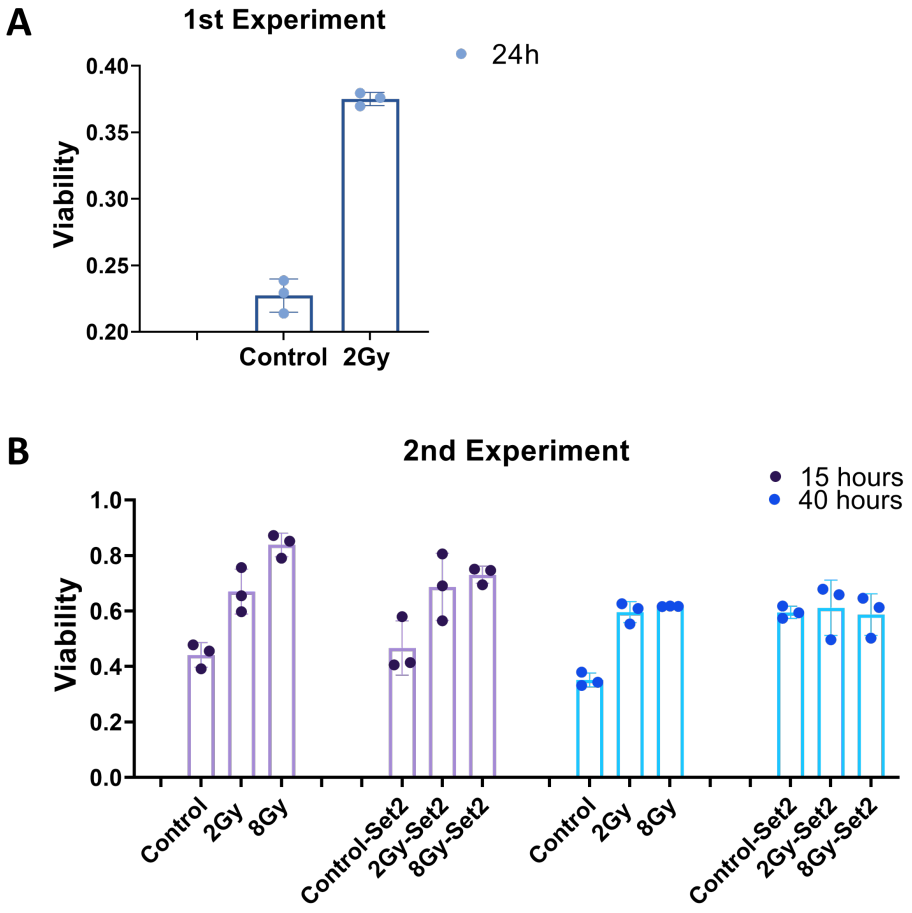

Figure 3.27: Viability graphs for the 1st and 2nd experiments.**A:**The first experiment was conducted with only the control and 2 Gy.The 2 Gy sample shows a higher cell viability than the control.**B:**2nd Experiment with multiple time points, and two different sets of samples. A higher dose shows a higher viability, which is opposite to the expected trend. Over time (from 15 to 40 hours), there is a reduction in viability for the 2Gy and 8Gy samples.

was to have a decreasing viability with an increasing dose of radiation. The test is a standard method used in literature and has yielded similar outcomes for the experiments. That has not been the case for the assays carried out for these experiments. In this experiment the results of the viability assay have differed between experiments, and in some cases shown greater number of cells in samples exposed to higher radiation doses.

The inconsistency of the results could be attributed to the time-points used for the analysis of the samples and the characterization of the samples before irradiation to ensure a similar number of cells were present in each sample. Due to the large amount of the dye required for the assay, the test had to be done with a less extensive manner, with only certain tests carried out based on previous results. The assay was studied for the samples immediately after irradiation, after 15 hours and after 40 hours too. The justification for the longer time points is that the cell-death induced by radiation, can also take longer time to occur. Since the cells become apoptotic after irradiation, the literature basis also implied that that a greater percentage of cells are positive for late apoptosis at 48 hours [76].

The cells were allowed to incubate for those periods of time, and then tested again for viability. Since the assay itself is non-toxic. For time-points test the same samples were by washing with PBS and adding new CCK-8 reagent. The results of these tests are summarised in the graphs shown in figures 3.27 and 3.28. The 1st experiment was conducted with only the control and 2 Gy, in which the samples show an increase in the number of cells. The 2nd experiment was carried out with two sets of samples

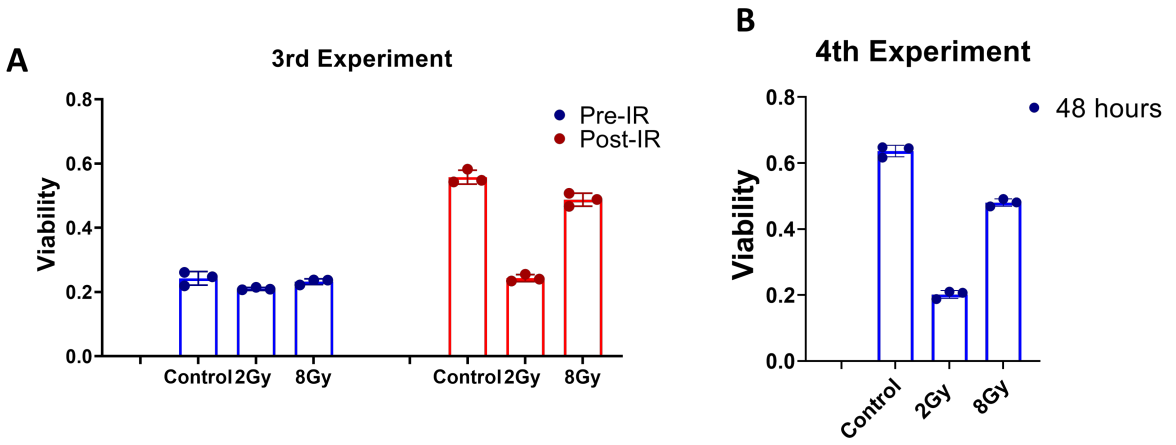

Figure 3.28: Viability graphs for the 3rd and the fourth experiment.**A:**Pre-IR refers to the viability assay carried out before irradiation and Post-IR refers to after irradiation. The aim was to characterize the cells before the experiment. The viability of all the conditions is similar, implying that cell numbers seeded are fairly constant. In Post-IR, the viability of an 8Gy sample is higher than 2 Gy. **B:**Experiment 4 is conducted at a 48 hour time point, and shows a viability trend similar to experiment 3

at two time points (15 and 40 hours). For both the samples, the cells showed a marginal increase in viability compared to samples irradiated with 8 Gy. To eliminate doubt, for the 3rd experiment, the cells were characterised before irradiation and showed a reasonable uniformity in the cell viability. After irradiation a decrease in viability for the lower dose and increase for the higher dose. For the fourth test the assay was conducted after 48 hours, and it replicated the results from the 3rd experiment.

To ensure that the errors found in the results were not an outcome of an uneven cell culture, the cells were characterised before irradiation which gave an output of similar number of cells per sample, and after irradiation gave the unexpected outcomes of an increase in cell number for higher doses. Making any solid conclusions for this assay has been tough due to the inconsistency of the data, but a few possible explanations seen have been enumerated below:

1. The mechanism by which the cells are undergoing apoptosis and death, or repair and continued proliferation are not fully understood with respect to proton beam irradiation. While there is some precedence to the method with other charged particle beams, the response of the cells with respect to 3D cell culture and irradiation could vary in this combination of parameters.

2. The damage induced in the DNA as indicated by a consistent Gamma-H2A.X marker, would not necessarily imply that the cells are entering the apoptosis cycle or death, and there could be the presence of mechanisms that lead to repair, or an increased rate of proliferation of cells. While this is not seen in most *in-vitro* studies, clinical data shows a very high rate of recurrence of Glioblastoma in patients, even with the sue of very high doses, and the presence of 3D structures could be the reason for these spikes in cell growth.

3. The last reason could be that the use of proton beam irradiation in the samples affects the enzyme (hydrogenases) produced by the cell which are required for the formazan dye production, and the response is inconsistent due to how radiation affects the enzyme itself, or its production in cells, giving an inaccurate output for the assay.

The output of the assay is also an average of the cells present in 2D and 3D on the samples, and therefore pin-pointing to the cause of the inconsistency as a result of the morphology is also not substantial.

3.5. Scanning Electron Microscopy

Scanning Electron Microscopy allows the visualisation of cells and structures at resolutions that cannot be achieved by other methods. The process is to fixate the cells using a slow fixation method with

Gluteraldehyde, and then dehydration with HMDS and Ethanol.

SEM is used as a tool for the morphological evaluation of the cultured GBM cells. When compared between 2D and 3D environments, the cells show distinct differences in their morphology that correlate with the images seen via IF. The 2D cells have a flat, spread out morphology with a raised central surface which is the nucleus. On the 3D structures, the cells form very long processes that are much longer than the cells itself. The cells adhere to the surface of the 3D scaffolds quite extensively. Additionally in the 2D samples very fine extensions can be seen between individual cells. These extensions are probably the nanotubules that have been observed in other GBM cells. There are specific antibodies to identify these tubules, but it can be visualised well with SEM. These tubules play an important role in the cell-cell interactions of the GBM cells. It may also contribute to drug an radiation response[77].Figure 3.29 shows the comparison between 2D and 3D cells. In the 3D configuration the cells attach to the

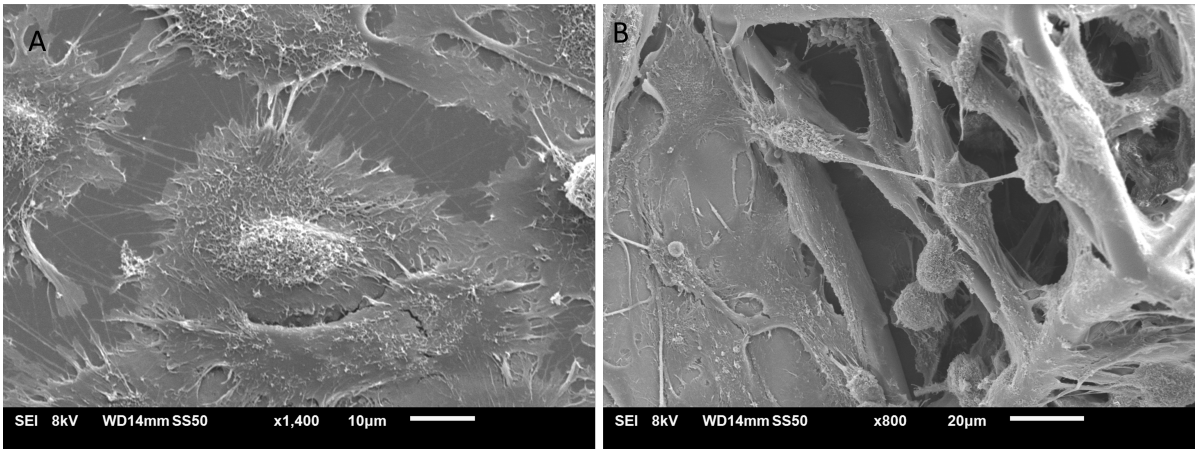

Figure 3.29: A: Cells cultured on the 2D substrates showing the typical spread out morphology of cells. Very fine tubules can be observed between individual cells **B:** 3D environment of the cells in which long processes can be seen extending from a single cell.

beams of the scaffolds extensively. These extensions are thicker and seem like the extension of the cell cytoplasm. These extensions are a characteristic of GBM cells and play an important role in cell migration and invasion [78]. These tubules can form extensive networks and are the methods by which the cells interact with one another. These extensions are seen more prominently in 3D scaffolds, and very dense region of the 2D cell cultures (where extensive networks would be formed), and that agrees with the observations that are made in 3D *in-vitro* and organoid models of GBM [78].The models of invasion are complex, and the development of better high-throughput methods are needed to quantify this information [78]. These processes can be seen in image 3.30

The SEM images in this experiment also corroborate the earlier observation that cells grown on 3D cell cultures have a more controlled growth and show lower rates of proliferation[75]. The 2D regions of the cells around the show lesser number of cells when compared to the region away from the scaffolds. This difference is more clearly visible when the cells are not a 100% confluent on the surface. This can be seen in figure 3.31

In the 2D regions the cells do not grow a particular direction, unless a very large mass of cells is present. Then the cells seem to migrate toward that region in 2D. The large mass of cells acts as an attractant to cells around it. This can be seen in the figure 3.32. In the 3D environment, many cells are seen at the nodes of the structure, along the inclined beams and stretched in between the lateral beams. The cells utilise the structure as pathways for migration. The direction of their movement cannot be determined without a time-period study, but it is known that cells migrate using blood-vessel architecture [18]. This observation can justify further study into the migratory behaviour of the GBM cells in 3D. The growth of the cells on the scaffolds can be seen in figure 3.34 The samples were also compared for between control and irradiated samples. Figure 3.34 shows a comparison between control 8 Gy-irradiated samples. These samples are fixed at about 12 hours after irradiation.There are no observed differences between the morphologies of the cells.The densities of the cells in the

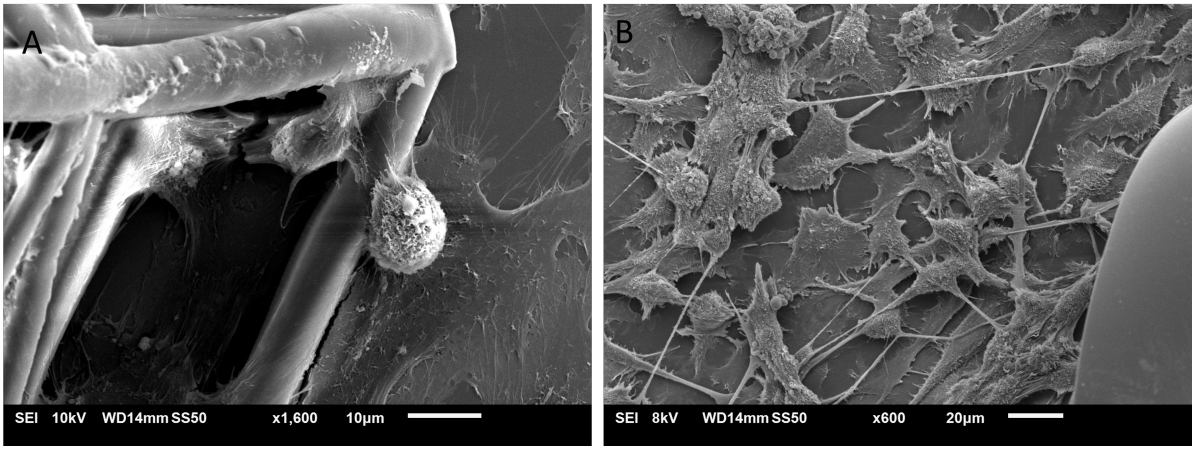

Figure 3.30: A: Cells growing on 3D environments with a spherical morphology and formation of processes that attach the cell to the scaffold. **B:**Cells in the 2D configuration also showing the formation of long processes in very cell-dense regions.

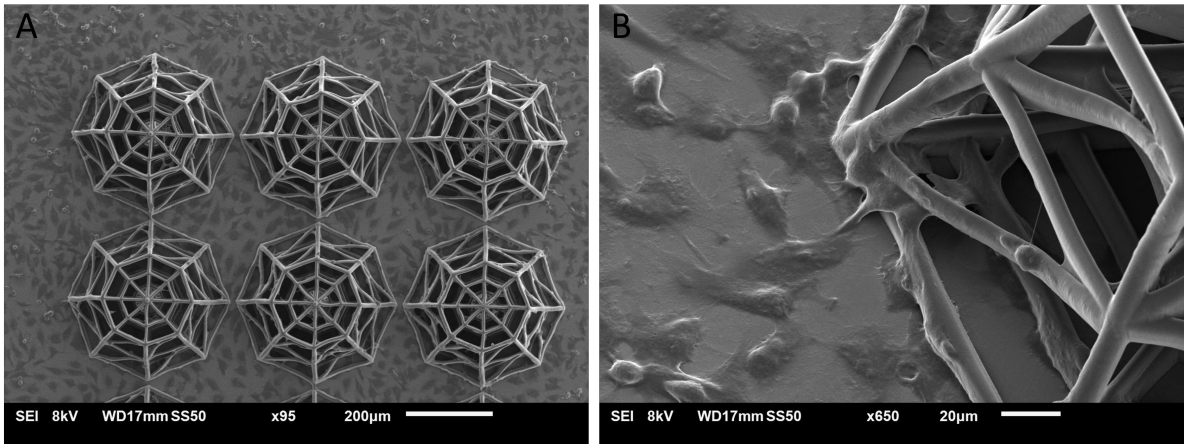

Figure 3.31: A: Regions in between scaffolds have lower cell densities that the regions around it, although they have been cultured together with the same density of cells. These samples were part of a test and cultured for a shorter duration of time (3days) **B:** A high magnification image of the scaffold base from A

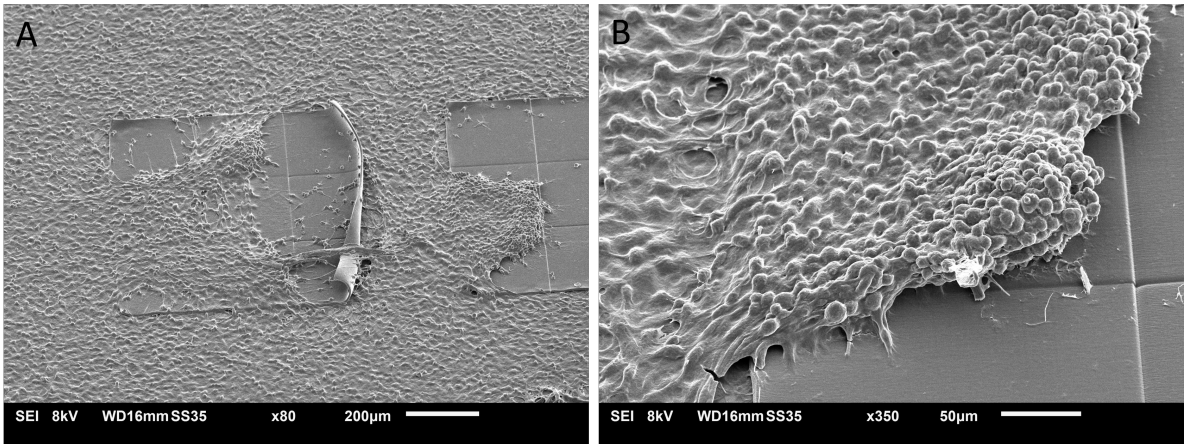

Figure 3.32: A: 2D pedestals with a very high confluency in the processes for forming aggregates **B:** Magnified view of the formed aggregate on a pedestal

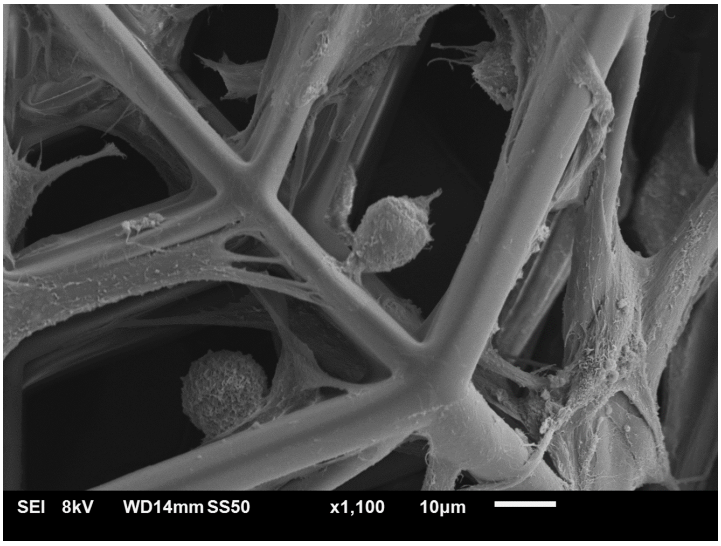

Figure 3.33: A typical view of the GBM cells on the scaffolds. The cells are present in between lateral beams, on inclined beams, and and in the corners formed by the structures attached to more than one beam. The cells proliferate the structures quite successfully.

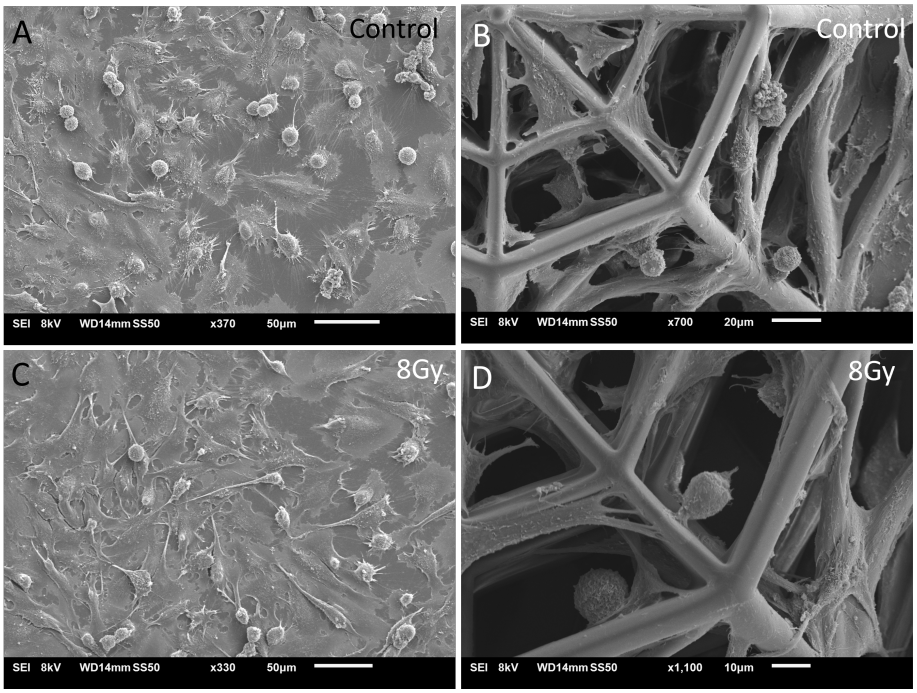

Figure 3.34: A: Cells in the control Sample on 2D**B:**Cells on the control sample in 3D scaffolds**C:**Cells on the 8Gy sample on 2D**D:** Cells on the 8Gy sample in 3D. No specific differences between the control and 8 Gy samples.

images are comparable, and does not show a large decrease in the 8 Gy. Although these results are not expected based on previous literature mentioned in this report [75, 48], they are consistent with the results of the other tests in the project. The cells show a high foci formation but not increased cell death in confocal imaging.

The development of the HMDS protocol is an important outcome of this method as it becomes possible to make more reliable observations of the cells, their morphologies, and the surface details of the cultured cells. Smaller extensions and cilia on the surface of the cells that could not be seen with an

ethanol-only protocol, could be preserved with HMDS. The implications of these results can go further beyond the scope of this project, and be used as a reliable high throughput method for cellular and 3D morphological studies.

4

Conclusions and Recommendations

This report provides a comprehensive overview of the project, and the directions selected for the experiments were done while keeping the original research questions in mind. In the conclusion, the extent to which these questions have been answered is discussed, and other insights that were found during the course of working on this topic.

The research questions mentioned in the section 1.4.1 are answered below. Some of the questions could be answered with reasonable confidence, some of the other questions posed caveats which have also be detailed.

1. Is replicating features of the vasculature effective for GBM?

The blood vessel architecture of the brain tissues provides a nutrient-rich and structural region for the adhesion, proliferation and migration of the cells. The 3D scaffolds were designed to mimic the branching-points of the vasculature of the brain. The blood vessels branch in a dendritic fashion and create a network and architecture on which glioblastoma tumour cells are known to proliferate. The formation of these mass of cells can be a result of the nutrient rich environment of the blood vessels, but there is also suggestion that the blood-vessel endothelium also contributes to providing a structural environment for the cells to adhere and grow on.

Within these scaffolds, the use of angular beams, and inclined beams in the structure provide complexity to the design without obstructing the field of view that would be needed for microscopes. These extra beams provide support to make the scaffolds stronger, but are also effective in adding variation and dimension at the nodes. The blood vessels in the brain expand and grow in all directions and have a large variation in sizes. Glioblastoma cells itself vary in dimension significantly between 2D and 3D environments, but an average of 20μm made it also necessary to have the features of the structures comparable to the size of the cells.

The iterative method of changing the design made it possible to document the variation that each change could bring to the design and the improvements each alteration provided. While using the earlier hexagonal pyramids, the structures did not effectively capture cells, but a reduction in height and increase in surface area made the samples more effective for culture and retained the characteristics from the original design idea. The final change to reduce some beams in the topmost layer of the structure was necessary from an imaging point of view, but the robustness of the structure, and its effectiveness in culture was not affected. It did not reduce the number or quality of cells that could be observed under the microscope. It is reasonable to estimate that cells would be adhered to horizontal trappings in the scaffolds more than the vertical ones during culture. In the SEM images of cells at the end of the culture period of 5 days, GBM cells can be seen on all the inclined beams of the structures. This suggests that the cells utilise the pathway of the inclined beams to migrate across the structure. Mimicking the vasculature, even without the presence of additional nutrient flow or functionalization, proved to be an effective method to enhance cell proliferation on 3D structures.

While it can be difficult to compare the rates of proliferation in the cells between 2D and 3D, since the regions are not confined spaces, the confluency of the cells in the regions around the scaffold was consistently observed to be higher than that in the 3D regions of the cells. In some cases a lower cell confluency in the regions around the scaffolds, implying that the 3D structures also limit the cell

proliferation as compared to 2D alone. This is a characteristic of *in-vivo* and 3D cell cultures, and is consistent with the state of the art studies with 3D cell cultures.

The design itself proved to be effective toward the stresses that would be induced by cells on it. Research has suggested that rougher surfaces provide for better migration and proliferation of cells [79]. The resolution of printing for these scaffolds would produce surfaces with a roughness and unevenness, which could be a contributing factor to the effective colonisation of the structure [79]. Figure 4.1 shows the surface roughness of the beams on the 3D scaffolds. The scaffolds required no other functionalization with biochemical coatings such as Laminin or collagen, making IP-Visio printed structures effective and high-throughput.

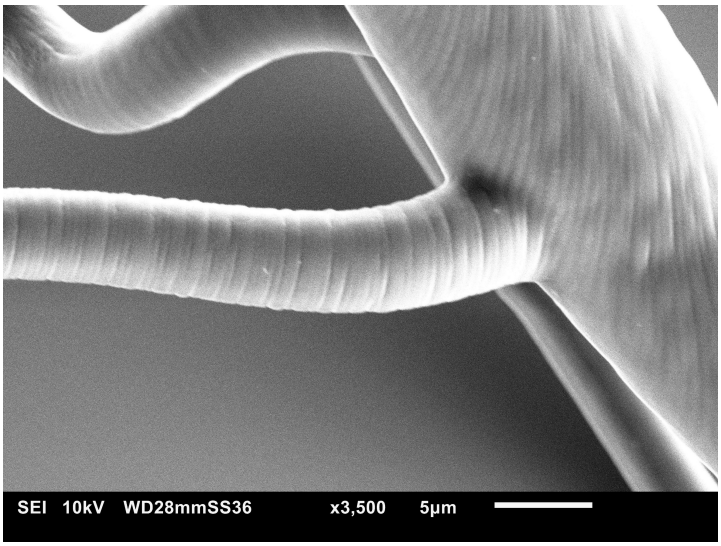

Figure 4.1: Roughness created on the surface due to the slicing and hatching parameter. It is only visible at a very high magnification

The use of two photon polymerization to print 3D structures for cell cultures has promising results with the samples in this project. 2PP provides the flexibility required to engineer these scaffolds based on specific biomimicry criteria. Laser Power and scanning speed value are recommended by Nanoscribe for most resin-lens combinations. Using these recommended values and settings as starting points of optimization can save a lot of time during design and fabrication

Conclusive tests were conducted with silanization of the samples with MAPTMS, before printing. Using a 2% v/v concentration of MAPTMS in Ethanol, gave very good adhesion of pedestals to the structures, and had no negative effects on the 3D structures. Silanization is also not cytotoxic to cells at all, and does not affect cellular characteristics. A combination of IP-Visio 3D structures with a silanised substrate also did not require any other functionalisation for effective colonisation by the cells. The MAPTMS protocol has since been used by other users of the Nanoscribe attempting to improve adhesion, and it has shown promise for many other resin-substrate combinations.

2.What differences in proton beam radiation response of GBM can be seen between 2D monolayers and 3D scaffold cultures?

This question is also answered with the results of the Gamma H2A.X Antibody experiment. The differences in the morphologies of the cells, and their organization on both these structures shows a clear difference in the way a 3D environment can alter the cells. These changed characteristics would also certainly be responsible for the resistance that cells can develop to irradiation, and a self defense mechanism, and radioresistance.

Through the course of this project, it became more important to define “damage” more specifically in the studies. The double strand breakage in the nucleus of the cells is very clearly seen differently between 2D and 3D with various radiation doses. Higher doses providing greater damage, and the cells in a 3D orientation having characteristics that show reduced DNA DSB.

The experiments that are conducted with cell-death, apoptosis and live cell proportions do not necessarily correlate to this information. This could imply that the processes by which the cells eventually die after ionizing radiation are not straightforward correlations. It could be possible that the cells have mechanisms of repair, that alter the results from expectation. Higher doses do not cause greater cell death, even when studied for time periods upto 48 hours.

Cell viability studies with CCK-8 were conducted in many research papers with reliable outcomes. It did not give conclusive results for this experiment.A more extensive investigation into the results CCK-8 is recommended. Although it is a high throughput and relatively easy method to characterize cells, finding another immunofluorescent method for the evaluation of dead or apoptotic cells, would give outputs that could also be distinguishable between 2D and 3D environments, and could evaluate that difference better than CCK-8. The results of the CCK-8 tests also average the output for cells in 2D and 3D simultaneously, and would therefore not be further recommended for studies with such integrated scaffolds.

That being said, apoptosis of cells is a very vast and detailed topic, and certainly requires a dedicated study associated with the topic, in terms or literature and optimization, to effectively use immunofluorescence or other tools to identify the markers, and cellular responses to radiation.It is therefore recommended that with respect to U251 studies it is essential to attempt additional correlating assay from the inception of the project.

The Live/Dead assay (DRAQ7, Calcein AM)and Apoptosis Assay (AnnexinV-PE) used in this experiment form a good starting point to have reliable results from these assays. Optimisation of timepoints, concentrations of the dyes, and the use of specialised buffer solutions, become important considerations for the improvement of these assays. Counterstaining with other dyes that indicate the cell morphology clearly (Such as Phalloidin) could also provide clearer indications to where the sites of the antibodies are present and whether the membrane specific staining is also being observed. It would further assist in the optimisation of the staining protocol.

3. Do 3D scaffolds affect the efficacy of Proton beam irradiation on the GBM culture?

This question was aimed at eliminating the structural hindrance to irradiation that could occur for the cells, and to understand that the response to irradiation is not altered due to the presence of the structures. An important insight through the course of the project has also been that these cells in *in-vivo* conditions do not exist in isolation, they exist within a complex network of cells, blood vessels, tissues, nutrients and an extra cellular matrix. The presence of these structures do not alter the dose deposited itself because of the very advanced ballistics and targeting of the beam that provides a very uniform dose in its field. The presence of this matrix though, is a better replication of the environment with some of its complexities, and makes the response more comprehensive that with 2D monolayer studies alone.

The main question that encompasses the overview of the project is:

How do 3D Engineered Glioblastoma microenvironments respond to Proton beam Irradiation?

With the aim to create create a reproducible bio-artefact, optimized to routinely assess GBM behavior and Proton Beam irradiation effectiveness, the 3D engineered microenvironments, and the subsequent protocols for cell culture and staining provide a robust method to evaluate GBM response to proton beam irradiation. Specifically, the engineered GBM microenvironments, which promote a 3D spatial arrangement of cells closer to *in-vivo* configuration, displayed a lower amount of DNA damage upon proton irradiation compared to 2D cell monolayers.

5

Future Work

This project has been unique in its scope and application of combining various aspects of 3D cell Culture, and radiobiology, with engineered microenvironments. It is a pilot project under the TU Delft Health initiative grant, and forms a starting point for evaluation of not only Glioblastoma cell lines, but the principles could also be applied for studies of other cancer types and engineering environments for them.

Considering the continuation of this project, the samples have to be tested and validated for other cell lines first. It could also be expanded with patient derived primary cells, once the robustness of the design can be established across cell lines. From studies it is known that the behaviour of primary cells is vastly different from cell lines, and the responses of these cells to these environments and radiation would be a step further in understanding GBM. The projects can also include correlating information with specific immunofluorescence markers for proliferation, migration, cell maintenance, radioresiatance etc.

The other interesting aspect to consider is the co-culture of Glioblastoma cells with endothelial cells on these structures. A successful culture of endothelial (blood vessel cells) cells could provide an a very effective blood vessel mimicry *in vitro*. The response of GBM cells to the mechanical characteristics of this structure, along with the biological functionalisation of cells, would make a better mimetic scaffold. The current design only takes inspiration for the structural aspect, but a co-culture with endothelial cells could also provide biological cues and signals to the GBM cells. The project in its scope can also further include radiation or chemotherapeutic studies.

A further extension of the project can be to then establish nutrient or chemical gradients with these 3D cell cultures, and study the migration and proliferation of cells in 3D, and if this behaviour is changed by radiation applications to the cells.

6

Reflection

During the course of this very collaborative project I acquired many new scientific and technical skills. As someone with a background of mechanical engineering, many of the aspects of the research have been an opportunity to learn and grow. Form planning and the literature survey, to executing the experiments, and working with various teams to bring this project to fruition, the experiences that I have gained are invaluable. Even before beginning my thesis on this topic, I joined the Micro and Nano Engineering specialisation with the intention to work on biomedical applications of the field. During the selection of my masters thesis topic, this particular project resonated with my very enthusiastic interest in the field, and presented a chance to make good on this intention. I am very grateful to Dr. Angelo Accardo for selecting me to work on this project, when I presented no other technical skill, except my enthusiasm, and an incredible curiosity to work with something so fascinating.

During the course of my literature survey, I was humbled to say the least. The possibilities and the research conducted in this field is immense, and evolves so rapidly. It came with a period of attempting to understand the disease itself, and its devastating outcomes for those suffering with it. This became the cornerstone of my work, to ensure that I never lose sight of why this research is important. It has been the source of my motivation to continue working, and better understand any aspect that I was considering for this project. These in-depth studies on specific topics is not something I have conducted often during the course of my education, and it taught me to be organised, and more importantly, to ask questions. I come from a culture where one can often be rebuked for asking an obvious question, and as banal as it may seem, it took some courage to ask innumerable questions, not only to my supervisors, but also to myself. Being able to freely question the work that other scientists are conducting, and drawing my own conclusions from it was a tremendous outcome of my literature survey.

The next was to plan this project. Considering its many facets the only way for an organised research was to meticulously plan for eventualities, and possible outcomes.The original plan included alternate research timelines in case of unsuccessful outcomes at various stages, and gave me the confidence to move ahead with the work. On top of that, working within the restrictions put upon us by COVID-19, it became imperative to include that reality in my timeline. It forced me to be organised, to express my realistic expectations and to stay grounded during my work. Even while delays could be expected, a framework to fall back on gave me assurance of my work.

I completed my literature survey in November 2020, and then immediately began experimental work. During the initial stages, there was consideration that the cell culture part of the project should be off-loaded to another member of the team at LUMC, as it may have been too much to do in a short time frame. At the time I distinctly remember my supervisor at LUMC, Dr Araci Rondon, asking me “Do you want to learn how to do it?” and the only answer I had was yes. And that was that. She expressed that faith in me, and painstakingly trained me for the work in sterile lab environments. I am very glad that I took those steps then, and learnt the tasks, because it came very much in handy toward the later stages of my project. It made me responsible for every aspect of my project, and giving me the chance to make changes and alterations.I learnt through my experimental work the respect I have for the independence I express in other parts of my life, and being able to expand that into my own work made the process very satisfying. I learnt to communicate quickly and effectively and to not mince words.

I was pleasantly surprised at how willing all my colleagues were to provide their help, inputs and suggestions, or sometimes even act as sounding boards to help me organise my thoughts. They have been my critics too, and pointed out errors that I may have overlooked, and without their help this project could not have moved forward. The delamination of the 2D pedestals was a particularly stressful period of the project, when it seemed that no solution that I was attempting was being fruitful, but persevering through it, I found a solution that worked with using MAPTMS for silanization, and that was a small victory. I could not fully determine the cause of the delamination, but it has led to a great possibility of using these structures in to create samples that could change over time, and could be useful for projects that demand more dynamic scaffold designs. It taught me that the fruits of labour in experimentation can sometimes come slowly, and patience is definitely a virtue here

Working for the experiments at Holland Proton therapy centre is is not an experience that is awarded to many masters students. Working with other researchers, and the many applications for which this technology is being used has been fascinating. On some days, it involved working at odd hours, and even the weekends, but the support of my supervisors, helping me transport the samples between Delft and Leiden, and the colleagues who stayed with me at the labs, made the journey very enjoyable. I kept reminding myself of the fact that this research could be a small step forward in understanding glioblastoma better and that kept me going. The work that I put into this project, has truly been its own reward. I learnt to create creative solutions to problems. I developed what I now call the “Cell-box” to develop a 3D printed carrier for the petri-dishes and to carry them in a plastic lunch box to make it easier to handle the samples during transport.

In this year, I have learnt to be more confident in my work, and to defend the process I used to work with something. I started with a less critical scientific perspective, and that has grown through the year I have spent on this topic. I learned that working with the technical aspects of the project was my forte, and I needed to spend more time in sharpening my scientific acumen. On a personal note, some friendships that I have cultivated during this project with my colleagues, is an immeasurable resource that I will carry with me. I am proud of the work I did in this year, and the growth I have had. I hope this project further contributes to valuable and exciting research in the field.

A

Cell Culture and Staining Protocols

A.1. Cell Culture Protocol

1. Samples are sterilised for 10 minutes with 70% Ethanol inside a flow cabinet.
2. Sampels are washed twice with PBS and allowed to air dry inside the cabinet.
3. Cells are trypsinised using 1ml of Trypsin (2.5%, Gibco) from a flask or dish, centrifuged and counted.
4. Fresh cell suspension made as per the density of 50,000 cells/ml.
5. Suspension is made in Dulbecco's Modified Eagle Medium (DMEM), with 1% L-Glutamine, 1% Pen-strep and 10% Foetal Bovine Serum.
6. Cells are seeded in droplets of 75 μL on the scaffold regions
7. Cells are allowed to adhere for 1 hour in the incubator at 37 deg C and 5% $C0_2$
8. 5ml of DMEM is added to the dishes, and the samples are cultured for 5 days before irradiation.

A.2. Direct Immunofluorescence Protocol with DAPI-Phalloidin

1. Cells are washed with Phosphate buffered saline (PBS). Two times.
2. Cells are fixed for 15 minutes in 4% paraformaldehyde solution in PBS, then washed 4 times with PBS.
3. Cells are permeablized with 0.1% Triton X-100 in PBS for 15 minutes, and washed again in PBS.
4. Cells are stained with a 50μg/ml fluorescent Phalloidin-FITC conjugate solution in PBS for 40 minutes at room temperature.
5. Washed several times to remove unbound conjugate.
6. Conterstained with a 1:1000 dilution of Hoechst33258(H-3569 Molecular probes) in PBS fo0r 5 minutes at room temperature.

A.3. Indirect Immunofluorescence for Gamma-H2A.X

1. Wash the cells 3x with PBS.
2. Fix with 4% paraformaledhyde in PBS for 15 minutes.
3. Wash 4x with PBS (directly staining or store in refrigerator with PBS).
4. 0.2% Triton in PBS for 15min for permeablization of the membrane and intracellular staining.
5. Wash 1x with PBS.
6. Incubate in 5% Bovine Serum Albumin (BSA) in PBS from 30min to 1h (IN A HUMID CHAMBER, room temperature) - to block nonspecific sites.

7. Incubate the primary antibody in PBS or 1% BSA / PBS. The Anti-Gamma-H2A.X antibody (ab81299, abcam) is used with 1:250 dilution. for 1h, room temperature.
8. Wash 2x with PBS.
9. Incubate with using FITC (Goat anti-Rabbit IgG, A11008, Molecular Probes)secondary antibody with a dilution of 1:500 in PBS 1% BSA in PBS for 1h. IN WET CHAMBER, room temperature
10. Wash 2x with PBS, for 5min each.
11. Do negative control without the primary antibody, counter stain with Hoechst33258(Molecular Probes). (1:1000)

A.4. Immunofluorescence with Unfixed Cells. Live/Dead Assay

1. Prepare Calcein AM (C3099, ThermoFisher, 1mg/ml) in a dilution of 1:3000 of the original solution in cell culture medium.
2. Prepare DRAQ7 (ab109202, abcam, 0.3mM) in a dilution of 1:100, diluted in cell culture medium.
3. Remove Medium from the dish
4. Add 100 μL of each dilutions directly to the cells. Usually in a small droplet for small quantities in the petri dish.
5. Allow to incubate for 30 minutes at 37°C.
6. Add 100 μL 1:1000 dilution of Hoechst33258 (Molecular Probes).
7. Add extra PBS (5ml) to the dish and proceed with imaging.
8. DRAQ7 can be seen with the CY5 setting and Calcein AM with the settings corresponding to FITC in the fluorescence microscope.

A.5. AnnexinV-Apoptosis Assay

1. PE AnnexinV(640907, Bioloegend) is prepared in a dilution of 1:20 in cell medium.
2. Prepare DRAQ7 (ab109202, abcam, 0.3mM) in a dilution of 1:100, diluted in cell culture medium.
3. Remove medium from the petri dish, and add 100μL of the AnnexinV-PE conjugate dilution, and 100μL of the DRAQ7 solution on the scaffold region.
4. incubate the cells for 30 minutes at 37°C.
5. Add 100 μL 1:1000 dilution of Hoechst33258 (Molecular Probes), allow to incubate for 5 minutes at room temperature.
6. Add extra 5ml PBS in the petri dish and proceed with Confocal imaging. the excitation/emission spectra for PE is 488/561 nm, CY5 can be used for DRAQ7.

B

Foci Counting with ImageJ

Macro for foci counting: The software used for this is ImageJ 1.8.0_172 found at:

https://imagej.nih.gov/ij/download.html. It is an open source software and freely available for use.

The .czi images taken form the Microscope are opened in this software. The channels are split into individual images and the macro below is run. The macro is not fully automatic, and has two regions when the image of choice has to be manually selected. The output is given as a label to the nuclear region and the number of foci maxima seen within it. The macro is written in the ”IJ1 Macro” language and is compatible with ImageJ.

The original code is sourced from :

https://forum.image.sc/t/counting-of-foci-per-nucleus/2156, and then edited for use in this experiment.

```
var tolerance = 5;
waitForUser("Select the image of Nuclei");
originalImage = getTitle();
run("8-bit");
run("Overlay Options...", "stroke=red width=1 fill=none set");
run("Median...", "radius=6");
run("Subtract Background...", "rolling=125 sliding");
setThreshold(30, 255);
setOption("BlackBackground", true);
run("Convert to Mask");
run("Fill Holes");
run("Remove Outliers...", "radius=5 threshold=50 which=Bright");
run("Watershed");


roiManager("Reset");
run("Analyze Particles...", "pixel exclude clear add");

waitForUser("Select the image for spot counting");
run("8-bit");

run("Gaussian Blur...", "sigma=1");
run("Subtract Background...", "rolling=125");

for(i=0; i<roiManager("count"); i++) {
  roiManager("select", i);
  run("Find Maxima...", "noise="+tolerance+" output=[Count]");
  run("Find Maxima...", "noise="+tolerance+" output=[Point Selection]");
  run("Add Selection...");
}
```

Figure B.1: ImageJ Code

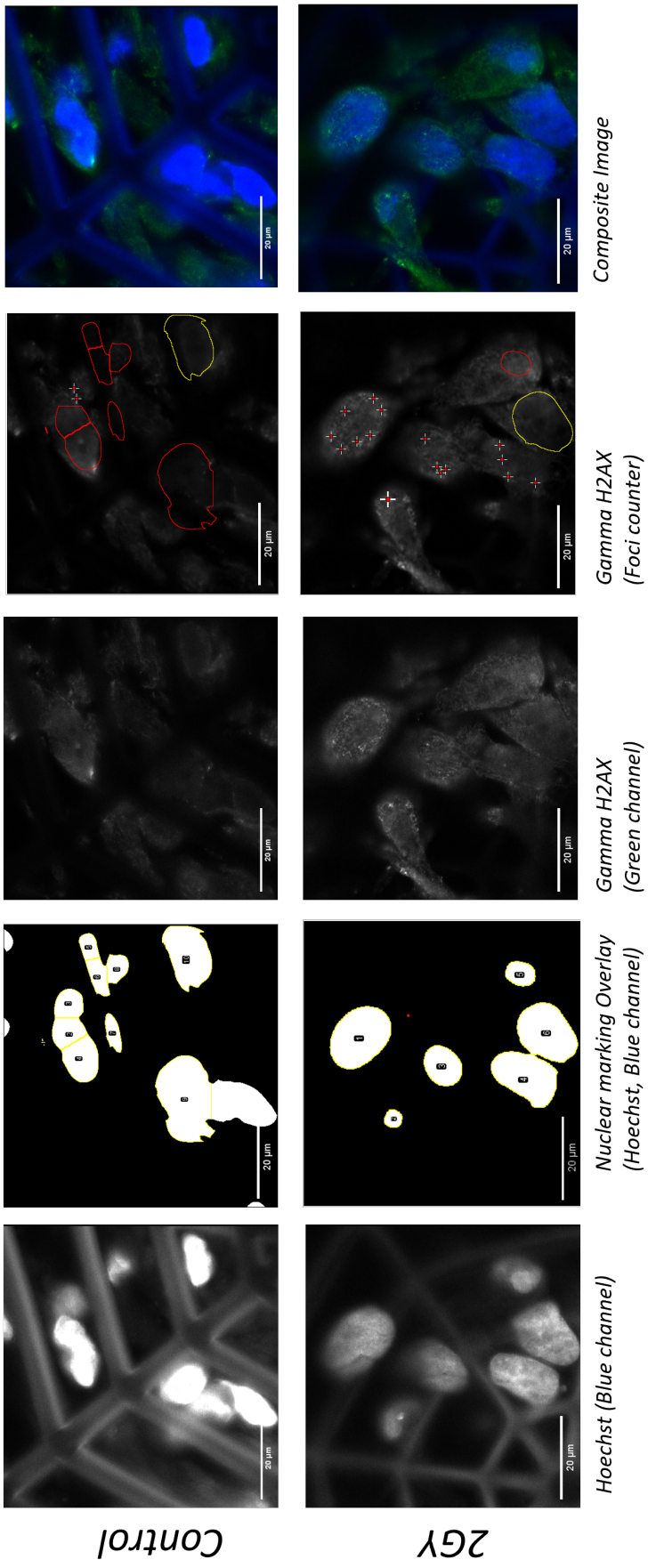

Figure B.2: The channels are separated and the nucleus channel is used to mark the boundaries of the region where the foci are counted.The sample image is shown for a sample with a control and 2Gy sample.

C

SEM Protocol

Reagents:

1. 4% Buffered Gluteraldehyde (in PBS)
2. 50%, 70%, 90% and 100% Ethanol
3. Hexamethyldisilazane (HMDS) (Sigma Aldrich)

Protocol:

1. Fix sample with 4% buffered glutaraldehyde, for 4 hours at room temperature. Fixative should be 10 to 20 times the volume of the sample.
2. Rinse with PBS 4 times for 5 minutes each with gentle agitation.
3. Alcohol series dehydration
   (a) 50 % ethanol, 4 minutes
   (b) 70 % ethanol, 4 minutes
   (c) 90 % ethanol, 4 minutes
   (d) 100 % ethanol, 4 minutes
4. Chemical drying:
   (a) (2 parts 100% EtOH : 1 part HMDS) for 15 minutes.
   (b) (1 parts 100% EtOH : 1 part HMDS) for 15 minutes.
   (c) (1 parts 100% EtOH : 2 parts HMDS) for 15 minutes.
   (d) HMDS alone for 15
   (e) let the last HMDS fully evaoprate
5. Note: Do not allow samples to dry up before the last dehydration step. Replace solutions quickly to avoid stresses on cells and structures.
6. Mount samples on holders with carbon tape and, sputter coat with the JEOL JFC-1300 Auto Fine coater with 13 nm Au and image.

D

2PP Protocol

Materials used for the 2PP Fabrication:

1. IP-Visio (Nanoscribe GmbH)
2. ITO-coated Glass substrates (25mmx25mm square slides)
3. Propylene glycol monomethyl ether acetate (PGMEA, 484431-Sigma Aldrich)
4. Iso-Propyl Alcohol (2-Propanol, IPA. Sigma Aldrich)
5. Ethanol(Sigma Aldrich)
6. Acetone (Sigma Aldrich)
7. 3-(Trimethoxysilyl)propyl methacrylate (MAPTMS,440159-Sigma Aldrich)
8. Calibrated pipette
9. Glass Petri Dish
10. 3D DiLL LF Sample holder (Provided by Nanoscribe)

Fabrication steps:

1. Prepare the .gwl job file that is read by Nanowrite software in the computer associated with the printer. For this the following steps are used:
   (a) Export the CAD model as an .stl sile.
   (b) Open the STL file in DeScribe import wizard.
   (c) Follow the steps, select the IP-Visio 25x recipe file.
   (d) Select the Slicing hatching parameters for the STL
   (e) Select array parameters
   (f) Export the GWL data file into the editor module
   (g) Edit the code and save the file as a job file(this code is shown in appendixE.)
2. Remove Glass slides from their packet, and check with a multimeter for the ITO-coated side. ITO coated side shows resistance values on the multimeter the other side does not. Keep slides facing up inside the flow cabinet
3. Rinse with Acetone and IPA. Clean any dust with a fine clean room cloth (Dastex). Dry with the compressed air gun
4. Put the slides with the ITO side facing upward in the Oxygen Plasma machine for cleaning. The parameters are 5cc/min and maximum power (80W) for 10 minutes.
5. Meanwhile, prepare the silanization solution. Remove the MAPTMS from the refrigerator about 20 minutes prior to opening. This is to avoid contamination with atmospheric moisture condensation.The solution required is 2% v/v MAPTMS in Ethanol. A final solution of 30-60ml is enough to

submerge the glass slides fully. Use a glass petri dish as MAPTMS reacts with plastic. Dissolve the MAPTMS in Ethanol.

6. Introduce the glass slides (ITO-side facing upwards) into the MAPTMS solution. Cover to avoid evaporation, and allow to silanize for one hour.
7. After 1h, remove the samples, discard the remaining solution. Clean the sample surface with minimum amount of Acetone, and the with demineralised water, and dry with an air gun. The water should form globules on the surface due to the increased hydrophobicity.
8. Open Nanowrite on the computer. Calibrate the stage, make sure the area is clear before. After that check that the minimum Z-value is reached and is displayed on the terminal.
9. Put the 25x objective in the printer, and put the felt ring.
10. Tape the clean slides to the sample holder, with the ITO side facing upward. Add small droplets of the IP-Visio resin in the centre of each slide. Avoid bubbles as they interfere with the printing.
11. Open the enclosure of the Printer and slide the holder into the grooves in with the side with the resin facing downwards.
12. Approach the sample, and find interface through the Nanowrite.
13. Load the job file into nanowrite, and begin the print.
14. After the print is completed (or aborted), remove the sample holder form the Nanoscribe.
15. Carefully remove the tape from the holder, and put the slides with the resin a Glass petri dish with PGMEA.
16. Allow the samples to develop for 25 minutes in PGMEA
17. After 25 minutes, transfer the samples to a dish containing IPA. Let the samples remain in IPA for 5 minutes.
18. After that remove and allow to air dry in the flow cabinet. IPA evaporates quickly. The samples are now ready for use.
19. Cleans the Objective lens with IPA and close the Nanoscribe.

E

DeScribe Code

```
% File generated by DeScribe 2.5.5
% System initialization
InvertZAxis 1

% Writing configuration
GalvoScanMode
ContinuousMode
PiezoSettlingTime 10
GalvoAcceleration 10
StageVelocity 200

% Scan field offsets
XOffset 0
YOffset 0
ZOffset 0


% Writing parameters
PowerScaling 1.0
var $solidLaserPower = 100
var $solidScanSpeed = 15000

% Base writing parameters
var $baseLaserPower = $solidLaserPower
var $baseScanSpeed =$solidScanSpeed
var $interfacePos = 1
```

```
%%%%%%%%%%%%%%%%%%%
% 3D Scaffold Print%
%%%%%%%%%%%%%%%%%%%
TextFontSize 3
WriteText "Oct V3" % Final Design of Scaffold
MoveStageY 300
var $i = 0
var $j = 0
for $j = 0 to 2
        for $i = 0 to 4
            % Array includes 0 in count.
            %This will print 15 samples.

% Include slicer output
include Oct V3 _data.gwl
MoveStageY 400
end
Stagegotoy 300
MoveStageX 400
end

% Writing parameters
StageGotoX 1500
StageGotoY 0
```

Figure E.1: The first half of the code

```
%%%%%%%%%%%%%%%%%%%
% 2DPedestal Print%
%%%%%%%%%%%%%%%%%%%
var $solidLaserPower = 80
var $solidScanSpeed = 50000

% Base writing parameters
var $baseLaserPower = $solidLaserPower
var $baseScanSpeed =$solidScanSpeed

var $interfacePos = 1

var $i = 0
var $j = 0
TextFontSize 30

WriteText "Pedestals"
MoveStageY 200

for $i = 0 to 2

    for $j = 0 to 2

var $interfacePos = 1

%1st Pedestal%
% Include slicer output
include 250X250X10_data.gwl
MoveStageX 247
            % 250 um pedestal, and the..
            %..stage moves 247 um leading..
            %to a 3um overlap
end
stagegotox 1500
Movestagey 247
end

MoveStageY 200
```

```
%2nd Pedestal%
var $i = 0
var $j = 0


for $i = 0 to 2

    for $j = 0 to 2
var $interfacePos = 1

% Include slicer output
include 250X250X10_data.gwl
MoveStageX 247
end
stagegotox 1500
Movestagey 247
end

MoveStageY 200


%3rd Pedestal%
var $i = 0
var $j = 0

for $i = 0 to 2

    for $j = 0 to 2
var $interfacePos = 1

% Include slicer output
include 250X250X10_data.gwl
MoveStageX 247
end
stagegotox 1500
Movestagey 247
end
```

Figure E.2: the second half of the code

F

Viability Protocol

Materials:

1. Cell counting Kit-8 (Sigma Aldrich,96992)
2. Dulbecco's Eagle Modified Medium (Gibco, 41966-029) (DMEM with 10% FCS, 1% L-Glu and 1% Penstrep)

Method:

1. Remove medium from the dishes
2. Add 3 mL of warm DMEM per dish
3. Add 300uL of CCK-8 solution per petri dish (Prepares a dilution of 1:10)
4. Let it incubate at 37° for 1.5 hours
5. Create dilutions with 100μL of respective Cell Culture medium and 900μL PBS (1:10)
6. Add 100μL of the medium from the dish in each well of the 96-well plate
7. Read with 450 nm in the plate reader.

A template layout used in the plate reader is shown in the image.Only a part of the 96-well plate is usually used. The grid is marked with numbers for columns and letters for rows

	2	3	4	5	6	7	8	9	10
B	PBS	DMEM 10% FCS, 1%PS, 1%L-glu	DMEM 1:10 Dilution in PBS	Sample U251 Control No irradiation	Sample U251 2 Gy Irradiation	Sample U251 8 Gy Irradiation	Sample U251 Control No Irradiation 1:10 Dilution in PBS	Sample U251 2 Gy Irradiation 1:10 Dilution in PBS	Sample U251 8 Gy Irradiation 1:10 Dilution in PBS
C	PBS	DMEM 10% FCS, 1%PS, 1%L-glu	DMEM 1:10 Dilution in PBS	Sample U251 Control No irradiation	Sample U251 2 Gy Irradiation	Sample U251 8 Gy Irradiation	Sample U251 Control No Irradiation 1:10 Dilution in PBS	Sample U251 2 Gy Irradiation 1:10 Dilution in PBS	Sample U251 8 Gy Irradiation 1:10 Dilution in PBS
D	PBS	DMEM 10% FCS, 1%PS, 1%L-glu	DMEM 1:10 Dilution in PBS	Sample U251 Control No irradiation	Sample U251 2 Gy Irradiation	Sample U251 8 Gy Irradiation	Sample U251 Control No Irradiation 1:10 Dilution in PBS	Sample U251 2 Gy Irradiation 1:10 Dilution in PBS	Sample U251 8 Gy Irradiation 1:10 Dilution in PBS

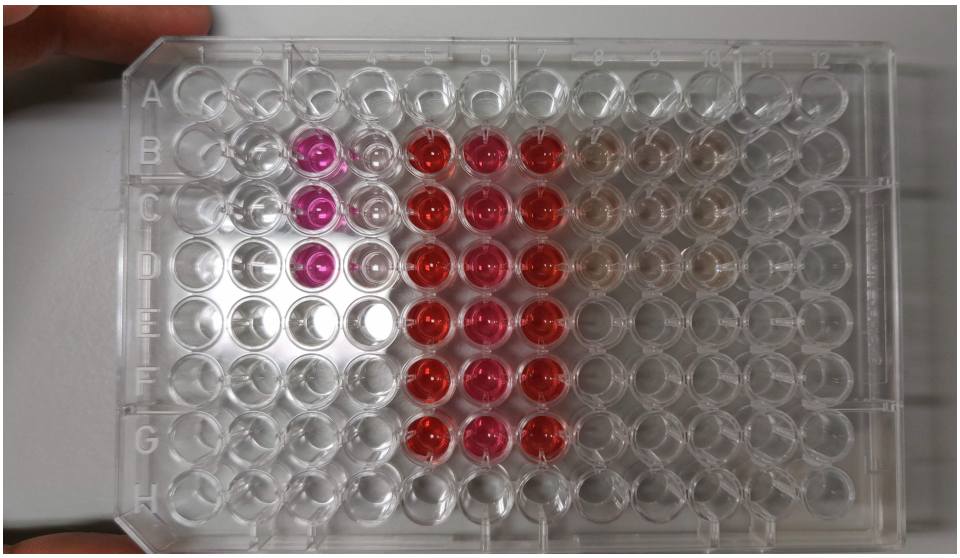

Figure F.1: The 96-well plate that is used to measure the absorbance of light in the extracted solution from the dishes

Bibliography

[1] David N. Louis et al. “The 2016 World Health Organization Classification of Tumors of the Central Nervous System: a summary”. In: *Acta Neuropathologica* 131.6 (June 2016), pp. 803–820. ISSN: 1432-0533.

[2] Hans-Georg Wirsching, Evanthia Galanis, and Michael Weller. “Chapter 23 - Glioblastoma”. In: *Gliomas*. Ed. by Mitchel S. Berger and Michael Weller. Vol. 134. Handbook of Clinical Neurology. Elsevier, 2016, pp. 381–397.

[3] Walter E. Dandy. “Removal of right cerebral hemisphere for certain tumors with hemiplegia: preliminary report”. In: *Journal of the American Medical Association* 90.11 (Mar. 1928), pp. 823–825. ISSN: 0002-9955.

[4] Shreyas S. Rao et al. “Toward 3D Biomimetic Models to Understand the Behavior of Glioblastoma Multiforme Cells”. In: *Tissue Engineering Part B: Reviews* 20.4 (2014). PMID: 24044776, pp. 314–327.

[5] Liang Ma et al. “The comparison genomics analysis with glioblastoma multiforme (GBM) cells under 3D and 2D cell culture conditions”. In: *Colloids and Surfaces B: Biointerfaces* 172 (2018), pp. 665–673. ISSN: 0927-7765.

[6] Andrew Rape, Badriprasad Ananthanarayanan, and Sanjay Kumar. “Engineering strategies to mimic the glioblastoma microenvironment”. eng. In: *Advanced drug delivery reviews* 79-80 (Dec. 2014). 25174308[pmid], pp. 172–183. ISSN: 1872-8294.

[7] Lawrence Rajendran et al. “Emerging Roles of Extracellular Vesicles in the Nervous System”. In: *The Journal of neuroscience : the official journal of the Society for Neuroscience* 34 (Nov. 2014), pp. 15482–9.

[8] Doris Lam et al. “Tissue-specific extracellular matrix accelerates the formation of neural networks and communities in a neuron-glia co-culture on a multi-electrode array”. In: *Scientific Reports* 9.1 (Mar. 2019), p. 4159.

[9] John Weingart. *Glioblastoma Multiforme (GBM): Advancing Treatment for a Dangerous Brain Tumor*.

[10] Pei Zhang et al. “Current Opinion on Molecular Characterization for GBM Classification in Guiding Clinical Diagnosis, Prognosis, and Therapy”. In: *Frontiers in Molecular Biosciences* 7 (2020), p. 241. ISSN: 2296-889X.

[11] Cancer Genome Atlas Research Network. “Comprehensive genomic characterization defines human glioblastoma genes and core pathways”. eng. In: *Nature* 455.7216 (Oct. 2008). nature07385[PII], pp. 1061–1068. ISSN: 1476-4687.

[12] Roel G. W. Verhaak et al. “Integrated genomic analysis identifies clinically relevant subtypes of glioblastoma characterized by abnormalities in PDGFRA, IDH1, EGFR, and NF1”. eng. In: *Cancer cell* 17.1 (Jan. 2010). S1535-6108(09)00432-2[PII], pp. 98–110. ISSN: 1878-3686.

[13] Seamus Caragher, Anthony J. Chalmers, and Natividad Gomez-Roman. “Glioblastoma’s Next Top Model: Novel Culture Systems for Brain Cancer Radiotherapy Research”. eng. In: *Cancers* 11.1 (Jan. 2019). cancers11010044[PII], p. 44. ISSN: 2072-6694.

[14] Ahmad R. Safa et al. “Glioblastoma stem cells (GSCs) epigenetic plasticity and interconversion between differentiated non-GSCs and GSCs”. In: *Genes Diseases* 2.2 (2015), pp. 152–163. ISSN: 2352-3042.

[15] Ahmed Musah-Eroje and Sue Watson. “A novel 3D in vitro model of glioblastoma reveals resistance to temozolomide which was potentiated by hypoxia”. eng. In: *Journal of neuro-oncology* 142.2 (Apr. 2019). PMC6449313[pmcid], pp. 231–240. ISSN: 1573-7373.

[16] Tormod Selbekk et al. “Tissue Motion and Strain in the Human Brain Assessed by Intraoperative Ultrasound in Glioma Patients”. In: *Ultrasound in Medicine and Biology* 36.1 (Jan. 2010), pp. 2–10. ISSN: 0301-5629.

[17] Christine Wang et al. “A comparative study of brain tumor cells from different age and anatomical locations using 3D biomimetic hydrogels”. In: *Acta Biomaterialia* 116 (2020), pp. 201–208. ISSN: 1742-7061.

[18] Azadeh Farin et al. “Transplanted glioma cells migrate and proliferate on host brain vasculature: A dynamic analysis”. In: *Glia* 53.8 (2006), pp. 799–808.

[19] Joshua B. Rubin et al. “A small-molecule antagonist of CXCR4 inhibits intracranial growth of primary brain tumors”. In: *Proceedings of the National Academy of Sciences* 100.23 (2003), pp. 13513–13518. ISSN: 0027-8424.

[20] David Zagzag et al. “Tenascin-C Expression by Angiogenic Vessels in Human Astrocytomas and by Human Brain Endothelial Cells in Vitro”. In: *Cancer Research* 56.1 (1996), pp. 182–189. ISSN: 0008-5472.

[21] Candece L. Gladson. “The Extracellular Matrix of Gliomas: Modulation of Cell Function”. In: *Journal of Neuropathology & Experimental Neurology* 58.10 (Oct. 1999), pp. 1029–1040.

[22] Attilio Marino et al. “Biomimicry at the nanoscale: current research and perspectives of two-photon polymerization”. In: *Nanoscale* 7 (7 2015), pp. 2841–2850.

[23] Sourabh Saha et al. “Effect of Proximity of Features on the Damage Threshold During Submicron Additive Manufacturing Via Two-Photon Polymerization”. In: *Journal of Micro and Nano-Manufacturing* 5 (Apr. 2017).

[24] Sofia Rodriguez. *Ultraprecise 3D Microprinting for Optical and Photonic Components*. Oct. 2018.

[25] Dieter Schardt, Thilo Elsässer, and Daniela Schulz-Ertner. “Heavy-ion tumor therapy: Physical and radiobiological benefits”. In: *Reviews of Modern Physics - REV MOD PHYS* 82 (Feb. 2010), pp. 383–425.

[26] Parisa Azimi and Amir Movafeghi. “Proton Therapy in Neurosurgery: A Historical Review and Future Perspective Based on Currently Available New Generation Systems”. In: *International Clinical Neuroscience Journal* 3 (Aug. 2016), pp. 59–80.

[27] Jay S. Loeffler and Marco Durante. “Charged particle therapy—optimization, challenges and future directions”. In: *Nature Reviews Clinical Oncology* 10.7 (July 2013), pp. 411–424. ISSN: 1759-4782.

[28] Dounia Houria Hamdi et al. “In vitro engineering of human 3D chondrosarcoma: a preclinical model relevant for investigations of radiation quality impact”. In: *BMC Cancer* 15.1 (Aug. 2015), p. 579.

[29] Eirini Terpsi Vitti and Jason L Parsons. “The Radiobiological Effects of Proton Beam Therapy: Impact on DNA Damage and Repair”. In: *Cancers* 11.7 (2019). ISSN: 2072-6694.

[30] Sonali Joshi and Dihua Yu. “Chapter 8 - Immunofluorescence”. In: *Basic Science Methods for Clinical Researchers*. Ed. by Morteza Jalali, Francesca Y.L. Saldanha, and Mehdi Jalali. Boston: Academic Press, 2017, pp. 135–150. ISBN: 978-0-12-803077-6.

[31] Michael Wangler and Hugo Bellen. “In Vivo Animal Modeling”. In: Dec. 2017, pp. 211–234. ISBN: 9780128030776.

[32] Iris Mironi-Harpaz et al. “Photopolymerization of cell-encapsulating hydrogels: Crosslinking efficiency versus cytotoxicity”. In: *Acta Biomaterialia* 8.5 (2012), pp. 1838–1848. ISSN: 1742-7061.

[33] Tzu-Wei Wang and Myron Spector. “Development of hyaluronic acid-based scaffolds for brain tissue engineering”. In: *Acta Biomaterialia* 5.7 (2009), pp. 2371–2384. ISSN: 1742-7061.

[34] Shreyas S. Rao et al. “Glioblastoma behaviors in three-dimensional collagen-hyaluronan composite hydrogels”. eng. In: *ACS applied materials & interfaces* 5.19 (Oct. 2013). PMC4333346[pmcid], pp. 9276–9284. ISSN: 1944-8252.

[35] Weikun Xiao, Alireza Sohrabi, and Stephanie K Seidlits. “Integrating the glioblastoma microenvironment into engineered experimental models”. In: *Future Science OA* 3.3 (2017), FSO189.

[36] Xiangyu Gong, Jonathan Kulwatno, and K.L. Mills. “Rapid fabrication of collagen bundles mimicking tumor-associated collagen architectures”. In: *Acta Biomaterialia* 108 (2020), pp. 128–141. ISSN: 1742-7061.

[37] Ashley R. Murphy et al. “Scaffolds for 3D in vitro culture of neural lineage cells”. In: *Acta Biomaterialia* 54 (2017), pp. 1–20. ISSN: 1742-7061.

[38] Stephen J. Florczyk et al. “Porous chitosan-hyaluronic acid scaffolds as a mimic of glioblastoma microenvironment ECM”. eng. In: *Biomaterials* 34.38 (Dec. 2013). S0142-9612(13)01117-4[PII], pp. 10143–10150. ISSN: 1878-5905.

[39] M.W. Hayman et al. “Growth of human stem cell-derived neurons on solid three-dimensional polymers”. In: *Journal of Biochemical and Biophysical Methods* 62.3 (2005), pp. 231–240. ISSN: 0165-022X.

[40] Natividad Gomez-Roman et al. “A novel 3D human glioblastoma cell culture system for modeling drug and radiation responses”. In: *Neuro-Oncology* 19.2 (Aug. 2016), pp. 229–241. ISSN: 1522-8517.

[41] Donglai Lv et al. “A three-dimensional collagen scaffold cell culture system for screening anti-glioma therapeutics”. eng. In: *Oncotarget* 7.35 (Aug. 2016). 10885[PII], pp. 56904–56914. ISSN: 1949-2553.

[42] Omar Tricinci et al. “A 3D Biohybrid Real-Scale Model of the Brain Cancer Microenvironment for Advanced In Vitro Testing”. In: *Advanced Materials Technologies* 5.10 (2020), p. 2000540.

[43] Angelo Accardo et al. “Multiphoton Direct Laser Writing and 3D Imaging of Polymeric Freestanding Architectures for Cell Colonization”. In: *Small* 13.27 (2017), p. 1700621.

[44] Barbara Spagnolo et al. “Three-dimensional cage-like microscaffolds for cell invasion studies”. In: *Scientific Reports* 5.1 (May 2015), p. 10531. ISSN: 2045-2322.

[45] Alexandra M. Greiner et al. “Multifunctional polymer scaffolds with adjustable pore size and chemoattractant gradients for studying cell matrix invasion”. In: *Biomaterials* 35.2 (2014), pp. 611–619. ISSN: 0142-9612.

[46] Attilio Marino et al. “A 3D Real-Scale, Biomimetic, and Biohybrid Model of the Blood-Brain Barrier Fabricated through Two-Photon Lithography”. In: *Small* 14.6 (2018), p. 1702959.

[47] Enrico Domenico Lemma et al. “Studying Cell Mechanobiology in 3D: The Two-Photon Lithography Approach”. In: *Trends in Biotechnology* 37.4 (2019), pp. 358–372. ISSN: 0167-7799.

[48] Ramon Lopez Perez et al. “DNA damage response of clinical carbon ion versus photon radiation in human glioblastoma cells”. In: *Radiotherapy and Oncology* 133 (Apr. 2019), pp. 77–86. ISSN: 0167-8140.

[49] Andres I. Roig et al. “DNA damage intensity in fibroblasts in a 3-dimensional collagen matrix correlates with the Bragg curve energy distribution of a high LET particle”. eng. In: *International journal of radiation biology* 86.3 (Mar. 2010). PMC3382085[pmcid], pp. 194–204. ISSN: 1362-3095.

[50] Iris Eke et al. “Three-dimensional Invasion of Human Glioblastoma Cells Remains Unchanged by X-ray and Carbon Ion Irradiation In Vitro”. In: *International Journal of Radiation Oncology, Biology, Physics* 84.4 (Nov. 2012), e515–e523. ISSN: 0360-3016.

[51] Dane Avondoglio et al. “High throughput evaluation of gamma-H2AX”. In: *Radiation Oncology* 4.1 (Aug. 2009), p. 31.

[52] Li Jia Jiang et al. “Two-photon polymerization: investigation of chemical and mechanical properties of resins using Raman microspectroscopy”. In: *Opt. Lett.* 39.10 (May 2014), pp. 3034–3037.

[53] Anja Torsvik et al. “U-251 revisited: genetic drift and phenotypic consequences of long-term cultures of glioblastoma cells”. eng. In: *Cancer medicine* 3.4 (Aug. 2014). PMC4303149[pmcid], pp. 812–824. ISSN: 2045-7634.

[54] Nobuaki Ishii et al. “Frequent Co-Alterations of TP53, p16/CDKN2A, p14ARF, PTEN Tumor Suppressor Genes in Human Glioma Cell Lines.” In: *Brain Pathology* 9.3 (1999), pp. 469–479.

[55] Felicite K. Noubissi et al. “Detection and quantification of γ-H2AX using a dissociation enhanced lanthanide fluorescence immunoassay”. In: *Scientific Reports* 11.1 (Apr. 2021), p. 8945. ISSN: 2045-2322.

[56] *Biolegend Spectral Analyzer*. URL: `https://www.biolegend.com/en-us/spectra-analyzer`.

[57] Adam J. Engler et al. “Matrix Elasticity Directs Stem Cell Lineage Specification”. In: *Cell* 126.4 (2006), pp. 677–689. ISSN: 0092-8674.

[58] Weihua Zhou et al. “Purine metabolism regulates DNA repair and therapy resistance in glioblastoma”. In: *Nature Communications* 11.1 (July 2020), p. 3811. ISSN: 2041-1723.

[59] Jiuping Ji et al. “Phosphorylated fraction of H2AX as a measurement for DNA damage in cancer cells and potential applications of a novel assay”. In: *PLOS ONE* 12.2 (Feb. 2017), pp. 1–18.

[60] Shibo Fu et al. “γ-H2AX kinetics as a novel approach to high content screening for small molecule radiosensitizers”. eng. In: *PloS one* 7.6 (2012). PONE-D-11-21700[PII], e38465–e38465. ISSN: 1932-6203.

[61] Michael Bobola et al. “Minimally Cytotoxic Doses of Temozolomide Produce Radiosensitization in Human Glioblastoma Cells Regardless of MGMT Expression”. In: *Molecular cancer therapeutics* 9 (May 2010), pp. 1208–18.

[62] Igor Buchwalow et al. “Non-specific binding of antibodies in immunohistochemistry: fallacies and facts”. In: *Scientific Reports* 1.1 (July 2011), p. 28. ISSN: 2045-2322.

[63] Vaibhavi Umesh et al. “Microenvironmental Stiffness Enhances Glioma Cell Proliferation by Stimulating Epidermal Growth Factor Receptor Signaling”. In: *PLOS ONE* 9 (July 2014), pp. 1–8.

[64] Brenda M. Rubenstein and Laura J. Kaufman. “The Role of Extracellular Matrix in Glioma Invasion: A Cellular Potts Model Approach”. In: *Biophysical Journal* 95.12 (Dec. 2008), pp. 5661–5680. ISSN: 0006-3495.

[65] Junwei Chen and Ning Wang. “Tissue cell differentiation and multicellular evolution via cytoskeletal stiffening in mechanically stressed microenvironments”. In: *Acta Mechanica Sinica* 35.2 (Apr. 2019), pp. 270–274. ISSN: 1614-3116.

[66] Shweta Sharma, Rishov Goswami, and Shaik O. Rahaman. “The TRPV4-TAZ mechanotransduction signaling axis in matrix stiffness- and TGFβ1-induced epithelial-mesenchymal transition”. eng. In: *Cellular and molecular bioengineering* 12.2 (Apr. 2019). 565[PII], pp. 139–152. ISSN: 1865-5025.

[67] Henry Ruiz-Garcia et al. “Engineering Three-Dimensional Tumor Models to Study Glioma Cancer Stem Cells and Tumor Microenvironment”. In: *Frontiers in Cellular Neuroscience* 14 (2020), p. 298. ISSN: 1662-5102.

[68] Md Yousuf Ali et al. “Radioresistance in Glioblastoma and the Development of Radiosensitizers”. eng. In: *Cancers* 12.9 (Sept. 2020). cancers12092511[PII], p. 2511. ISSN: 2072-6694.

[69] Divya Khaitan et al. “Establishment and characterization of multicellular spheroids from a human glioma cell line; Implications for tumor therapy”. eng. In: *Journal of translational medicine* 4 (Mar. 2006). PMC1420330[pmcid], pp. 12–12.

[70] Gang Xue et al. “Reprogramming mediated radio-resistance of 3D-grown cancer cells”. eng. In: *Journal of radiation research* 56.4 (July 2015). rrv018[PII], pp. 656–662. ISSN: 1349-9157.

[71] Muhammad Jamal et al. “The brain microenvironment preferentially enhances the radioresistance of CD133(+) glioblastoma stem-like cells”. eng. In: *Neoplasia (New York, N.Y.)* 14.2 (Feb. 2012). 22431923[pmid], pp. 150–158. ISSN: 1476-5586.

[72] U. Fischer and E. Meese. “Glioblastoma multiforme: the role of DSB repair between genotype and phenotype”. In: *Oncogene* 26.56 (Dec. 2007), pp. 7809–7815. ISSN: 1476-5594.

[73] Dong Pan et al. “Ionizing radiation induced biological effects in three-dimensional cell cultures”. In: *RENDICONTI LINCEI* 25 (Mar. 2014).

[74] Dong Pan et al. “Methylation of promoter of RBL1 enhances the radioresistance of three dimensional cultured carcinoma cells”. In: *Oncotarget* 8 (Oct. 2016).

[75] Natividad Gomez-Roman et al. “A novel 3D human glioblastoma cell culture system for modeling drug and radiation responses”. eng. In: *Neuro-oncology* 19.2 (Feb. 2017). now164[PII], pp. 229–241. ISSN: 1523-5866.

[76] S.-H. Chu et al. “In vitro and in vivo radiosensitization of human glioma U251 cells induced by upregulated expression of SLC22A18”. In: *Cancer Gene Therapy* 21.3 (Mar. 2014), pp. 103–109. ISSN: 1476-5500.

[77] Silvana Valdebenito et al. “Tunneling Nanotubes Mediate Adaptation of Glioblastoma Cells to Temozolomide and Ionizing Radiation Treatment”. In: *iScience* 23.9 (2020), p. 101450. ISSN: 2589-0042.

[78] Matthew J. Rybin et al. “Organoid Models of Glioblastoma and Their Role in Drug Discovery”. In: *Frontiers in Cellular Neuroscience* 15 (2021), p. 4. ISSN: 1662-5102.

[79] Fatemeh Zamani et al. “The influence of surface nanoroughness of electrospun PLGA nanofibrous scaffold on nerve cell adhesion and proliferation”. In: *Journal of Materials Science: Materials in Medicine* 24.6 (June 2013), pp. 1551–1560. ISSN: 1573-4838.